

# **MXene/MnO<sub>2</sub> nanocomposite coated superior salt-rejecting biodegradable luffa sponge for efficient solar steam generation**

Ahmed Mortuza Saleque<sup>1a,b</sup>, Sainan Ma<sup>2,\*</sup>, Amrit Kumar Thakur<sup>3\*</sup>, R. Saidur<sup>4a,b,\*\*</sup>, Tan Kim Han<sup>4a</sup>, Mohammad Ismail Hossain<sup>5</sup>, Wayesh Qarony<sup>6</sup>, Y. Ma<sup>3</sup>, Ravishankar Sathyamurthy<sup>7</sup>, Yuen Hong Tsang<sup>1a,b,\*</sup>

1a.) Department of Applied Physics, Photonic Research Institute, and Materials Research Center, The Hong Kong Polytechnic University, Hung Hom, Kowloon, Hong Kong

1b.) Shenzhen Research Institute, The Hong Kong Polytechnic University, 518057 Shenzhen, Guangdong, People's Republic of China

2.) Ningbo Research Institute, Zhejiang University, Ningbo 315100, China

3.) Department of Mechanical Engineering, University of California, Merced, CA, 95343, USA

4a.) Research Center for Nano-Materials and Energy Technology (RCNMET), School of Engineering and Technology, Sunway University, Bandar Sunway, Petaling Jaya 47500, Selangor Darul Ehan, Malaysia

4b.) School of Engineering, Lancaster University, Lancaster LA1 4YW, UK

5.) Department of Electrical and Computer Engineering, University of California, Davis, CA 95616, USA

6.) Department of Electrical Engineering and Computer Sciences, University of California, Berkeley, CA 94720, USA

7.) Mechanical Engineering Department, King Fahd University of Petroleum and Minerals, Dhahran, Saudi Arabia

\*) Corresponding authors.

\*\*.) Correspondence to: R. Saidur, Department of Engineering, Lancaster University, Lancaster LA1 4YW, UK.

E-mail addresses: [sainanma@hotmail.com](mailto:sainanma@hotmail.com) (S. Ma), [saidur@sunway.edu.my](mailto:saidur@sunway.edu.my) (R. Saidur), [amritt1@gmail.com](mailto:amritt1@gmail.com) (A. K.Thakur), [yuen.tsang@polyu.edu.hk](mailto:yuen.tsang@polyu.edu.hk) (Y. H. Tsang).

## ABSTRACT

Solar steam generation is widely regarded as one of the potential green approaches for freshwater regeneration by utilizing solar energy. Herein, the MXene/MnO<sub>2</sub> nanocomposite-coated biodegradable luffa sponge (Ti<sub>3</sub>C<sub>2</sub>-MnO<sub>2</sub>@LS) is proposed as an efficient solar evaporator for solar steam generation. The thin layer of Ti<sub>3</sub>C<sub>2</sub>-MnO<sub>2</sub> coated on the surface of the luffa sponge (LS) serves as the solar absorber and enhances the hydrophilicity of the LS, while the thermally insulating LS layer with microporous structure endows sufficient water transportation and localizes heat for interfacial water evaporation. Combining MXene with MnO<sub>2</sub> can increase the surface area as well as the stability. The Ti<sub>3</sub>C<sub>2</sub>-MnO<sub>2</sub>@LS delivers a solar evaporation rate as high as 1.36 kg m<sup>-2</sup> h<sup>-1</sup>, with a solar steam conversion efficiency of 85.28% under one sun irradiation. Furthermore, this Ti<sub>3</sub>C<sub>2</sub>-MnO<sub>2</sub>@LS exhibits superior salt-rejecting properties even under highly concentrated saltwater desalination and excellent wastewater purification performance. This work demonstrates the prospects of combining novel 2D materials with biomass-based materials for practical solar steam generation.

**Keywords:** Solar energy, desalination, 2D materials, MXene, biomaterials

## 1. INTRODUCTION

With the rapid progress of modern industry and highly increased population, water shortage has become a severe issue.[1] Intensive research have been devoted to exploring efficient, renewable, and economic water treatment strategies for fresh and clean water regeneration. Traditional desalination and wastewater treatment technologies, such as reverse osmosis, electrodialysis, thermal desalination and multi-effect distillation, still face complex equipment, high cost, high energy consumption and secondary pollution problems. Solar energy, as the most promising, and sustainable energy source, has attracted high attention to be utilized for water treatment [2,3]. However, the traditional solar steam generation system has a poor efficiency, which involves high heat loss [4,5]. Over the past decades, solar-driven interfacial steam generation has become an important research branch for seawater desalination and wastewater treatment because of its sustainability, environmental friendliness, and low cost [6–9].

For an efficient solar steam generation system, the light absorption ability, photothermal conversion efficiency, water transportability, and durability of the solar evaporator determine the solar water evaporation efficiency [10]. Various photothermal materials have been developed, including carbon materials [11,12], metal nanoparticles [13,14], semiconductor materials [15,16], and organic photothermal materials [17,18]. Among them, biomass-based materials, generally possessing natural porous structure, low thermal conductivity, and low cost, have drawn tremendous interest. For instance, a series of wood-based materials have been reported as solar evaporators for efficient solar steam generation [19–22]. Besides, carbonized bamboo, which possesses excellent water

transport channels, good mechanical strength, and effective heat localization effect, has also been explored [23–29]. Liao et al. prepared carbonized lotus seedpods with a hierarchical porous structure and good light absorption, achieving a photothermal evaporation rate and efficiency of  $1.30 \text{ kg m}^{-2} \text{ h}^{-1}$  and 86.5%, respectively [30]. Beyond these, many vegetable or fruit-based materials were investigated, such as mushroom [31], sunflower heads [32], potato [33], coconut husk [34], corncob [35], daikon [36], carrot [37], and eggplant [38]. Recently, loofah, which is a vigorous, productive, and widely distributed reticulated fibrous plant, has been investigated as good solar evaporator [39,40]. The outstanding mechanical strength and microporous structure present promising potential for continuous solar driven water transpiration.

However, for most biomass-based materials, the pristine solar absorption property is poor. Surface treatment like coating with photothermal materials can be a feasible way to enhance solar absorption. MXene, as a new family of multifunctional 2D material, has been widely applied in a variety of fields, including supercapacitor [41], microwave absorption [42], catalysis [43], and dye separation [44], etc. Wang et al. [45] reported that the  $\text{Ti}_3\text{C}_2$  MXene shows an internal light-to-heat conversion efficiency of 100% measured by a designed droplet-based light absorption and heating system, indicating the great potential of MXene as photothermal materials for solar steam generation. Because of the semi-metal character of  $\text{Ti}_3\text{C}_2$  nanosheets, the photothermal conversion mechanism of MXene is considered to be localized surface plasmon resonance effect. However, due to the commonly presented smooth surface of the  $\text{Ti}_3\text{C}_2$  nanosheets, the light absorption is weak with strong light reflection [46]. Nevertheless, the 2D  $\text{Ti}_3\text{C}_2$  nanosheets often restack spontaneously, which could hinder the water transport and

vapor escaping process. Thus, it is necessary to further modify the  $Ti_3C_2$  for efficient solar steam generation. Introducing the interlayer barrier can effectively avoid spontaneous stacking as well as increase surface area. Materials like CNTs [47], metal oxides [48], and polymers [49] have been investigated to prevent the restack of MXene nanosheets. Among them, manganese dioxide ( $MnO_2$ ) has drawn more attention due to its low cost and environmental friendliness. Wang et al. [50] demonstrated the  $MnO_2$ /MXene composite as film electrodes for electronics, in which the combination of  $MnO_2$  and MXene effectively increased the surface area and reduced the spontaneous stacking of the MXene nanosheets. Moreover,  $MnO_2$  is also a promising photothermal material for solar steam generation [51–53].

While significant advancements have been made for photothermal materials, considerable hurdles remain, particularly in regard to the problem of severe salt accumulation, which is seen as one of the largest impediments preventing their actual solar desalination applications. Water molecules undergo a phase transition from liquid to gas during solar evaporation, migrating through the porous channels of the photothermal material where salt may readily precipitate and clog the channels. The deposition of salt on the surface of photothermal materials may reduce their performance as a heat generator when exposed to light. The researchers exhibited two types of salt rejection mechanisms to solve these difficulties. A double-layered Janus structure on the photothermal material's surface hinders salt crystallization and emigration [54–56]. The simplest method is to construct aligned channels with large diameters to allow crystallized salts to dissolve quickly and be transferred back into the bulk water [57,58].

Herein, we utilized the low-cost biodegradable luffa sponge (LS), which has a 3D

microporous structure, as the solar evaporator via surface coated with  $\text{Ti}_3\text{C}_2\text{-MnO}_2$  nanocomposite. The hydrophilicity and solar absorption properties of LS have been highly enhanced by surface coating of  $\text{Ti}_3\text{C}_2\text{-MnO}_2$  nanocomposite. The water evaporation and seawater desalination performance enabled by the  $\text{Ti}_3\text{C}_2\text{-MnO}_2\text{@LS}$  are investigated and discussed. The obtained solar evaporator presents a high evaporation efficiency and long-term stability for solar water evaporation under one sun irradiation. In addition, the  $\text{Ti}_3\text{C}_2\text{-MnO}_2\text{@LS}$  shows excellent salt-rejecting performance owing to large diameters porous structure of LS which helps to dissolve crystallized salts and transferred back into the bulk water as known as salt ion diffusion backflow mechanism. Therefore, it can be used for highly concentrated saline desalination. The wastewater treatment performance has also been evaluated, in which dye contaminants can be completely removed. All of these allow the synthesized  $\text{Ti}_3\text{C}_2\text{-MnO}_2\text{@LS}$  for practical solar water treatment.

## **2. EXPERIMENTAL SECTION**

### **2.1 Synthesis of MXene ( $\text{Ti}_3\text{C}_2$ )**

MAX phase material ( $\text{Ti}_3\text{AlC}_2$ ),  $\text{NH}_4\text{HF}_2$  (95% reagent grade), and NaOH (97% purity, pellets) were purchased from Y-Carbon limited and Sigma Aldrich, USA for MXene ( $\text{Ti}_3\text{C}_2\text{T}_x$ ) synthesis. The purchased chemicals were used without being purified further. 20 ml of a 2 M solution of  $\text{NH}_4\text{HF}_2$  were prepared, followed by 1 hour of magnetic stirring at 300 rpm and 30 °C. Slowly 1 g of  $\text{Ti}_3\text{AlC}_2$  was added to a 2 M  $\text{NH}_4\text{HF}_2$  solution, which was magnetically stirred for 48 hours at 300 rpm and 30 ° C. Throughout the stirring procedure, Al was etched from the MAX phase material ( $\text{Ti}_3\text{AlC}_2$ ). Continuous pH monitoring and the addition of diluted NaOH solution allowed for the solution's pH to be

maintained at 6. After the etching procedure was complete, the solution was filtered and repeatedly washed with DI water. 4 repetitions of ultrahigh centrifugation were performed at 3500 rpm (10 mins for each cycle). The resultant multilayered  $Ti_2C_2T_x$  solution was sonicated for 1 hour with an ultrasonic probe to produce delaminated MXene (d-  $Ti_2C_2T_x$ ). Finally, the delaminated flakes of synthesized MXene were dried in a vacuum oven overnight.

## 2.2 Material Characterizations

The microstructures of the  $Ti_3C_2-MnO_2@LS$  were investigated using a scanning electron microscope (SEM, TESCAN, VEGA3, 20 kV). Energy dispersive X-ray (EDS) images were acquired using X-ray spectroscopy (INCA X-Act, Oxford) in conjunction with SEM equipment. A UV-Vis-NIR spectrometer was used to measure the absorption spectra (PerkinElmer Lambda 1050). X-ray diffraction (XRD) patterns of the materials were obtained using a Cu-K $\alpha$  radiation X-ray diffractometer (Smart Lab, Rigaku, 40 kV, 100 mA). X-ray photoelectron spectroscopy (XPS) measurements were performed using Al-K $\alpha$  radiation on a Thermo Fisher Nexsa G2 XPS instrument. The Raman spectroscopy was conducted using WITEC Confocal Raman system with 532 nm laser. The hydrophilicity of the surface was decided through the water contact angle measurement (WCA, KINO SL 200 KB). Transients hot-wire approach with computer-controlled equipment was used to measure thermal conductivity (Thermtest Instruments, THW L2). Using a linear heat source implanted in the material being tested, the hot-wire method is a transient dynamic approach that measures the temperature increase in a predetermined distance. The rate of temperature rises or fall over a certain time period is a direct measure of thermal conductivity [59].

### 2.3 Preparation of $\text{Ti}_3\text{C}_2\text{-MnO}_2\text{@LS}$ photothermal absorber

The cylindrical form of luffa sponge extracted from the ripe fruit of *Luffa cylindrica* was washed and cleaned before being tailored into a circular shape with a 20 mm radius and a 12 mm thickness. The prepared sample was ultrasonically cleaned with deionized (DI) water and dried in a 50 °C oven.  $\text{Ti}_3\text{C}_2$  MXene synthesized in a laboratory and purchased  $\text{MnO}_2$  powder were both dissolved in Isopropyl alcohol (IPA). 6 different concentrations of  $\text{Ti}_3\text{C}_2$  and  $\text{MnO}_2$  were prepared, and their corresponding average absorbance were measured. As the major objective of this solution was to improve the absorption of luffa sponge in the AM 1.5 solar spectrum, each of the produced solutions was tested in a separate cuvette for its absorption spectrum. The supporting information note S3 contains the detail description of the preparation and table S1 (supporting information) shows the various concentration of  $\text{Ti}_3\text{C}_2$  and  $\text{MnO}_2$  and their average absorbance as measured by UV-Vis-NIR spectroscopy. Based on the average absorbance,  $\text{Ti}_3\text{C}_2\text{-MnO}_2$  (2 – 5) sample provided highest average absorbance (table S1, supporting information). Therefore, it was chosen as the optimum concentration for fabricating the  $\text{Ti}_3\text{C}_2\text{-MnO}_2\text{@LS}$ .  $\text{Ti}_3\text{C}_2$  and  $\text{MnO}_2$  with a concentration of 2 mg ml<sup>-1</sup> and 5 mg ml<sup>-1</sup>, respectively are dissolved in IPA. The prepared solutions were ultrasonically treated for 4 hours. After that, 60 ml of  $\text{Ti}_3\text{C}_2$  and 40 ml of  $\text{MnO}_2$  solutions were mixed in a beaker, and the mixture was magnetically stirred at 600 rpm for 2 hours. Afterward, the prepared luffa sponge (LS) sample was dip coated several times into the  $\text{Ti}_3\text{C}_2\text{-MnO}_2$  solution. The sample was then dried in a 65 °C oven for 6 hours. The preparation method is illustrated in **Fig. 1a**. To perform sun evaporation experiments, the as-prepared  $\text{Ti}_3\text{C}_2\text{-MnO}_2\text{@LS}$  was placed on top of a beaker containing water, as shown in **Fig. 1b**.



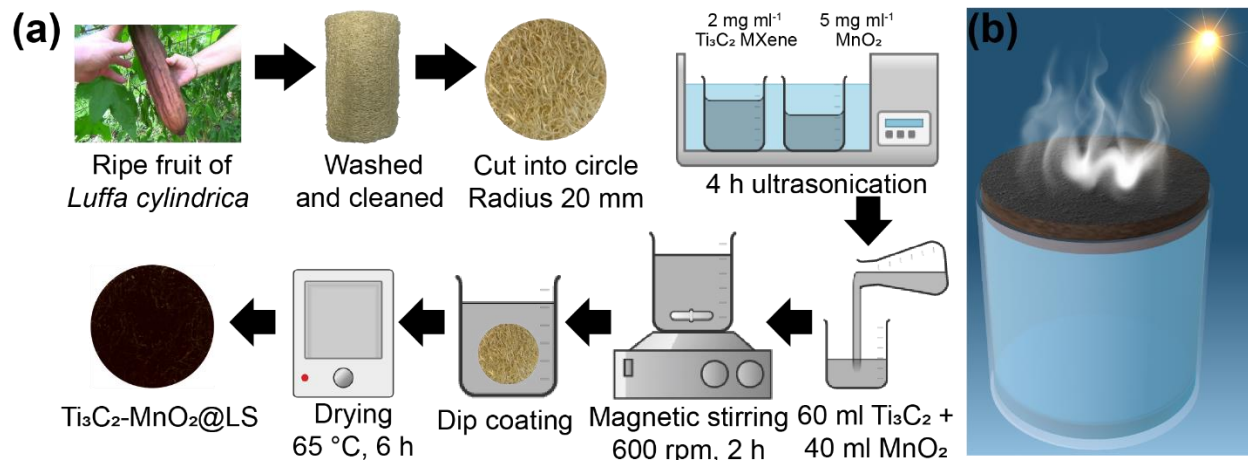


**Fig. 1** (a) Schematic representation of  $\text{Ti}_3\text{C}_2\text{-MnO}_2\text{@LS}$  preparation process; (b) Illustration of solar steam generation by  $\text{Ti}_3\text{C}_2\text{-MnO}_2\text{@LS}$ .

## 2.4 Solar-driven desalination experiment

The solar desalination experiments were conducted in a laboratory environment where the solar irradiance was provided by a xenon lamp (300 W, PLS-SXE300, Beijing Perfect Light Technology Co., Ltd). The intensity of the incident solar irradiance was measured by a power meter (THORLABS, S314C). The setup was placed on an electronic microbalance (Ohaus Corporation, C213, deviation  $\sim 0.1$  mg) to measure the mass loss. The temperature of the solar evaporator surface and underneath bulk water was recorded using an infrared camera (FLIR-E64501, Tallinn, Estonia, error range of  $\pm 2$  °C). **The  $\text{Ti}_3\text{C}_2\text{-MnO}_2\text{@LS}$  structure was wrapped by an Expanded Polyethylene (EPE) foam in order to make it float and reduce the heat loss. Then, it was placed in a beaker containing seawater to conduct the solar evaporation experiments. A separate experiment was conducted without EPE foam to understand the improvement in solar evaporation rate and efficiency and the corresponding results are provided in Fig. S2, supporting information. At first, the thickness of the LS was varied from 6 mm to 18 mm and the**

corresponding evaporation efficiency were measured under 1 sun illumination. The maximum evaporation efficiency of 85.28% has been achieved at 14 mm thickness of LS. Therefore, rest of the experiments were conducted using 14 mm thickness. The solar irradiance was varied from 1 to 5 kW/m<sup>2</sup> and the corresponding mass losses were recorded. To measure the mass loss due to the solar irradiance, the Ti<sub>3</sub>C<sub>2</sub>-MnO<sub>2</sub>@LS was put on top of a beaker holding 150 ml of seawater. The beaker was then placed within a custom-made glass structure, as shown in **Fig. S1, supporting information**. The evaporated steam is collected through an output channel on the structure's upper side. The outflow channel is linked to a pipe, with the other end connected to a container to collect the condensed water droplet. The majority of the evaporated steam flows via the output route at the top of the pipe to the water droplet collecting container. The steam gradually releases heat and condenses into water droplets as it travels along this path. However, some steam condenses inside the custom-made structure and condenses into a water droplet, which is deposited at the bottom. As a consequence, at the end of the experiment, the water deposited at the bottom of the custom-made structure was also collected. The evaporation rate and efficiency were calculated from the measured evaporated mass loss under various solar irradiance.

### 3. RESULTS AND DISCUSSION

#### 3.1 Material Structure and Morphology

Due to the low solar absorption of natural LS, Ti<sub>3</sub>C<sub>2</sub>-MnO<sub>2</sub> nanocomposite with excellent light absorption was utilized to coat the surface of natural LS. The surface morphology of the Ti<sub>3</sub>C<sub>2</sub>-MnO<sub>2</sub>@LS was characterized by SEM, as shown in **Fig. 2a-d**. The natural LS

possesses a fiber-shaped porous structure, which is feasible for water transport from the underneath bulk water. After coating with  $\text{Ti}_3\text{C}_2\text{-MnO}_2$ , the fiber surface of the LS is entirely covered by a large number of nanoparticles. Compared with the pristine surface (inset of Fig. 2d), it becomes rougher, which can be beneficial to reduce light reflection. The LS has a fibrous porous structure that is advantageous to soak the  $\text{Ti}_3\text{C}_2\text{-MnO}_2$  nanocomposite during the dip coating process.

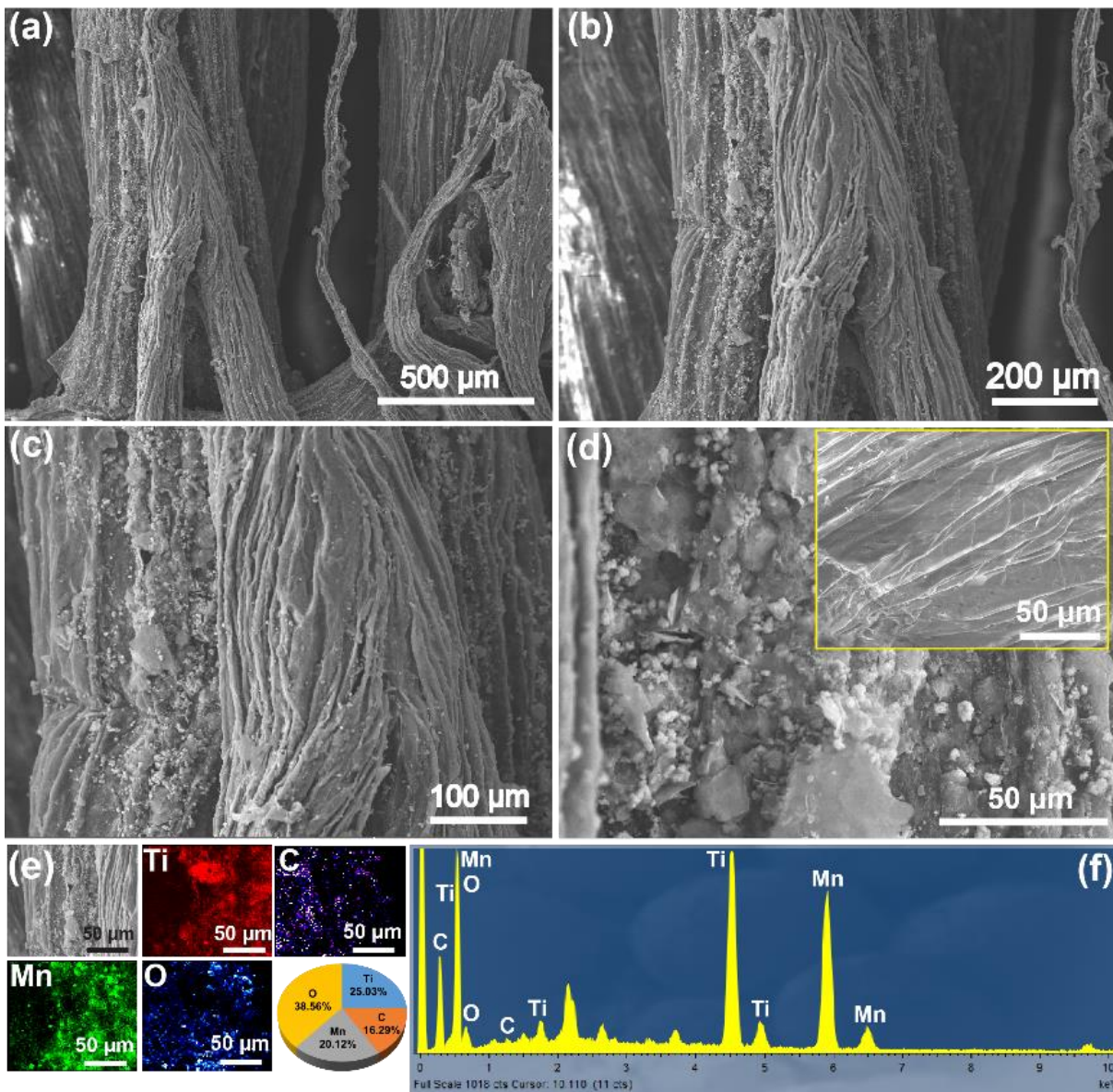


**Fig. 2** (a-d) SEM images of  $\text{Ti}_3\text{C}_2\text{-MnO}_2$ @LS in different magnitude. Inset of (d) is pristine LS; (e) EDS elemental mapping; (f) EDS spectrum with the elemental composition

analysis.

**Fig. 2e** shows the corresponding elemental distribution information by EDX elemental mapping. It is clear that the Ti, Mn, C, and O elements are homogeneously and continuously distributed throughout the LS surface, with the ratio of 25.03%, 20.12%, 16.29%, and 38.56%, respectively. The coexistence of  $\text{Ti}_3\text{C}_2$  and  $\text{MnO}_2$  is also indicated by the EDS spectrum in **Fig. 2f**.

The structural features of  $\text{Ti}_3\text{C}_2\text{-MnO}_2$  nanocomposite have been investigated by the Raman measurement as shown in **Fig. 3a**. As for the Raman spectrum of  $\text{MnO}_2$ , the two Raman bands at 486.52 and 652.81  $\text{cm}^{-1}$  are observed, corresponding to the symmetrical vibrations of  $\text{MnO}_2$ .<sup>[53,60]</sup> Generally, the two Raman bands at around 159.52 and 409.21  $\text{cm}^{-1}$  correspond to the vibrations from Ti-C bonds for  $\text{Ti}_3\text{C}_2$ , and the two bands at around 1386 and 1576.92  $\text{cm}^{-1}$  are attributed to the D band and G band of graphitic carbon.<sup>[61,62]</sup> The ratio of intensity between  $I_D$  and  $I_G$  of the  $\text{Ti}_3\text{C}_2$  is 1.048, suggesting a high graphitization degree. The Raman spectrum of  $\text{Ti}_3\text{C}_2\text{-MnO}_2$  shows both the typical characteristic bands of  $\text{MnO}_2$  and  $\text{Ti}_3\text{C}_2$ , indicating the hybrid structure of  $\text{Ti}_3\text{C}_2\text{-MnO}_2$  nanocomposite.

In order to further confirm the crystalline structure of  $\text{Ti}_3\text{C}_2\text{-MnO}_2\text{@LS}$ , XRD spectra of  $\text{MnO}_2$ ,  $\text{Ti}_3\text{C}_2$ , and  $\text{Ti}_3\text{C}_2\text{-MnO}_2$  nanocomposite were recorded, as presented in **Fig. 2b**. The diffraction peaks of the  $\text{MnO}_2$  at the angles of 29.29, 37.45, 43.07, 56.59, 72.91 are assigned to the (100), (110), (111), (211) and (301) planes, respectively. While the peaks at angles of 4.388, 14.52, 24.81, 34.89, 60.76 are assigned to the (002), (006), (008), (103) and (110) planes of  $\text{Ti}_3\text{C}_2$ , respectively. Coexisting phases of  $\text{MnO}_2$  and  $\text{Ti}_3\text{C}_2$  can be observed in  $\text{Ti}_3\text{C}_2\text{-MnO}_2$  nanocomposite.

The elemental compositions of Ti, Mn, C and O species in the  $\text{Ti}_3\text{C}_2\text{-MnO}_2$  hybrid are investigated by X-ray photoelectron spectroscopy (XPS). As shown in **Fig. 3c**, the peaks at a binding energy of 665.04, 658.67 and 453.81 eV in the  $\text{Ti}_3\text{C}_2\text{-MnO}_2$  hybrid are assigned to Mn  $2p_{1/2}$ , Mn  $2p_{3/2}$  and Ti  $2p$ , respectively. The XPS spectra indicate that the  $\text{Ti}_3\text{C}_2\text{-MnO}_2@\text{LS}$  is composed of Ti, Mn, C and O, indicating the introduction of  $\text{Ti}_3\text{C}_2\text{-MnO}_2$  hybrid into the LS. The water contact angles of the LS before and after surface coating with  $\text{Ti}_3\text{C}_2\text{-MnO}_2$  nanocomposite were measured and shown in **Fig. 3d**. The results that the contact angle decreases from  $78.56^\circ$  to  $45.21^\circ$  after coating (standard deviation  $\pm 0.05^\circ$ ), indicates that the coating can improve the hydrophilicity, which can contribute to a fast and efficient water supply from the bottom bulk water to the evaporating surface. The higher affinity for water of the  $\text{Ti}_3\text{C}_2\text{-MnO}_2$  coating in comparison to the pristine luffa sponge causes the water droplets to disperse and the water contact angle to be maximized. **Fig. 3e** shows the absorption properties of the  $\text{Ti}_3\text{C}_2\text{-MnO}_2@\text{LS}$  and uncoated LS. The solar absorption of the LS has been greatly enhanced after being coated with  $\text{Ti}_3\text{C}_2\text{-MnO}_2$ , which should be attributed to the excellent light absorption property of  $\text{Ti}_3\text{C}_2\text{-MnO}_2$  and the rougher surface with reduced reflection. The absorption covers the entire UV-Vis-NIR region and matches well with the AM 1.5 solar spectrum, which is beneficial to efficient photothermal conversion. All the above results suggest the successful synthesis of  $\text{Ti}_3\text{C}_2\text{-MnO}_2@\text{LS}$  and the great potential for application in solar steam generation.

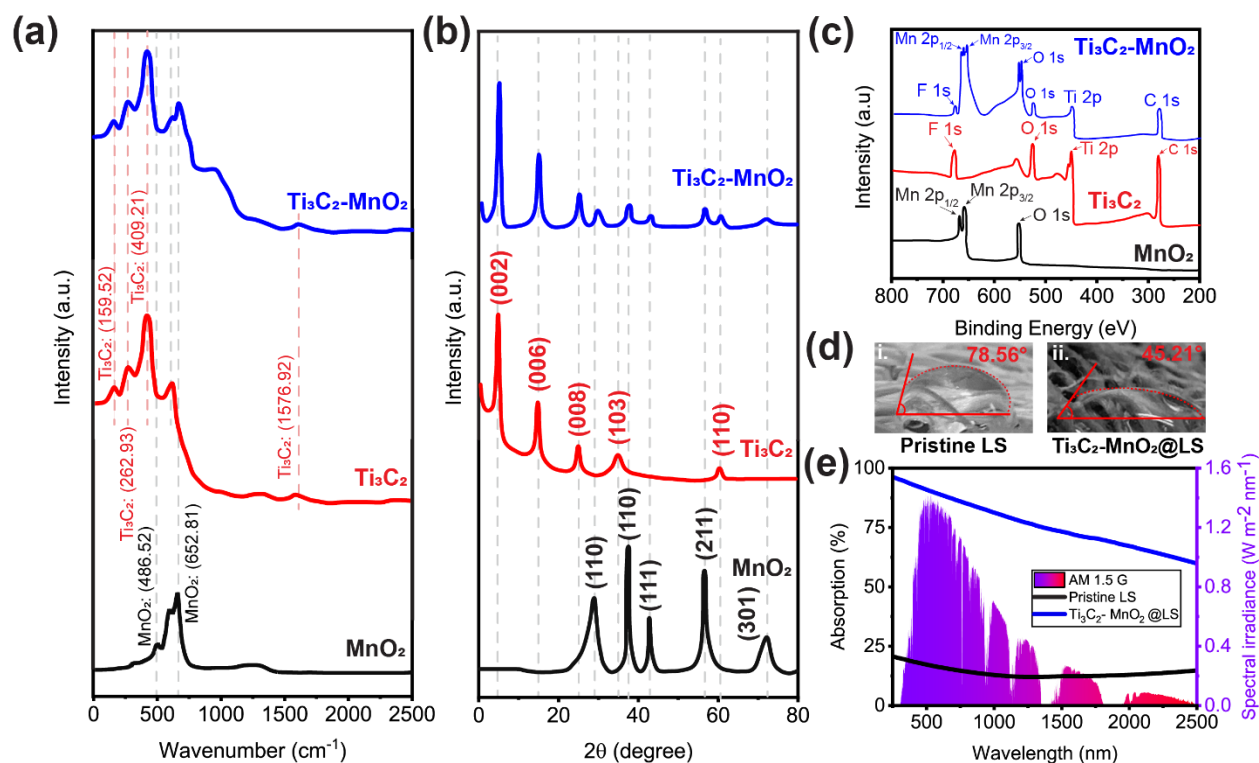


**Fig. 3** (a) Raman spectra of Ti<sub>3</sub>C<sub>2</sub>-MnO<sub>2</sub>, Ti<sub>3</sub>C<sub>2</sub>, and MnO<sub>2</sub>; (b) XRD patterns of Ti<sub>3</sub>C<sub>2</sub>-MnO<sub>2</sub>, Ti<sub>3</sub>C<sub>2</sub>, and MnO<sub>2</sub>; (c) XPS spectra of Ti<sub>3</sub>C<sub>2</sub>-MnO<sub>2</sub>, Ti<sub>3</sub>C<sub>2</sub>, and MnO<sub>2</sub>; (d) Water contact angle of pristine LS and Ti<sub>3</sub>C<sub>2</sub>-MnO<sub>2</sub>@LS; (e) UV-Vis-NIR absorption spectra of pristine LS and Ti<sub>3</sub>C<sub>2</sub>-MnO<sub>2</sub>@LS.

### 3.2 Evaluation of the solar evaporation by Ti<sub>3</sub>C<sub>2</sub>-MnO<sub>2</sub>@LS

The water evaporation performance of the synthesized Ti<sub>3</sub>C<sub>2</sub>-MnO<sub>2</sub>@LS was investigated. **Fig. 4a** displays the time-dependent mass changes of water only, pristine LS and Ti<sub>3</sub>C<sub>2</sub>-MnO<sub>2</sub>@LS under simulated solar irradiation of 1 kW m<sup>-2</sup>. The corresponding spontaneous evaporations under dark have been subtracted. It can be observed that the water evaporation rate has been greatly enhanced in the presence of Ti<sub>3</sub>C<sub>2</sub>-MnO<sub>2</sub>@LS compared to that of pristine LS. The evaporation rate of the system with Ti<sub>3</sub>C<sub>2</sub>-MnO<sub>2</sub>@LS reaches to 1.36 kg m<sup>-2</sup> h<sup>-1</sup>, which is more than 3.5 times higher than that of pristine LS (0.39 kg m<sup>-2</sup> h<sup>-1</sup>) and 6.8 times higher than that of water only (0.20 kg m<sup>-2</sup> h<sup>-1</sup>). **The evaporation efficiency and rate attained are comparatively higher than several**

biodegradable solar evaporators shown in the literature (table S2, supporting information). **Fig. 4b** shows the water mass change of  $\text{Ti}_3\text{C}_2\text{-MnO}_2\text{@LS}$  under various light densities ranging from  $1 \text{ kW m}^{-2}$  to  $5 \text{ kW m}^{-2}$ . The evaporation rate increases almost linearly with the light density. The evaporation rate reaches up to  $6.65 \text{ kg m}^{-2} \text{ h}^{-1}$  when the irradiation intensity scaled to  $5 \text{ kW m}^{-2}$ .

The solar evaporation efficiency ( $\eta_{th}$ ) of the samples can be calculated by the following equation (1).

$$\eta_{th} = \frac{\dot{m}h_{LV}}{q_{solar}} \quad (1)$$

Where  $\dot{m}$  is the steady-state water evaporation rate ( $\text{kg m}^{-2} \text{ h}^{-1}$ ) excluding the evaporation rate under the dark field,  $h_{LV}$  is the total phase change enthalpy of water ( $2260 \text{ J/g}$ ) including the sensible heat and latent heat,  $q_{solar}$  is the power density of solar irradiation ( $\text{W/m}^2$ ).

The evaporation rate,  $m_e$  can be calculated by following equation:

$$m_{ev} = \frac{m_h}{A} \quad (2)$$

Where,  $m_h$  is mass loss of water per hour ( $\text{kg/h}$ ) due to evaporation and  $A$  is the area ( $\text{m}^2$ ) of evaporation surface. As shown in **Fig. 4c**, the solar evaporation efficiency of  $\text{Ti}_3\text{C}_2\text{-MnO}_2\text{@LS}$  can reach 85.28% under 1 sun irradiation and 83.48% under 5 sun irradiation. The slight decrease in the efficiency may be due to the increased heat loss along with higher light intensity. Another set of experiments has been carried out in order to better understand the influence of EPE sponge on solar evaporation efficiency. The evaporation efficiency has increased from 80.12% to 85.28% and 78.37% to 83.97% after surrounding the  $\text{Ti}_3\text{C}_2\text{-MnO}_2\text{@LS}$  solar evaporator with EPE sponge under 1 sun and 2 sun

illumination, respectively. The corresponding results are provided in **Fig. S2, supporting information**. This improvement in evaporation efficiency is attributed to the EPE sponge's heat insulation property, which limits the amount of photothermal induced heat that is radiated into the environment, hence aiding in heat localization. The cycling stability of the  $\text{Ti}_3\text{C}_2\text{-MnO}_2\text{@LS}$  for solar evaporation was measured by repeating the same evaporation experiment for 25 cycles under 1 sun irradiation. The results are presented in **Fig. 4d**, in which the water evaporation rates are quite stable with ignorable fluctuation. It demonstrates that the as-prepared  $\text{Ti}_3\text{C}_2\text{-MnO}_2\text{@LS}$  has a very stable solar evaporation ability.

Besides, the solar water evaporation performances of  $\text{Ti}_3\text{C}_2\text{-MnO}_2\text{@LS}$  with different thicknesses of LS under 1 sun were investigated to find out the most efficient thickness. As shown in **Fig. 4e**, the evaporation efficiency increases from 50% to 85.28% as the thickness increases from 6 mm to 12 mm and reaches the highest at a thickness of 14 mm. After that, the efficiency drops as the thickness continues to increase. Similarly, the evaporation rate at 6 mm of luffa sponge thickness is just  $0.79 \text{ kg m}^{-2} \text{ h}^{-1}$ . At 14 mm thickness, the evaporation rate reaches its maximum value of  $1.36 \text{ kg m}^{-2} \text{ h}^{-1}$ . The rate of evaporation then reduces with increasing thickness, reaching  $1.15 \text{ kg m}^{-2} \text{ h}^{-1}$  at 18 mm thickness. When the thickness of LS is small, more heat loss occurs to the underlying bulk water. Whereas when the thickness increases to be too thick, water may not be sufficiently transported to the evaporation surface due to the long transfer path, leading to the lower evaporation efficiency. **Fig. 4f** shows that the thermal conductivity of the LS is extremely low, which is  $0.18 \text{ W m}^{-1} \text{ K}^{-1}$  in dry state and  $0.35 \text{ W m}^{-1} \text{ K}^{-1}$  in wet state with



a standard deviation of  $\pm 0.007 \text{ W m}^{-1} \text{ K}^{-1}$ , indicating the good heat confinement effect of LS.

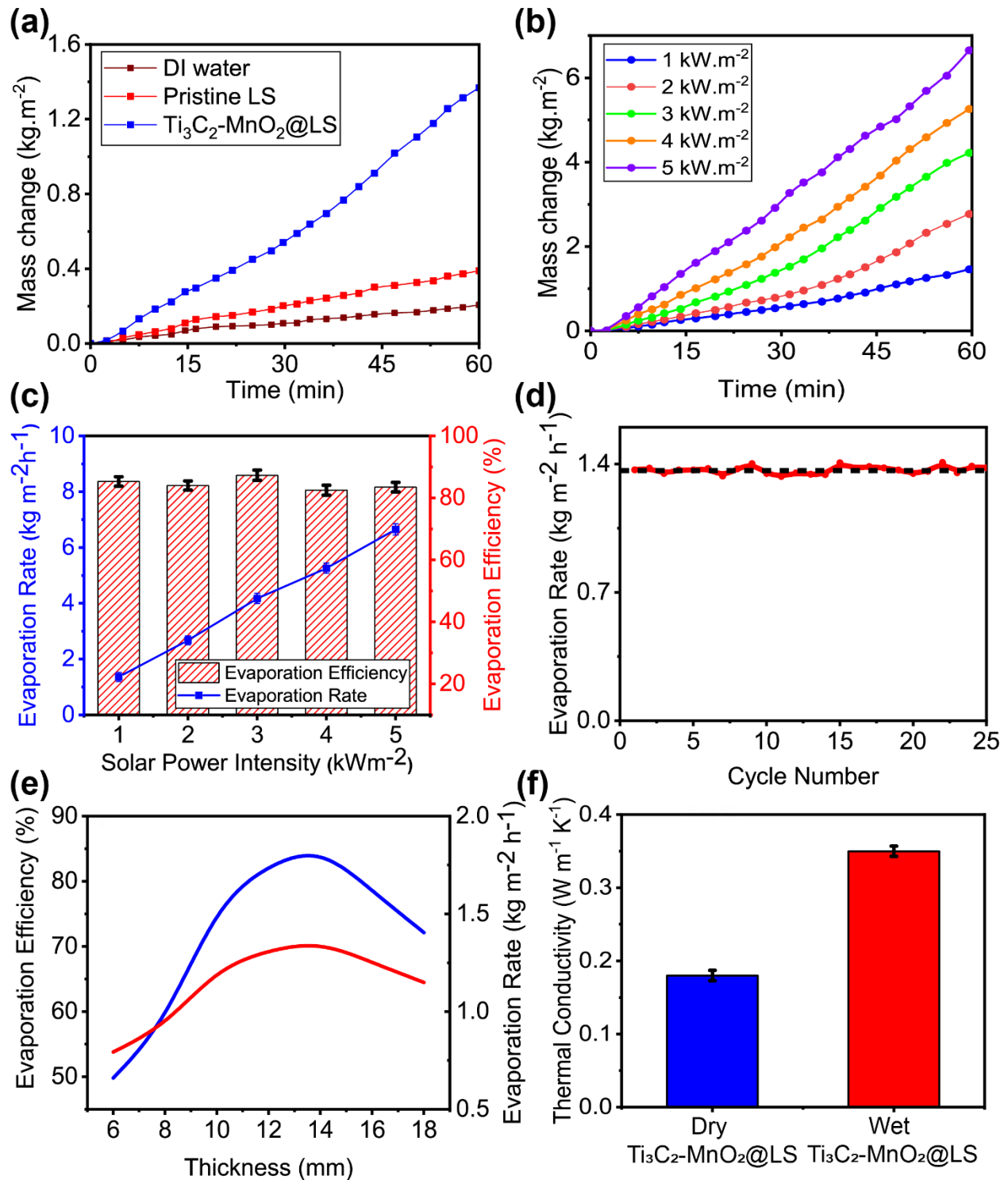


**Fig. 4** The solar water evaporation mass change over time of the system with water only,

pristine LS, and  $\text{Ti}_3\text{C}_2\text{-MnO}_2@\text{LS}$  under one sun irradiation; (b) Solar evaporation performance of  $\text{Ti}_3\text{C}_2\text{-MnO}_2@\text{LS}$  under various light intensity irradiation; (c) Corresponding evaporation rate (line) and evaporation efficiency (bars) under various solar irradiance with error bars; (d) The cyclic performance of the  $\text{Ti}_3\text{C}_2\text{-MnO}_2@\text{LS}$  for water evaporation for 1h over 25 cycles. (e) Evaporation efficiency and rate at different thickness; (f) Thermal conductivity of  $\text{Ti}_3\text{C}_2\text{-MnO}_2@\text{LS}$  at dry and wet state.

The heat confinement performance was further investigated by measuring the cross-sectional temperature distribution of the beaker with and without  $\text{Ti}_3\text{C}_2\text{-MnO}_2@\text{LS}$  floating on the air-water interface under 1 sun irradiation via the IR camera. As shown in **Fig. 5a**, after 30 mins illumination, the beaker with water only presents a homogeneously increased temperature distribution. In contrast, from the cross-sectional IR image of the system with  $\text{Ti}_3\text{C}_2\text{-MnO}_2@\text{LS}$ , an obvious temperature gradient can be observed between the top layer and underlying bulk water. A temperature of as high as 63.9 °C can be achieved at the top surface, whereas the temperature of underlying bulk water was only slightly higher than room temperature (~ 27.3 °C).

### 3.3 Desalination and salt rejecting performance evaluation

To evaluate the desalination performance of the prepared  $\text{Ti}_3\text{C}_2\text{-MnO}_2@\text{LS}$ , seawater collected from Whampoa Harbor, Hong Kong and high concentration NaCl solutions including 10, 20, and 30 wt% were prepared for solar evaporation under simulated 1 sun irradiation. As shown in **Fig. 5b**, the evaporation rate drops with the increasing saline concentration owing to the fact that the vapor pressure of water decreases with the increased salinity.[63] Nonetheless, the evaporation rate of seawater keeps above 1.3 kg  $\text{m}^{-2} \text{h}^{-1}$  and even for 30 wt% NaCl solution, the evaporation rate is still larger than 1.1 kg  $\text{m}^{-2} \text{h}^{-1}$ , indicating the excellent desalination performance of  $\text{Ti}_3\text{C}_2\text{-MnO}_2@\text{LS}$ . Furthermore, the salt-resistant performance of the  $\text{Ti}_3\text{C}_2\text{-MnO}_2@\text{LS}$  has also been evaluated.

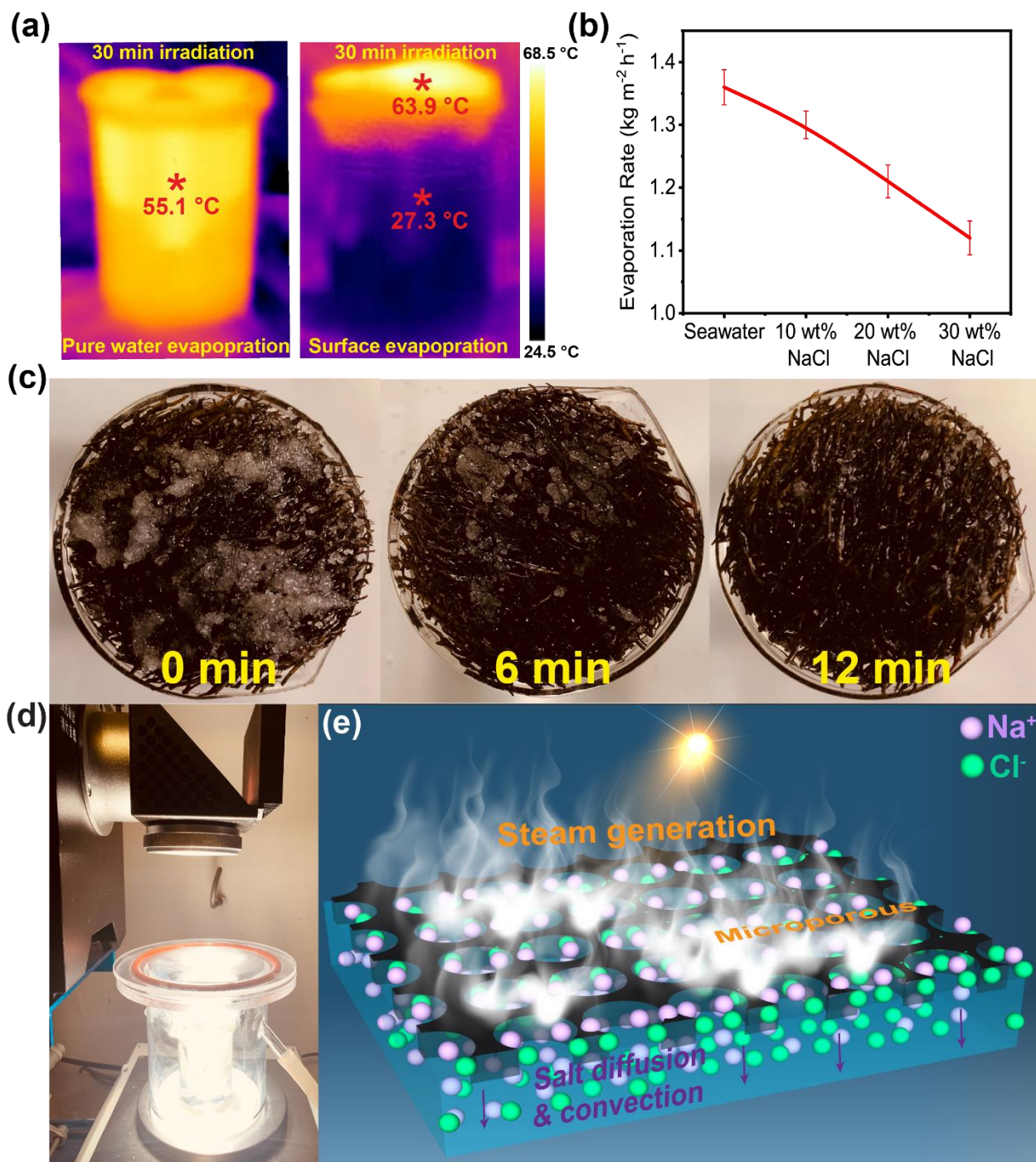


**Fig. 5** (a) IR images of the side view temperature distribution of the system with water only and  $\text{Ti}_3\text{C}_2\text{-MnO}_2\text{@LS}$  after 30 min irradiation; (b) Solar evaporation rate of  $\text{Ti}_3\text{C}_2\text{-MnO}_2\text{@LS}$  under different salinity (seawater, 10, 20, 30 wt%); (c) Progression of salt-resistance under 1 sun irradiation; (d) Image of the homemade setup for seawater desalination; (e) Schematic illustration of the possible salt rejection mechanism of the  $\text{Ti}_3\text{C}_2\text{-MnO}_2\text{@LS}$ .

As illustrated in Fig. 5c, 5 g NaCl salt crystals were directly placed on the top surface of  $\text{Ti}_3\text{C}_2\text{-MnO}_2@\text{LS}$ , irradiating the surface with 1 sun solar illumination. The solid NaCl is gradually dissolved within 12 min, confirming the remarkable salt ion diffusion backflow property of  $\text{Ti}_3\text{C}_2\text{-MnO}_2@\text{LS}$ . **Supporting movie** demonstrates the salt rejection and ion back flow of the proposed the  $\text{Ti}_3\text{C}_2\text{-MnO}_2@\text{LS}$ . The salt rejection property of the evaporator of the interfacial solar desalination is of great importance. Salt accumulation will block the water transportation channels as well as hinder solar absorption, resulting in a lower evaporation efficiency. The mechanism of salt ion diffusion backflow may be described as follows. First, luffa sponge's porous structure provides linked channels for rapid water transport and vapor escape. The hydrophilic characteristic of the luffa sponge keeps it moist, allowing for adequate water flow through capillary action and rapid steam production.

The salt particles formed on the surface of the  $\text{Ti}_3\text{C}_2\text{-MnO}_2@\text{LS}$  solar evaporator dissolve rapidly and create a high salt region at the interface between the solar evaporator and bulk water. The difference in salt concentration between the high salt region and the bulk water induces diffusion and convection, therefore reducing salt concentration in the solar evaporator and preventing salt deposition. **Fig. 5e** illustrates that due to the natural microporous structure of LS, efficient salt ion diffusion backflow mechanism can be achieved. Thus, the  $\text{Ti}_3\text{C}_2\text{-MnO}_2@\text{LS}$  can effectively prevent salt deposition during the desalination process. To demonstrate the potential applicability for seawater and wastewater purification, the solar desalination experiment was conducted on a homemade setup with natural seawater and simulated wastewater, as shown in **Fig. 5d**. The vapor will condense in the chamber and be collected for further analysis.

To evaluate the quality of purified water (i.e., desalinated water), the potential of hydrogen (pH), salinity, total dissolved solids (TDS), and conductivity of actual seawater, desalinated water, and DI water were measured. As shown in **Fig. 6a**, the pH of three water samples is kept neutral, while the salinity of desalinated water is very close to zero. **Fig. 6b** shows that the TDS and conductivity of desalinated water are both reduced by more than 2 orders of magnitude compared to the actual seawater, indicating a greatly improvement in water quality. The ion ( $\text{Na}^+$ ,  $\text{K}^+$ ,  $\text{Ca}^{2+}$ ,  $\text{Mg}^{2+}$ ) concentrations of actual seawater before and after desalination were measured by inductive-coupled plasma mass spectrometry. As presented in **Fig. 6c**, the ion concentration of desalinated water treated by  $\text{Ti}_3\text{C}_2\text{-MnO}_2@\text{LS}$  is nearly 3-4 orders of magnitude significantly reduced compared to the actual seawater, which is far below the salinity levels for drinkable water defined by the World Health Organization (WHO). Moreover, wastewater treatment experiment was further conducted to evaluate the wastewater treatment performance of  $\text{Ti}_3\text{C}_2\text{-MnO}_2@\text{LS}$ . Methylene blue (MB) solution was chosen to simulate wastewater. As shown in **Fig. 6d**, the absorbance of purified water is similar to that of DI water without the characteristic peaks of MB shown, indicating that the MB should be completely removed from the purified water. All the above results indicate that the  $\text{Ti}_3\text{C}_2\text{-MnO}_2@\text{LS}$  has great prospects to be applied in practical solar water treatment to address the issues of freshwater shortage.

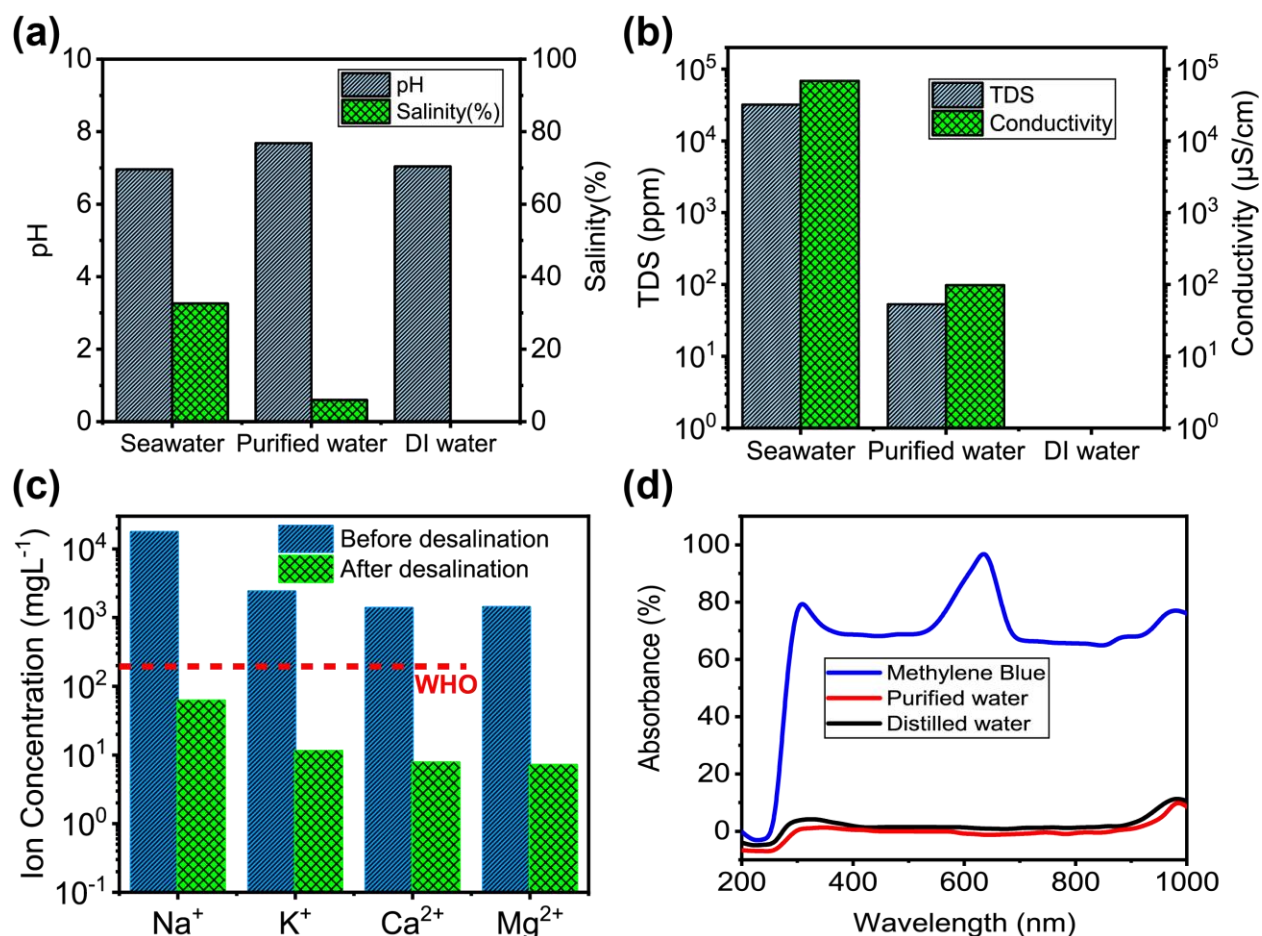


**Fig. 6** (a) pH and salinity of seawater, desalted water, and DI water; (b) TDS and conductivity of seawater, desalted water, and DI water; (c) Concentration of four main salt ions of actual seawater before and after desalination. (d) The UV-Vis spectra of methylene blue before and after solar thermal purification with  $\text{Ti}_3\text{C}_2\text{-MnO}_2@\text{LS}$  under one sun irradiation.

#### 4. Conclusion

In summary, highly effective  $\text{Ti}_3\text{C}_2\text{-MnO}_2$  nanocomposite coated LS has been developed for interfacial solar steam generation. The  $\text{Ti}_3\text{C}_2\text{-MnO}_2@\text{LS}$  was synthesized by a facial dip-drying method to improve the solar absorption and hydrophilicity of pristine biodegradable LS. The as-prepared evaporator achieves a superb water evaporation rate of  $1.36 \text{ kg m}^{-2} \text{ h}^{-1}$  and photothermal conversion efficiency of 85.28% under one sun irradiation. Excellent desalination performance has also been achieved, in which an

evaporation rate of above  $1.1 \text{ kg m}^{-2} \text{ h}^{-1}$  can be realized even under 30 wt% saline evaporation. The outstanding performance could be attributed to the excellent photothermal conversion efficiency of  $\text{Ti}_3\text{C}_2$  composited with  $\text{MnO}_2$  and the natural microporous structure and low thermal conductivity of LS. The porous structure of the luffa sponge provides salt ion diffusion backflow mechanism to reject the salt deposition on the surface of the evaporator. Moreover, the  $\text{Ti}_3\text{C}_2\text{-MnO}_2\text{@LS}$  is also feasible for efficient wastewater purification. The long-term durability, outstanding evaporation rate, low cost, and excellent salt rejection make it possible for widespread practical solar water evaporation to meet the freshwater demand.

## **Acknowledgments**

This work is financially supported by the Innovation and Technology Fund, Hong Kong, China (GHP/040/19SZ), the Hong Kong Polytechnic University (Project number: 1-ZE14), Photonic Research Institute, The Hong Kong Polytechnic University (Project number: 1-CD6V), the Hong Kong Polytechnic University Shenzhen Research Institute, Shenzhen, China (Grant Code: the science and technology innovation commission of Shenzhen (JCYJ20210324141206017)), Zhejiang Provincial Natural Science Foundation of China (Grant No. LQ21E020009), Ningbo Natural Science Foundation (Grant No. 2021J172), NSF (Award # 1856112) and California DWR (No. RS-2014-08).

## **Conflicts of interest**

There is no conflict to declare.

## Reference

- [1] H. Cheng, Y. Hu, J. Zhao, Meeting China's Water Shortage Crisis: Current Practices and Challenges, *Environ Sci Technol.* 43 (2009) 240–244. <https://doi.org/10.1021/es801934a>.
- [2] J. Gong, C. Li, M.R. Wasielewski, Advances in solar energy conversion, *Chem Soc Rev.* 48 (2019) 1862–1864. <https://doi.org/10.1039/C9CS90020A>.
- [3] K. Yu, P. Shao, P. Meng, T. Chen, J. Lei, X. Yu, R. He, F. Yang, W. Zhu, T. Duan, Superhydrophilic and highly elastic monolithic sponge for efficient solar-driven radioactive wastewater treatment under one sun, *J Hazard Mater.* 392 (2020) 122350. <https://doi.org/10.1016/j.jhazmat.2020.122350>.
- [4] A. Lenert, E.N. Wang, Optimization of nanofluid volumetric receivers for solar thermal energy conversion, *Solar Energy.* 86 (2012) 253–265. <https://doi.org/10.1016/j.solener.2011.09.029>.
- [5] G. Ahmadi, D. Toghraie, A. Azimian, O.A. Akbari, Evaluation of synchronous execution of full repowering and solar assisting in a 200 MW steam power plant, a case study, *Appl Therm Eng.* 112 (2017) 111–123. <https://doi.org/10.1016/j.applthermaleng.2016.10.083>.
- [6] A.M. Saleque, S. Ahmed, Md.N.A.S. Ivan, M.I. Hossain, W. Qarony, P.K. Cheng, J. Qiao, Z.L. Guo, L. Zeng, Y.H. Tsang, High-temperature solar steam generation by MWCNT-HfTe<sub>2</sub> van der Waals heterostructure for low-cost sterilization, *Nano Energy.* 94 (2022) 106916. <https://doi.org/10.1016/j.nanoen.2022.106916>.
- [7] A.M. Saleque, N. Nowshin, Md.N.A.S. Ivan, S. Ahmed, Y.H. Tsang, Natural Porous Materials for Interfacial Solar Steam Generation toward Clean Water Production, *Solar RRL.* (2022) 2100986. <https://doi.org/10.1002/solr.202100986>.
- [8] Z. Wang, T. Horseman, A.P. Straub, N.Y. Yip, D. Li, M. Elimelech, S. Lin, Pathways and challenges for efficient solar-thermal desalination, *Sci Adv.* 5 (2019). <https://doi.org/10.1126/sciadv.aax0763>.
- [9] A.K. Menon, I. Haechler, S. Kaur, S. Lubner, R.S. Prasher, Enhanced solar evaporation using a photo-thermal umbrella for wastewater management, *Nat Sustain.* 3 (2020) 144–151. <https://doi.org/10.1038/s41893-019-0445-5>.
- [10] P. Tao, G. Ni, C. Song, W. Shang, J. Wu, J. Zhu, G. Chen, T. Deng, Solar-driven



- interfacial evaporation, *Nat Energy*. 3 (2018) 1031–1041. <https://doi.org/10.1038/s41560-018-0260-7>.
- [11] P. Cao, L. Zhao, Z. Yang, P. Yuan, Y. Zhang, Q. Li, Carbon Nanotube Network-Based Solar-Thermal Water Evaporator and Thermoelectric Module for Electricity Generation, *ACS Appl Nano Mater.* 4 (2021) 8906–8912. <https://doi.org/10.1021/acsanm.1c01551>.
- [12] T. Yang, H. Lin, K.-T. Lin, B. Jia, Carbon-based absorbers for solar evaporation: Steam generation and beyond, *Sustainable Materials and Technologies*. 25 (2020) e00182. <https://doi.org/10.1016/j.susmat.2020.e00182>.
- [13] Z. Wang, Y. Liu, P. Tao, Q. Shen, N. Yi, F. Zhang, Q. Liu, C. Song, D. Zhang, W. Shang, T. Deng, Bio-Inspired Evaporation Through Plasmonic Film of Nanoparticles at the Air-Water Interface, *Small*. 10 (2014) 3234–3239. <https://doi.org/10.1002/smll.201401071>.
- [14] H. Wang, R. Zhang, D. Yuan, S. Xu, L. Wang, Gas Foaming Guided Fabrication of 3D Porous Plasmonic Nanoplatfrom with Broadband Absorption, Tunable Shape, Excellent Stability, and High Photothermal Efficiency for Solar Water Purification, *Adv Funct Mater.* 30 (2020) 2003995. <https://doi.org/10.1002/adfm.202003995>.
- [15] T. Wang, S. Gao, G. Wang, H. Wang, J. Bai, S. Ma, B. Wang, Three-dimensional hierarchical oxygen vacancy-rich WO<sub>3</sub>-decorated Ni foam evaporator for high-efficiency solar-driven interfacial steam generation, *J Colloid Interface Sci.* 602 (2021) 767–777. <https://doi.org/10.1016/j.jcis.2021.06.065>.
- [16] W. Huang, P. Su, Y. Cao, C. Li, D. Chen, X. Tian, Y. Su, B. Qiao, J. Tu, X. Wang, Three-dimensional hierarchical Cu<sub>x</sub>S-based evaporator for high-efficiency multifunctional solar distillation, *Nano Energy*. 69 (2020) 104465. <https://doi.org/10.1016/j.nanoen.2020.104465>.
- [17] Z. Li, X. Ma, D. Chen, X. Wan, X. Wang, Z. Fang, X. Peng, Polyaniline-Coated MOFs Nanorod Arrays for Efficient Evaporation-Driven Electricity Generation and Solar Steam Desalination, *Advanced Science*. 8 (2021) 2004552. <https://doi.org/10.1002/advs.202004552>.
- [18] X. Wang, Q. Liu, S. Wu, B. Xu, H. Xu, Multilayer Polypyrrole Nanosheets with Self-Organized Surface Structures for Flexible and Efficient Solar–Thermal Energy

- Conversion, *Advanced Materials*. 31 (2019) 1807716. <https://doi.org/10.1002/adma.201807716>.
- [19] G. Xue, K. Liu, Q. Chen, P. Yang, J. Li, T. Ding, J. Duan, B. Qi, J. Zhou, Robust and Low-Cost Flame-Treated Wood for High-Performance Solar Steam Generation, *ACS Appl Mater Interfaces*. 9 (2017) 15052–15057. <https://doi.org/10.1021/acsami.7b01992>.
- [20] C. Jia, Y. Li, Z. Yang, G. Chen, Y. Yao, F. Jiang, Y. Kuang, G. Pastel, H. Xie, B. Yang, S. Das, L. Hu, Rich Mesostructures Derived from Natural Woods for Solar Steam Generation, *Joule*. 1 (2017) 588–599. <https://doi.org/10.1016/j.joule.2017.09.011>.
- [21] M.M. Ghafurian, H. Niazmand, E. Ebrahimnia-Bajestan, R.A. Taylor, Wood surface treatment techniques for enhanced solar steam generation, *Renew Energy*. 146 (2020) 2308–2315. <https://doi.org/10.1016/j.renene.2019.08.036>.
- [22] L. Huang, L. Ling, J. Su, Y. Song, Z. Wang, B.Z. Tang, P. Westerhoff, R. Ye, Laser-Engineered Graphene on Wood Enables Efficient Antibacterial, Anti-Salt-Fouling, and Lipophilic-Matter-Rejection Solar Evaporation, *ACS Appl Mater Interfaces*. 12 (2020) 51864–51872. <https://doi.org/10.1021/acsami.0c16596>.
- [23] J. Liu, J. Yao, Y. Yuan, Q. Liu, W. Zhang, X. Zhang, J. Gu, Surface-Carbonized Bamboos with Multilevel Functional Biostructures Deliver High Photothermal Water Evaporation Performance, *Adv Sustain Syst*. 4 (2020) 1–8. <https://doi.org/10.1002/adsu.202000126>.
- [24] C. Sheng, N. Yang, Y. Yan, X. Shen, C. Jin, Z. Wang, Q. Sun, Bamboo decorated with plasmonic nanoparticles for efficient solar steam generation, *Appl Therm Eng*. 167 (2020) 114712. <https://doi.org/10.1016/j.applthermaleng.2019.114712>.
- [25] Y. Bian, Q. Du, K. Tang, Y. Shen, L. Hao, D. Zhou, X. Wang, Z. Xu, H. Zhang, L. Zhao, S. Zhu, J. Ye, H. Lu, Y. Yang, R. Zhang, Y. Zheng, S. Gu, Carbonized Bamboos as Excellent 3D Solar Vapor-Generation Devices, *Adv Mater Technol*. 4 (2019) 1800593. <https://doi.org/10.1002/admt.201800593>.
- [26] Z. Li, C. Wang, T. Lei, H. Ma, J. Su, S. Ling, W. Wang, Arched Bamboo Charcoal as Interfacial Solar Steam Generation Integrative Device with Enhanced Water Purification Capacity, *Adv Sustain Syst*. 3 (2019) 1800144.

- <https://doi.org/10.1002/adsu.201800144>.
- [27] B. Gong, H. Yang, S. Wu, Y. Tian, X. Guo, C. Xu, W. Kuang, J. Yan, K. Cen, Z. Bo, K. (Ken) Ostrikov, Multifunctional solar bamboo straw: Multiscale 3D membrane for self-sustained solar-thermal water desalination and purification and thermoelectric waste heat recovery and storage, *Carbon* N Y. 171 (2021) 359–367. <https://doi.org/10.1016/j.carbon.2020.09.033>.
- [28] Md.N.A.S. Ivan, A.M. Saleque, S. Ahmed, Z.L. Guo, D. Zu, L. Xu, T.I. Alam, S.U. Hani, Y.H. Tsang, Jute stick derived self-regenerating sustainable solar evaporators with different salt mitigation mechanisms for highly efficient solar desalination, *J Mater Chem A Mater.* (2023). <https://doi.org/10.1039/D2TA08237C>.
- [29] A.M. Saleque, Md.N.A.S. Ivan, S. Ahmed, Y.H. Tsang, Light-trapping texture bio-hydrogel with anti-biofouling and antibacterial properties for efficient solar desalination, *Chemical Engineering Journal.* 458 (2023) 141430. <https://doi.org/10.1016/j.cej.2023.141430>.
- [30] Y. Liao, J. Chen, D. Zhang, X. Wang, B. Yuan, P. Deng, F. Li, H. Zhang, Lotus leaf as solar water evaporation devices, *Mater Lett.* 240 (2019) 92–95. <https://doi.org/10.1016/j.matlet.2018.12.133>.
- [31] N. Xu, X. Hu, W. Xu, X. Li, L. Zhou, S. Zhu, J. Zhu, Mushrooms as Efficient Solar Steam-Generation Devices, *Advanced Materials.* 29 (2017) 1–5. <https://doi.org/10.1002/adma.201606762>.
- [32] P. Sun, W. Zhang, I. Zada, Y. Zhang, J. Gu, Q. Liu, H. Su, D. Pantelić, B. Jelenković, D. Zhang, 3D-Structured Carbonized Sunflower Heads for Improved Energy Efficiency in Solar Steam Generation, *ACS Appl Mater Interfaces.* 12 (2020) 2171–2179. <https://doi.org/10.1021/acsami.9b11738>.
- [33] C. Wang, J. Wang, Z. Li, K. Xu, T. Lei, W. Wang, Superhydrophilic porous carbon foam as a self-desalting monolithic solar steam generation device with high energy efficiency, *J Mater Chem A Mater.* 8 (2020) 9528–9535. <https://doi.org/10.1039/D0TA01439G>.
- [34] T.T. Pham, T.H. Nguyen, T.A.H. Nguyen, D.D. Pham, D.C. Nguyen, D.B. Do, H.V. Nguyen, M.H. Ha, Z.H. Nguyen, Durable, scalable and affordable iron (III) based coconut husk photothermal material for highly efficient solar steam generation,

- Desalination. 518 (2021) 115280. <https://doi.org/10.1016/j.desal.2021.115280>.
- [35] Y. Sun, Z. Zhao, G. Zhao, L. Wang, D. Jia, Y. Yang, X. Liu, X. Wang, J. Qiu, High performance carbonized corncob-based 3D solar vapor steam generator enhanced by environmental energy, *Carbon N Y.* 179 (2021) 337–347. <https://doi.org/10.1016/j.carbon.2021.04.037>.
- [36] M. Zhu, J. Yu, C. Ma, C. Zhang, D. Wu, H. Zhu, Carbonized daikon for high efficient solar steam generation, *Solar Energy Materials and Solar Cells.* 191 (2019) 83–90. <https://doi.org/10.1016/j.solmat.2018.11.015>.
- [37] Y. Long, S. Huang, H. Yi, J. Chen, J. Wu, Q. Liao, H. Liang, H. Cui, S. Ruan, Y.-J. Zeng, Carrot-inspired solar thermal evaporator, *J Mater Chem A Mater.* 7 (2019) 26911–26916. <https://doi.org/10.1039/C9TA08754K>.
- [38] Y. Kong, Y. Gao, B. Gao, Y. Qi, W. Yin, S. Wang, F. Yin, Z. Dai, Q. Yue, Tubular polypyrrole enhanced elastomeric biomass foam as a portable interfacial evaporator for efficient self-desalination, *Chemical Engineering Journal.* 445 (2022) 136701. <https://doi.org/10.1016/j.cej.2022.136701>.
- [39] C. Liu, K. Hong, X. Sun, A. Natan, P. Luan, Y. Yang, H. Zhu, An “antifouling” porous loofah sponge with internal microchannels as solar absorbers and water pumps for thermal desalination, *J Mater Chem A Mater.* 8 (2020) 12323–12333. <https://doi.org/10.1039/d0ta03872e>.
- [40] A.M. Saleque, S. Ma, S. Ahmed, M.I. Hossain, W. Qarony, Y.H. Tsang, Solar Driven Interfacial Steam Generation Derived from Biodegradable Luffa Sponge, *Adv Sustain Syst.* 5 (2021) 2000291. <https://doi.org/10.1002/adsu.202000291>.
- [41] J. Zheng, X. Pan, X. Huang, D. Xiong, Y. Shang, X. Li, N. Wang, W.-M. Lau, H.Y. Yang, Integrated NiCo<sub>2</sub>-LDHs@MXene/rGO aerogel: Componential and structural engineering towards enhanced performance stability of hybrid supercapacitor, *Chemical Engineering Journal.* 396 (2020) 125197. <https://doi.org/10.1016/j.cej.2020.125197>.
- [42] Y. Li, F. Meng, Y. Mei, H. Wang, Y. Guo, Y. Wang, F. Peng, F. Huang, Z. Zhou, Electrospun generation of Ti<sub>3</sub>C<sub>2</sub>T<sub>x</sub> MXene@graphene oxide hybrid aerogel microspheres for tunable high-performance microwave absorption, *Chemical Engineering Journal.* 391 (2020) 123512.

- <https://doi.org/10.1016/j.cej.2019.123512>.
- [43] G. Liu, Q. Xiong, Y. Xu, Q. Fang, K.C.-F. Leung, M. Sang, S. Xuan, L. Hao, Sandwich-structured MXene@Au/polydopamine nanosheets with excellent photothermal-enhancing catalytic activity, *Colloids Surf A Physicochem Eng Asp.* 633 (2022) 127860. <https://doi.org/10.1016/j.colsurfa.2021.127860>.
- [44] Q. Lin, Y. Liu, G. Zeng, X. Li, B. Wang, X. Cheng, A. Sengupta, X. Yang, Z. Feng, Bionics inspired modified two-dimensional MXene composite membrane for high-throughput dye separation, *J Environ Chem Eng.* 9 (2021) 105711. <https://doi.org/10.1016/j.jece.2021.105711>.
- [45] R. Li, L. Zhang, L. Shi, P. Wang, MXene Ti<sub>3</sub>C<sub>2</sub>: An Effective 2D Light-to-Heat Conversion Material, *ACS Nano.* 11 (2017) 3752–3759. <https://doi.org/10.1021/acsnano.6b08415>.
- [46] X. Zhao, X.-J. Zha, L.-S. Tang, J.-H. Pu, K. Ke, R.-Y. Bao, Z. Liu, M.-B. Yang, W. Yang, Self-assembled core-shell polydopamine@MXene with synergistic solar absorption capability for highly efficient solar-to-vapor generation, *Nano Res.* 13 (2020) 255–264. <https://doi.org/10.1007/s12274-019-2608-0>.
- [47] Y. Dall’Agnese, P. Rozier, P.-L. Taberna, Y. Gogotsi, P. Simon, Capacitance of two-dimensional titanium carbide (MXene) and MXene/carbon nanotube composites in organic electrolytes, *J Power Sources.* 306 (2016) 510–515. <https://doi.org/10.1016/j.jpowsour.2015.12.036>.
- [48] J. Zhu, Y. Tang, C. Yang, F. Wang, M. Cao, Composites of TiO<sub>2</sub> Nanoparticles Deposited on Ti<sub>3</sub>C<sub>2</sub> MXene Nanosheets with Enhanced Electrochemical Performance, *J Electrochem Soc.* 163 (2016) A785–A791. <https://doi.org/10.1149/2.0981605jes>.
- [49] M. Pi, X. Wang, Z. Wang, R. Ran, Sustainable MXene/PDA hydrogel with core-shell structure tailored for highly efficient solar evaporation and long-term desalination, *Polymer (Guildf).* 230 (2021) 124075. <https://doi.org/10.1016/j.polymer.2021.124075>.
- [50] D. Wen, G. Ying, L. Liu, C. Sun, Y. Li, Y. Zhao, Z. Ji, Y. Wu, J. Zhang, J. Zhang, X. Wang, Flexible and High-Performance MXene/MnO<sub>2</sub> Film Electrodes Fabricated by Inkjet Printing: Toward a New Generation Supercapacitive Application, *Adv*

- Mater Interfaces. 8 (2021) 2101453. <https://doi.org/10.1002/admi.202101453>.
- [51] Z. Zhang, P. Mu, J. Han, J. He, Z. Zhu, H. Sun, W. Liang, A. Li, Superwetting and mechanically robust MnO<sub>2</sub> nanowire–reduced graphene oxide monolithic aerogels for efficient solar vapor generation, *J Mater Chem A Mater.* 7 (2019) 18092–18099. <https://doi.org/10.1039/C9TA04509K>.
- [52] D. Li, D. Han, C. Guo, C. Huang, Facile Preparation of MnO<sub>2</sub>-Deposited Wood for High-Efficiency Solar Steam Generation, *ACS Appl Energy Mater.* 4 (2021) 1752–1762. <https://doi.org/10.1021/acsaem.0c02902>.
- [53] M.S. Irshad, X. Wang, M.S. Abbasi, N. Arshad, Z. Chen, Z. Guo, L. Yu, J. Qian, J. You, T. Mei, Semiconductive, Flexible MnO<sub>2</sub> NWs/Chitosan Hydrogels for Efficient Solar Steam Generation, *ACS Sustain Chem Eng.* 9 (2021) 3887–3900. <https://doi.org/10.1021/acssuschemeng.0c08981>.
- [54] G. Ni, S.H. Zandavi, S.M. Javid, S. V. Boriskina, T.A. Cooper, G. Chen, A salt-rejecting floating solar still for low-cost desalination, *Energy Environ Sci.* 11 (2018) 1510–1519. <https://doi.org/10.1039/C8EE00220G>.
- [55] Y. Liu, J. Chen, D. Guo, M. Cao, L. Jiang, Floatable, Self-Cleaning, and Carbon-Black-Based Superhydrophobic Gauze for the Solar Evaporation Enhancement at the Air–Water Interface, *ACS Appl Mater Interfaces.* 7 (2015) 13645–13652. <https://doi.org/10.1021/acsaami.5b03435>.
- [56] X. Wang, Y. He, X. Liu, Synchronous steam generation and photodegradation for clean water generation based on localized solar energy harvesting, *Energy Convers Manag.* 173 (2018) 158–166. <https://doi.org/10.1016/j.enconman.2018.07.065>.
- [57] Y. Kuang, C. Chen, S. He, E.M. Hitz, Y. Wang, W. Gan, R. Mi, L. Hu, A High-Performance Self-Regenerating Solar Evaporator for Continuous Water Desalination, *Advanced Materials.* 31 (2019) 1900498. <https://doi.org/10.1002/adma.201900498>.
- [58] F. Wang, D. Wei, Y. Li, T. Chen, P. Mu, H. Sun, Z. Zhu, W. Liang, A. Li, Chitosan/reduced graphene oxide-modified spacer fabric as a salt-resistant solar absorber for efficient solar steam generation, *J Mater Chem A Mater.* 7 (2019) 18311–18317. <https://doi.org/10.1039/C9TA05859A>.

- [59] H. Xie, H. Gu, M. Fujii, X. Zhang, Short hot wire technique for measuring thermal conductivity and thermal diffusivity of various materials, *Meas Sci Technol.* 17 (2006) 208–214. <https://doi.org/10.1088/0957-0233/17/1/032>.
- [60] Y. Wu, Y. Liu, W. Wang, J. Wang, C. Zhang, Z. Wu, P. Yan, K. Li, Microwave absorption enhancement and loss mechanism of lamellar MnO<sub>2</sub> nanosheets decorated reduced graphene oxide hybrid, *Journal of Materials Science: Materials in Electronics.* 30 (2019) 842–854. <https://doi.org/10.1007/s10854-018-0354-9>.
- [61] M. Boota, B. Anasori, C. Voigt, M.-Q. Zhao, M.W. Barsoum, Y. Gogotsi, Pseudocapacitive Electrodes Produced by Oxidant-Free Polymerization of Pyrrole between the Layers of 2D Titanium Carbide (MXene), *Advanced Materials.* 28 (2016) 1517–1522. <https://doi.org/10.1002/adma.201504705>.
- [62] R. Zhao, H. Di, X. Hui, D. Zhao, R. Wang, C. Wang, L. Yin, Self-assembled Ti<sub>3</sub>C<sub>2</sub> MXene and N-rich porous carbon hybrids as superior anodes for high-performance potassium-ion batteries, *Energy Environ Sci.* 13 (2020) 246–257. <https://doi.org/10.1039/C9EE03250A>.
- [63] L. Li, N. He, B. Jiang, K. Yu, Q. Zhang, H. Zhang, D. Tang, Y. Song, Highly Salt-Resistant 3D Hydrogel Evaporator for Continuous Solar Desalination via Localized Crystallization, *Adv Funct Mater.* 2104380 (2021) 2104380. <https://doi.org/10.1002/adfm.202104380>.

### **Authors' Response to Reviewer**

We thank the reviewers for the valuable comments. We believe that the provided feedback helped to enhance the quality of the manuscript (**Manuscript ID: DES-D-22-01838**) and make it well-suited now for the Desalination.

The manuscript has been modified by addressing the comments made by the reviewers.

### **Response to Comments and Questions**

#### **Comments from the reviewers:**

##### **Reviewer 1:**

**Comment 1:** This study applied a new 2D material for efficient solar steam generation. The material synthesis/preparation is confirmed by various characterisation (SEM, EDS, XRD, Raman, and XPS). The prepared nanocomposite demonstrated an excellent desalination performance. This study fits the scopes of the journal. However, there are some major issues which are as follows.

**Response 1:** We thank the reviewer for the positive comment. In the following, we have tried to address all the concerns from the reviewer.

**Question 1:** The procedure of measuring the thermal conductivity should be explained in more detail in the material and methods.

**Answer 1:** We thank the reviewer for the question. The thermal conductivity was measured using transient hot-wire method using a computer-controlled equipment (Thermtest Instruments, model no. THW L2). The hot-wire method is a transient dynamic technique based on the measurement of the temperature rise in a defined distance from a linear heat source embedded in the test material. The thermal conductivity can be derived directly from the resulting change in the temperature over a known time interval.

The procedure of measuring the thermal conductivity is now added in the revised manuscript and highlighted in yellow color.

*“Transients hot-wire approach with computer-controlled equipment was used to measure thermal conductivity (Thermtest Instruments, THW L2). Using a linear heat source implanted in the material being tested, the hot-wire method is a transient dynamic approach that measures the temperature increase in a predetermined distance. The rate of temperature rises or fall over a certain time period is a direct measure of thermal conductivity [57].”*



**Question 2:** Raman spectroscopy and water contact angle measurement should be mentioned in the material and methods (Section 2.2)

**Answer 2:** Thank you very much for your suggestions. The Raman spectroscopy and water contact angle measurement are now mentioned in section 2.2 in the revised manuscript. The corresponding lines are highlighted in yellow color.

*“The Raman spectroscopy was conducted using WITEC Confocal Raman system with 532 nm laser. The hydrophilicity of the surface was decided through the water contact angle measurement (WCA, KINO SL 200 KB).”*

**Question 3:** What is  $\text{TiTe}_2$  QD-decorated rGO-coated facemask that is mentioned in the section 2.2 and 2.4?

**Answer 3:** Thank you very much for pointing out the mistake. We sincerely apologize for our typing mistake. “ $\text{TiTe}_2$  QD-decorated rGO-coated facemask” is not a part of this manuscript. However, in the revised manuscript the corresponding lines are corrected and highlighted in yellow color.

*“The microstructures of the  $\text{Ti}_3\text{C}_2\text{-MnO}_2\text{@LS}$  were investigated using a scanning electron microscope (SEM, TESCAN, VEGA3, 20 kV).”*

*“The  $\text{Ti}_3\text{C}_2\text{-MnO}_2\text{@LS}$  structure was wrapped by an Expanded Polyethylene (EPE) foam in order to make it float and reduce the heat loss.”*

**Question 4:** The standard deviations of presented data (e.g., contact angle and thermal conductivity) need to be reported.

**Answer 4:** Thank you very much for helping us to improve the quality of the manuscript. The standard deviations for contact angle and thermal conductivity measurement have been added in the revised manuscript. The updated lines are highlighted in yellow color. Also, error bars are added for the thermal conductivity graph at Figure 4(f).

*“The results that the contact angle decreases from  $78.56^\circ$  to  $45.21^\circ$  after coating (standard deviation  $\pm 0.05^\circ$ ), indicates that the coating can improve the hydrophilicity, which can contribute to a fast and efficient water supply from the bottom bulk water to the evaporating surface.”*

*“Fig. 4f shows that the thermal conductivity of the LS is extremely low, which is  $0.18 \text{ W m}^{-1} \text{ K}^{-1}$  in dry state and  $0.35 \text{ W m}^{-1} \text{ K}^{-1}$  in wet state with a standard deviation of  $\pm 0.007 \text{ W m}^{-1} \text{ K}^{-1}$ , indicating the good heat confinement effect of LS.”*

**Question 5:** The details of the solar system and the setup are missing. Section 2.4 should be in more detail.

**Answer 5:** Thank you for the suggestions. The details of the solar evaporation experiment and setup are provided in the revised manuscript. The changes are highlighted in yellow color.

*“The  $Ti_3C_2-MnO_2@LS$  structure was wrapped by an Expanded Polyethylene (EPE) foam in order to make it float and reduce the heat loss. Then, it was placed in a beaker containing seawater to conduct the solar evaporation experiments. A separate experiment was conducted without EPE foam to understand the improvement in solar evaporation rate and efficiency. At first, the thickness of the LS was varied from 6 mm to 18 mm and the corresponding evaporation efficiency were measured under 1 sun illumination. The maximum evaporation efficiency of 85.28% has been achieved at 14 mm thickness of LS. Therefore, rest of the experiments were conducted using 14 mm thickness. The solar irradiance was varied from 1 to 5 kW/m<sup>2</sup> and the corresponding mass losses were recorded. To measure the mass loss due to the solar irradiance, the  $Ti_3C_2-MnO_2@LS$  was put on top of a beaker holding 150 ml of seawater. The beaker was then placed within a custom-made glass structure, as shown in **Figure S1, supporting information**. The evaporated steam is collected through an output channel on the structure's upper side. The outflow channel is linked to a pipe, with the other end connected to a container to collect the condensed water droplet. The majority of the evaporated steam flows via the output route at the top of the pipe to the water droplet collecting container. The steam gradually releases heat and condenses into water droplets as it travels along this path. However, some steam condenses inside the custom-made structure and condenses into a water droplet, which is deposited at the bottom. As a consequence, at the end of the experiment, the water deposited at the bottom of the custom-made structure was also collected. The evaporation rate and efficiency were calculated from the measured evaporated mass loss under various solar irradiance.”*

**Question 6:** In the section 2.4., EPE should be defined/ spelled out.

**Answer 6:** We thank the reviewer for the suggestion. The full form of EPE foam (Expanded Polyethylene) is added in the revised manuscript.

*“The  $Ti_3C_2-MnO_2@LS$  structure was wrapped by an Expanded Polyethylene (EPE) foam in order to make it float and reduce the heat loss.”*

**Reviewer 2:**

**Comment 1:** This study investigated the performance of a MXene/MnO<sub>2</sub> coated luffa sponge for solar water evaporation application. The results indicated good evaporation rate and salt rejection. The manuscript is generally written fine, however, the novelty of the study is not clear, and critical and depth analysis in the discussion is very much lacking. Besides, the experimental design needs to be further improved. There is only one coated sample tested and compared with pristine luffa. I did not see any optimisation tests, and the evaporation performance is very much average, thus, begging the question of how the new design is more attractive compared to cheaper and simpler materials that many others in literature have already tested. It can be argued that carbonization of the top part or using cheap black paints or materials can be used directly on the luffa, without the need for expensive nanomaterials. The following are my further comments to help improve this manuscript:

**Response 1:** We thank the reviewer for valuable comments. We attempted to address all of the reviewer's concerns in the following section.

**Question 1:** -Highlights: Make sure that what you claim here. There are already a number of studies using luffa for SWE. Besides, avoid using the term "1st demonstration.."

**Answer 1:** Thank you very much for correcting us. The highlights are updated as per suggestion. Many studies have employed luffa sponge for SWE. However, the use of MXene/MnO<sub>2</sub> nanomaterials coating on top of the luffa sponge has not been explored yet. Our unique and previously unreported application of MXene/MnO<sub>2</sub> coated luffa sponge for SWE has been proposed in this manuscript.

**Question 2:** -Improve the graphical abstract. From the current one, it is hard to get the message here as it is generally presented and there are no details about what materials are those and their unique designs.

**Answer 2:** Thank you very much for your valuable suggestion. We have updated the graphical abstract. We hope that the new graphical abstract will convey the message to broad readers.

**Question 3:** -Always make a habit to put page numbers. It is very difficult to make detailed review if there are no page numbers.

**Answer 3:** Thank you very much for correcting us. Page numbers are added in the revised manuscript and revised supporting information file.

**Question 4:** -It is not clear as to what is the novelty of this current work. What is the advantage of having 2D material coating on a biodegradable luffa considering the cost and performance?

**Answer 4:** Thank you very much for your question. Many researchers demonstrated the use of biodegradable materials for solar steam generation using various 2D materials and expensive plasmonic nanoparticles coating. However, the demonstrated MXene/MnO<sub>2</sub> coated luffa sponge has significantly higher evaporation efficiency compared to other relevant works. For instance, L. Hu et al. demonstrated the use of Pd and Au nanoparticles deposited on biodegradable wood which resulted in an evaporation efficiency of 68% under 1 sun[1], whereas the proposed MXene/MnO<sub>2</sub> coated luffa sponge provides an evaporation efficiency of 85.25%. When compared to MXene/MnO<sub>2</sub>, the cost of Au nanoparticles is much higher. Similarly, another research group used graphite spray on wood for enhancing the performance of interfacial steam generation system and the reported evaporation efficiency under 1 sun is 80%[2]. Graphene oxide is also used on wood for desalination application with an evaporation efficiency of 83%[3], which is also less than our reported efficiency and involved complex preparation process. Researchers also used candle soot on luffa sponge and obtained a comparatively lower efficiency of 79.98%[4]. Bamboo was also used as a biodegradable material with Ag@TiO<sub>2</sub> nanoparticle coating for solar steam generation and 84% of evaporation efficiency had been achieved[5] which is lower than the evaporation efficiency of MXene/MnO<sub>2</sub> coated luffa sponge reported in this work. Therefore, the reported MXene/MnO<sub>2</sub> coated luffa sponge has performance in terms of evaporation efficiency and facile fabrication process. Moreover, the use of MnO<sub>2</sub> interlayer barrier ease the restacking problem of MXene which is another novelty of this work. Among the family of MXene materials, particularly Ti<sub>3</sub>C<sub>2</sub> exhibited excellent photo-thermal conversion behavior with a conversion efficiency ('light' to 'heat') of 100%, which can completely absorb and dissipate the electromagnetic radiation as heat. With the aforementioned absorption behavior of MXene, it is potentially very beneficial for solar steam generation and evaporation. To highlight the superior performance of the proposed MXene/MnO<sub>2</sub> coated luffa sponge, a performance comparison table is provided in the revised supporting information file (Table S1). Also, the following lines are added in the revised manuscript and highlighted in yellow color.

*"The evaporation efficiency and rate attained are comparatively higher than several biodegradable solar evaporators shown in the literature (table S2, supporting information)."*

The MXene production is still limited to laboratory scale, and it requires state of the art facilities for its synthesis. Therefore, the cost of MXene could limit its wide-spread application. However, this could be overcome through community-level procurement of MXene-loaded paint from local research institutes or through collaboration with local councils. Moreover, with increasing demand and application of this material, its price will be drastically reduced similar to graphene-based materials and with the exceptional thermal and physical properties of MXene, the proposed unit could be a game changer in the field of water evaporation.

**Question 5:** -2.2 and 2.4: I am very confused why you are talking about "TiTe2 QD-decorated rGO-coated facemask"? What is this?

**Answer 5:** Thank you very much for pointing to the mistake. We sincerely regret for the typing error. "TiTe<sub>2</sub> QD-decorated rGO-coated facemask" is not a part of this manuscript. However, in the revised manuscript the corresponding lines are corrected and highlighted in yellow color.

*"The microstructures of the Ti<sub>3</sub>C<sub>2</sub>-MnO<sub>2</sub>@LS were investigated using a scanning electron microscope (SEM, TESCAN, VEGA3, 20 kV)."*

*"The Ti<sub>3</sub>C<sub>2</sub>-MnO<sub>2</sub>@LS structure was wrapped by an Expanded Polyethylene (EPE) foam in order to make it float and reduce the heat loss."*

**Question 6:** -2.3: What are the concentrations of  $Ti_3C_2$  and  $MnO_2$  in the coating mixture? Make a table for the preparation and their mixture concentrations. Also, the naming convention of the different samples.

**Answer 6:** Thank you very much for helping us to improve the quality of the manuscript.  $Ti_3C_2$  and  $MnO_2$  with a concentration of  $2 \text{ mg ml}^{-1}$  and  $5 \text{ mg ml}^{-1}$ , respectively were used in the coating mixture.

As per suggestions, the different concentration of the  $Ti_3C_2$  and  $MnO_2$  used in coating were presented in a Table S1 (supporting information). The following lines are added in the revised supporting information file.

*“Different concentrations of  $Ti_3C_2$  MXene and  $MnO_2$  were utilized to formulate the coating solution for the cleaned luffa sponge. As  $Ti_3C_2$  MXene is more expensive than  $MnO_2$  powder, we adjusted the concentration so that the amount of  $Ti_3C_2$  MXene required was less than that of  $MnO_2$  powder. Both the materials were dissolved in isopropyl alcohol (IPA). The prepared solutions were ultrasonically treated for 4 hours. After that, 60 ml of  $Ti_3C_2$  and 40 ml of  $MnO_2$  solutions were mixed in a beaker, and the mixture was magnetically stirred at 600 rpm for 2 hours. As the major purpose of this solution is to improve the absorption in the AM 1.5 solar spectrum, each of the produced solutions was tested in a separate cuvette for its absorption spectrum. The following table S1 summarizes the various concentration of  $Ti_3C_2$  and  $MnO_2$  in the coating mixture and their average absorbance in the AM 1.5 solar spectrum.*

**Table S1.** Evaluating different concentration of  $Ti_3C_2$  and  $MnO_2$  for preparing photothermal absorber

Sample Name	Concentration of $Ti_3C_2$ MXene	Concentration of $MnO_2$	Average absorbance (60% MXene + 40% $MnO_2$ )
$Ti_3C_2$ - $MnO_2$ (1 – 1)	$1 \text{ mg ml}^{-1}$	$1 \text{ mg ml}^{-1}$	62.3%
$Ti_3C_2$ - $MnO_2$ (1 – 3)	$1 \text{ mg ml}^{-1}$	$3 \text{ mg ml}^{-1}$	64.8%
$Ti_3C_2$ - $MnO_2$ (1 – 5)	$1 \text{ mg ml}^{-1}$	$5 \text{ mg ml}^{-1}$	66.3%
$Ti_3C_2$ - $MnO_2$ (2 – 2)	$2 \text{ mg ml}^{-1}$	$2 \text{ mg ml}^{-1}$	63.8%
$Ti_3C_2$ - $MnO_2$ (2 – 5)	$2 \text{ mg ml}^{-1}$	$5 \text{ mg ml}^{-1}$	78.3%
$Ti_3C_2$ - $MnO_2$ (2 – 8)	$2 \text{ mg ml}^{-1}$	$7 \text{ mg ml}^{-1}$	74.2%

*From the table S1, it can be observed that the highest absorbance of 78.3% has been achieved for  $2 \text{ mg ml}^{-1}$  of  $Ti_3C_2$  MXene and  $5 \text{ mg ml}^{-1}$   $MnO_2$  combination. Therefore, sample  $Ti_3C_2$ - $MnO_2$  (2 – 5) has been chosen as the optimum concentration for dip coating of the cleaned luffa sponge.”*

**Question 7:** -What is the optimum concentration and how did you come up with it?

**Answer 7:** Thank you for your query. The optimum concentration for the  $Ti_3C_2$  and  $MnO_2$  were  $2 \text{ mg ml}^{-1}$  and  $5 \text{ mg ml}^{-1}$ , respectively.

As the major purpose of this solution is to improve the absorption in the AM 1.5 solar spectrum, each of the produced solutions was tested in a separate cuvette for its absorption spectrum. From the table S2, it can be observed that the highest absorbance of 78.3% has been achieved for  $2 \text{ mg ml}^{-1}$  of  $Ti_3C_2$  MXene and  $5 \text{ mg ml}^{-1}$   $MnO_2$  combination. Therefore, sample  $Ti_3C_2$ - $MnO_2$  (2 – 5) has been chosen as the optimum concentration for dip coating of the cleaned luffa sponge.

The following lines are added in the revised manuscript and highlighted in yellow color.

*“6 different concentrations of  $Ti_3C_2$  and  $MnO_2$  were prepared, and their corresponding average absorbance were measured. As the major objective of this solution was to improve the absorption of luffa sponge in the AM 1.5 solar spectrum, each of the produced solutions was tested in a separate cuvette for its absorption spectrum. The supporting information note S3 contains the detail description of the preparation and table S1 (supporting information) shows the various concentration of  $Ti_3C_2$  and  $MnO_2$  and their average absorbance as measured by UV-Vis-NIR spectroscopy. Based on the average absorbance,  $Ti_3C_2$ - $MnO_2$  (2 – 5) sample provided highest average absorbance (table S1, supporting information). Therefore, it was chosen as the optimum concentration for fabricating the  $Ti_3C_2$ - $MnO_2$  @LS.”*

**Question 8:** -In 2.4: Indicate the range of solar intensities you tested. Indicate how evaporation rate was calculated.

**Answer 8:** Thank you for your question. The desalination performance and mass loss of the  $Ti_3C_2$ - $MnO_2$ @LS were tested at different range of solar intensities. As depicted in Figure 4b and 4c, the mass loss, evaporation rate and efficiency were found with a varying solar intensity ranging from  $1 \text{ kW m}^{-2}$  to  $5 \text{ kW m}^{-2}$ . The following line is added in the revised manuscript and highlighted in yellow color.

*“Fig. 4b shows the water mass change of  $Ti_3C_2$ - $MnO_2$  @LS under various light densities ranging from  $1 \text{ kW m}^{-2}$  to  $5 \text{ kW m}^{-2}$ .”*

The equation for calculating the evaporation rate is now provided in equation (2) of the revised manuscript.

*“The evaporation rate,  $m_e$  can be calculated by following equation:*

$$m_{ev} = \frac{m_h}{A} \quad (2)$$

*Where,  $m_h$  is mass loss of water per hour (kg/h) due to evaporation and  $A$  is the area ( $\text{m}^2$ ) of evaporation surface.”*

**Question 9:** -Indicate the actual concentration of the coating layers in the luffa.

**Answer 9:** Thank you for your question. The actual concentration for the  $Ti_3C_2$  and  $MnO_2$  were  $2 \text{ mg ml}^{-1}$  and  $5 \text{ mg ml}^{-1}$ , respectively. The following lines are added in the revised manuscript and highlighted in yellow color.

*“As the major objective of this solution was to improve the absorption of luffa sponge in the AM 1.5 solar spectrum, each of the produced solutions was tested in a separate cuvette for its absorption spectrum. The supporting information note S3 contains the detail description of the preparation and table S1 (supporting information) shows the various concentration of  $Ti_3C_2$  and  $MnO_2$  and their average absorbance as measured by UV-Vis-NIR spectroscopy. Based on the average absorbance,  $Ti_3C_2$ - $MnO_2$  (2 – 5) sample provided highest average absorbance (table S1, supporting information). Therefore, it was chosen as the optimum concentration for fabricating the  $Ti_3C_2$ - $MnO_2$  @LS.”*

**Question 10:** -3.1: How does the coating improve the hydrophilicity? Expound this.

**Answer 10:** Thank you for the question. The pristine luffa sponge has moderate hydrophilicity property. However, the hydrophilicity can be further increased by material coating.[6] Water contact angle is the measure of the hydrophilic nature of photothermal evaporator. As shown in Figure 3d, the water contact angle of the pristine luffa sponge was as high as 78.56° but after the Ti<sub>3</sub>C<sub>2</sub>-MnO<sub>2</sub> coating, the water contact angle reduces to 45.21° which indicates that the coating improves the hydrophilicity of the luffa sponge. The Ti<sub>3</sub>C<sub>2</sub>-MnO<sub>2</sub> coating has higher affinity for water compared to pristine luffa sponge therefore, water droplet spreads across which maximize the water contact angle.

The following lines are added in the revised manuscript and highlighted in yellow color.

*“The water contact angles of the LS before and after surface coating with Ti<sub>3</sub>C<sub>2</sub>-MnO<sub>2</sub> nanocomposite were measured and shown in **Fig. 3d**. The results that the contact angle decreases from 78.56° to 45.21° after coating (standard deviation ± 0.05°), indicates that the coating can improve the hydrophilicity, which can contribute to a fast and efficient water supply from the bottom bulk water to the evaporating surface. The higher affinity for water of the Ti<sub>3</sub>C<sub>2</sub>-MnO<sub>2</sub> coating in comparison to the pristine luffa sponge causes the water droplets to disperse and the water contact angle to be maximized.”*

**Question 11:** -In equation 1, add the values used for enthalpy. Include the units in the discussion.

**Answer 11:** Thank you for the question. The value used for enthalpy and the units for other parameters are added in the revised manuscript. The updated lines are mentioned below for your convenience.

*“The solar evaporation efficiency ( $\eta_{th}$ ) of the samples can be calculated by the following equation (1).*

$$\eta_{th} = \frac{\dot{m}h_{LV}}{q_{solar}} \quad (1)$$

*Where  $\dot{m}$  is the steady-state water evaporation rate ( $\text{kg m}^{-2} \text{h}^{-1}$ ) excluding the evaporation rate under the dark field,  $h_{LV}$  is the total phase change enthalpy of water (2260 J/g) including the sensible heat and latent heat,  $q_{solar}$  is the power density of solar irradiation ( $\text{W/m}^2$ ).*

*The evaporation rate,  $m_e$  can be calculated by following equation:*

$$m_{ev} = \frac{m_h}{A} \quad (2)$$

*Where,  $m_h$  is mass loss of water per hour (kg/h) due to evaporation and  $A$  is the area ( $\text{m}^2$ ) of evaporation surface.”*

**Question 12:** -When you tested for various thicknesses of the luffa, what were the effect on evaporation rate?

**Answer 12:** Thank you for the question. Figure 4e has been updated in the revised manuscript to present the evaporate rate with the varying thickness. The following lines are added and highlighted in yellow color in the revised manuscript.

*“As shown in Fig. 4e, the evaporation efficiency increases from 50% to 85.28% as the thickness increases from 6 mm to 12 mm and reaches the highest at a thickness of 14 mm. After that, the efficiency drops as the thickness continues to increase. Similarly, the evaporation rate at 6 mm of luffa sponge thickness is just  $0.79 \text{ kg m}^{-2} \text{ h}^{-1}$ . At 14 mm thickness, the evaporation rate reaches its maximum value of  $1.36 \text{ kg m}^{-2} \text{ h}^{-1}$ . The rate of evaporation then reduces with increasing thickness, reaching  $1.15 \text{ kg m}^{-2} \text{ h}^{-1}$  at 18 mm thickness. When the thickness of LS is small, more heat loss occurs to the underlying bulk water. Whereas when the thickness increases to be too thick, water may not be sufficiently transported to the evaporation surface due to the long transfer path, leading to the lower evaporation efficiency.”*

**Question 13:** -In Fig 4c: The evaporation rate has drastically increased with the increase in solar intensity, while evap efficiency almost stay the same. Can you explain this?

**Answer 13:** Thank you for the question. The equation for calculating evaporation efficiency has a term ( $q_{\text{solar}}$ ) at the denominator which is the solar intensity per  $\text{m}^2$  area. For higher solar irradiance (2 to 5 sun), the mass loss due to evaporation increases. However, while calculating the evaporation efficiency, we need to divide this higher mass loss with the corresponding higher solar irradiance.

For example, for 1 sun irradiance, the mass loss was  $1.3585 \text{ kg/m}^2$  in 1 hour. Therefore, the equation for calculating the evaporation efficiency becomes:

$$\eta_{1 \text{ sun}} = \frac{\dot{m}h_{LV}}{q_{\text{solar}}} = \frac{\left(\frac{1.3585}{3600}\right) \left(\frac{\text{kg}}{\text{m}^2 \times \text{sec}}\right) \times 2260000 \left(\frac{\text{J}}{\text{kg}}\right)}{1000 \left(\frac{\text{Watt}}{\text{m}^2}\right)} = 85.28\%$$

Similarly, for 2 sun irradiances, the mass loss was  $2.675 \text{ kg/m}^2$  in 1 hour. Therefore, the equation for calculating the evaporation efficiency becomes:

$$\eta_{1 \text{ sun}} = \frac{\dot{m}h_{LV}}{q_{\text{solar}}} = \frac{\left(\frac{2.675}{3600}\right) \left(\frac{\text{kg}}{\text{m}^2 \times \text{sec}}\right) \times 2260000 \left(\frac{\text{J}}{\text{kg}}\right)}{2000 \left(\frac{\text{Watt}}{\text{m}^2}\right)} = 83.97\%$$

So, it is clear that a higher solar irradiance corresponds to a higher mass loss. However, we must divide it by the increased solar irradiation when calculating efficiency (1000 for 1 sun and 2000 for 2 sun). As a result, efficiency is almost unchanged. However, the denominator of the equation used to calculate the solar evaporation rate (equation 2, revised manuscript) does not have the  $q_{\text{solar}}$  term. As a result, we observed larger mass loss and higher evaporation rates with increasing sun irradiation.



**Question 14:** -The discussions lack critical analysis. It is mostly just description of the results.

**Answer 14:** Thank you for your advice. The following analyses are added in various parts of the revised manuscript and highlighted in yellow color.

*“The surface morphology of the  $Ti_3C_2-MnO_2@LS$  was characterized by SEM, as shown in **Fig. 2a-d**. The natural LS possesses a fiber-shaped porous structure, which is feasible for water transport from the underneath bulk water. After coating with  $Ti_3C_2-MnO_2$ , the fiber surface of the LS is entirely covered by a large number of nanoparticles. Compared with the pristine surface (inset of **Fig. 2d**), it becomes rougher, which can be beneficial to reduce light reflection. The LS has a fibrous porous structure that is advantageous to soak the  $Ti_3C_2-MnO_2$  nanocomposite during the dip coating process.”*

*“The water contact angles of the LS before and after surface coating with  $Ti_3C_2-MnO_2$  nanocomposite were measured and shown in **Fig. 3d**. The results that the contact angle decreases from  $78.56^\circ$  to  $45.21^\circ$  after coating (standard deviation  $\pm 0.05^\circ$ ), indicates that the coating can improve the hydrophilicity, which can contribute to a fast and efficient water supply from the bottom bulk water to the evaporating surface. The higher affinity for water of the  $Ti_3C_2-MnO_2$  coating in comparison to the pristine luffa sponge causes the water droplets to disperse and the water contact angle to be maximized.”*

*“The solar absorption of the LS has been greatly enhanced after being coated with  $Ti_3C_2-MnO_2$ , which should be attributed to the excellent light absorption property of  $Ti_3C_2-MnO_2$  and the rougher surface with reduced reflection. The absorption covers the entire UV-Vis-NIR region and matches well with the AM 1.5 solar spectrum, which is beneficial to efficient photothermal conversion.”*

*“When the thickness of LS is small, more heat loss occurs to the underlying bulk water. Whereas when the thickness increases to be too thick, water may not be sufficiently transported to the evaporation surface due to the long transfer path, leading to the lower evaporation efficiency.”*

*“The salt rejection property of the evaporator of the interfacial solar desalination is of great importance. Salt accumulation will block the water transportation channels as well as hinder solar absorption, resulting in a lower evaporation efficiency. The mechanism of salt ion diffusion backflow may be described as follows. First, luffa sponge's porous structure provides linked channels for rapid water transport and vapor escape. The hydrophilic characteristic of the luffa sponge keeps it moist, allowing for adequate water flow through capillary action and rapid steam production. The salt particles formed on the surface of the  $Ti_3C_2-MnO_2@LS$  solar evaporator dissolve rapidly and create a high salt region at the interface between the solar evaporator and bulk water. The difference in salt concentration between the high salt region and the bulk water induces diffusion and convection, therefore reducing salt concentration in the solar evaporator and preventing salt deposition.”*

**Question 15:** -The evap rate result at 1 Sun is just average, and some other biomass materials without nanoparticle coatings have better performance. I am not too sure what is the role of the nanoparticle coating here. It does not seem to drastically help in the performance, while certainly the salt resistance is attributed to the luffa structure mainly.

**Answer 15:** Thank you for the question. However, many recent relevant works with other biomass materials coated with various materials has lower performance compared to our work. A performance comparison table (table S2, supporting information) has been added which will make more convincing. Also, a comparative analysis has been added in the revised supporting information file.

The following table and lines are added in the revised supporting information file.

**“Table S2.** Performance comparison of  $Ti_3C_2-MnO_2@LS$  with other biodegradable photothermal evaporators

Materials used	Evaporation efficiency (%) under 1 Sun	Evaporation rate ( $kg\ m^{-2}\ h^{-1}$ ) under 1 Sun	Salt rejection ability	Ref.
Candle soot@LS	79.98	1.3	No	[1]
Pd NPs, Au NPs on wood	68	1.28	No	[2]
Graphite spray on wood	80	1.15	No	[3]
Wood graphene oxide composite	83	1.40	No	[4]
Ag@TiO <sub>2</sub> NP on bamboo	84	0.71	No	[5]
$Ti_3C_2-MnO_2@LS$	85.28%	1.36	Yes	This work

Many researchers demonstrated the use of biodegradable materials for solar steam generation using various 2D materials and expensive plasmonic nanoparticles coating. However, the demonstrated MXene/MnO<sub>2</sub> coated luffa sponge has significantly higher evaporation efficiency compared to other relevant works. For instance, L. Hu et al. demonstrated the use of Pd and Au nanoparticles deposited on biodegradable wood which resulted in an evaporation efficiency of 68% under 1 sun[2], whereas the proposed MXene/MnO<sub>2</sub> coated luffa sponge provides an evaporation efficiency of 85.25%. When compared to MXene/MnO<sub>2</sub>, the cost of Au nanoparticles is much greater. Similarly, another research group used graphite spray on wood for enhancing the performance of interfacial steam generation system and the reported evaporation efficiency under 1 sun is 80%[3]. Graphene oxide is also used on wood for desalination application with an evaporation efficiency of 83%[4], which is also less than our reported efficiency and involved complex preparation process. Researchers also used candle soot on luffa sponge and obtained a comparatively lower efficiency of 79.98%[1]. Bamboo was also used as a biodegradable

*material with Ag@TiO<sub>2</sub> nanoparticle coating for solar steam generation and 84% of evaporation efficiency had been achieved[5] which is lower than the evaporation efficiency of MXene/MnO<sub>2</sub> coated luffa sponge reported in this work. Therefore, the reported MXene/MnO<sub>2</sub> coated luffa sponge has performance in terms of evaporation efficiency and facile fabrication process. Moreover, the use of MnO<sub>2</sub> interlayer barrier ease the restacking problem of MXene which is another novelty of this work.”*

**Question 16:** -Add a schematic of the salt rejecting mechanism and further expound.

**Answer 16:** Thank you very much for helping us to improve the quality of our manuscript. The schematic of the salt rejecting mechanism has been added in Figure 5e. The following lines are added in the revised manuscript.

*“The mechanism of salt ion diffusion backflow may be described as follows. First, luffa sponge's porous structure provides linked channels for rapid water transport and vapor escape. The hydrophilic characteristic of the luffa sponge keeps it moist, allowing for adequate water flow through capillary action and rapid steam production. The salt particles formed on the surface of the Ti<sub>3</sub>C<sub>2</sub>-MnO<sub>2</sub>@LS solar evaporator dissolve rapidly and create a high salt region at the interface between the solar evaporator and bulk water. The difference in salt concentration between the high salt region and the bulk water induces diffusion and convection, therefore reducing salt concentration in the solar evaporator and preventing salt deposition. **Fig. 5e** illustrates that due to the natural microporous structure of LS, efficient salt ion diffusion backflow mechanism can be achieved. Thus, the Ti<sub>3</sub>C<sub>2</sub>-MnO<sub>2</sub>@LS can effectively prevent salt deposition during the desalination process.”*

**Question 17:** -How did you do the regeneration tests?

**Answer 17:** Thank you very much for your question. To perform the regeneration test, we have conducted the solar evaporation experiments for 25 cycles under 1 sun irradiance. Before conducting each cycle, the Ti<sub>3</sub>C<sub>2</sub>-MnO<sub>2</sub>@LS solar evaporator was dried in an oven and it was made sure that the initial seawater temperature remained always same at the beginning of the experiment. Also, the laboratory temperature and humidity were also kept constants for all the experiment. The result for regeneration test is provided in Figure 4d in the revised manuscript. The following lines are also added and highlighted in yellow color.

*“The cycling stability of the Ti<sub>3</sub>C<sub>2</sub>-MnO<sub>2</sub>@LS for solar evaporation was measured by repeating the same evaporation experiment for 25 cycles under 1 sun irradiation. The results are presented in **Fig. 4d**, in which the water evaporation rates are quite stable with ignorable fluctuation. It demonstrates that the as-prepared Ti<sub>3</sub>C<sub>2</sub>-MnO<sub>2</sub>@LS has a very stable solar evaporation ability.”*

**Question 18:** -You need to compare your results with those similar things in literature for good comparison. Add a table of comparison and discuss.

**Answer 18:** Thank you very much for your question. A performance comparison table (table S2, supporting information) has been added which will make more convincing. Also, a comparative analysis has been added in the revised supporting information file.

**Question 19:** -Any leakage tests? How did you ensure that MXene/MnO<sub>2</sub> are robustly attached on the luffa? What is the binding mechanism.

**Answer 19:** Thank you very much for your question. The prepared luffa sponge (LS) sample was dip coated several times into the Ti<sub>3</sub>C<sub>2</sub>-MnO<sub>2</sub> solution. Then, the sample was dried in an oven at 65 °C for 6 hours. During the dip coating, the Ti<sub>3</sub>C<sub>2</sub>-MnO<sub>2</sub> solution was soaked by the luffa sponge and after the drying process, the soaked Ti<sub>3</sub>C<sub>2</sub>-MnO<sub>2</sub> solution dried inside the fiber of luffa sponge. The sample was immersed into water for several hours to observe any leakage. However, there is no visible leakage found in water after immersing the sample for 6 hours into the water. The corresponding images (Figure S4) for leakage test are provided in the supporting information file.

**Reviewer 3:**

**Comment 1:** This manuscript presents the development of a MXene/MnO<sub>2</sub> nanocomposite coated luffa sponge for solar steam generation from seawater and wastewater. I would recommend its publication after addressing these comments:

**Response 1:** We appreciate the reviewer's favorable feedback. We attempted to address all of the reviewer's concerns in the following section.

**Question 1:** In Section 2.2 and 2.4, "TiTe<sub>2</sub> QD-decorated rGO-coated facemask" was mentioned. Is this a mistake, as there is no context of what this is referring to?

**Answer 1:** Thank you very much for pointing to the mistake. We sincerely regret for the typing error. "TiTe<sub>2</sub> QD-decorated rGO-coated facemask" is not a part of this manuscript. However, in the revised manuscript the corresponding lines are corrected and highlighted in yellow color.

*"The microstructures of the Ti<sub>3</sub>C<sub>2</sub>-MnO<sub>2</sub>@LS were investigated using a scanning electron microscope (SEM, TESCAN, VEGA3, 20 kV)."*

*"The Ti<sub>3</sub>C<sub>2</sub>-MnO<sub>2</sub>@LS structure was wrapped by an Expanded Polyethylene (EPE) foam in order to make it float and reduce the heat loss."*

**Question 2:** In Section 2.4, it was stated that the whole structure was wrapped in an EPE sponge to make it float. Does this have an effect on the solar absorption/evaporation efficiency?

**Answer 2:** We thank the reviewer for addressing this issue. The use of EPE sponge provides two benefits in this research. It helps to keep the structure afloat while also reducing heat loss. A new set of experiments has been carried out in order to better understand the influence of EPE sponge on solar evaporation efficiency. The evaporation efficiency has increased from 80.12% to 85.28% after surrounding the Ti<sub>3</sub>C<sub>2</sub>-MnO<sub>2</sub>@LS solar evaporator with EPE sponge under 1 sun illumination. This improvement in evaporation efficiency is attributed to the EPE sponge's heat insulation property, which limits the amount of photothermal induced heat that is radiated into the environment, hence aiding in heat localization. The corresponding results are provided in the supporting information note S2.

Following lines are added in the revised manuscript and highlighted in yellow color.

*"Another set of experiments has been carried out in order to better understand the influence of EPE sponge on solar evaporation efficiency. The evaporation efficiency has increased from 80.12% to 85.28% and 78.37% to 83.97% after surrounding the Ti<sub>3</sub>C<sub>2</sub>-MnO<sub>2</sub>@LS solar evaporator with EPE sponge under 1 sun and 2 sun illumination, respectively. The corresponding results are provided in **Fig. S2, supporting information**. This improvement in evaporation efficiency is attributed to the EPE sponge's heat insulation property, which limits the amount of photothermal induced heat that is radiated into the environment, hence aiding in heat localization."*

**Question 3:** In Section 3.1 and Figure 2e, usually quantification of carbon using EDS is not reliable due to carbon contamination.

**Answer 3:** We thank the reviewer for the question. Due to the high background counts in SEM-EDS, an artificial carbon (C) peak is always visible and thus a value of more than 2% carbon is normally measured even though there is no carbon in the specimen. This artefact is due to the window in the detector. Therefore, while taking the EDS value of carbon, we subtracted 2% carbon value from the EDS spectrum to eliminate this artefact. The EDS spectrum is provided in the updated supporting information file.

**Question 4:** Please check Figure 3e. It seems that pristine LS has higher absorption than that of  $\text{Ti}_3\text{C}_2\text{-MnO}_2\text{@LS}$ ?

**Answer 4:** Thank you very much for correcting us. There was a mistake in figure legend. However, the Figure 3e has been corrected in the revised manuscript.

**Question 5:** It would be good to include a graph or table to compare the solar evaporation rate, photothermal conversion efficiency and salt rejection ability of MXene/ $\text{MnO}_2\text{@LS}$  with other materials in the literature.

**Answer 5:** Thank you for the suggestions. Table S2 (supporting information) is provided to compare the solar evaporation rate, photothermal conversion efficiency and salt rejection ability of MXene/ $\text{MnO}_2\text{@LS}$  with other materials.

**Question 6:** There are some grammatical errors, like "most potential" in the abstract section and "will generate" in paragraph 3 of Section 3.2.

**Answer 6:** Thank you for pointing out the errors. The mentioned grammatical errors have been corrected in the revised manuscript. Also, the whole manuscript has been revised carefully.

## Reference

- [1] M. Zhu, Y. Li, F. Chen, X. Zhu, J. Dai, Y. Li, Z. Yang, X. Yan, J. Song, Y. Wang, E. Hitz, W. Luo, M. Lu, B. Yang, L. Hu, Plasmonic Wood for High-Efficiency Solar Steam Generation, *Adv Energy Mater.* 8 (2018) 1701028. <https://doi.org/10.1002/aenm.201701028>.
- [2] T. Li, H. Liu, X. Zhao, G. Chen, J. Dai, G. Pastel, C. Jia, C. Chen, E. Hitz, D. Siddhartha, R. Yang, L. Hu, Scalable and Highly Efficient Mesoporous Wood-Based Solar Steam Generation Device: Localized Heat, Rapid Water Transport, *Adv Funct Mater.* 28 (2018) 1707134. <https://doi.org/10.1002/adfm.201707134>.
- [3] K.-K. Liu, Q. Jiang, S. Tadepalli, R. Raliya, P. Biswas, R.R. Naik, S. Singamaneni, Wood–Graphene Oxide Composite for Highly Efficient Solar Steam Generation and Desalination, *ACS Appl Mater Interfaces.* 9 (2017) 7675–7681. <https://doi.org/10.1021/acsami.7b01307>.
- [4] A.M. Saleque, S. Ma, S. Ahmed, M.I. Hossain, W. Qarony, Y.H. Tsang, Solar Driven Interfacial Steam Generation Derived from Biodegradable Luffa Sponge, *Adv Sustain Syst.* 5 (2021) 2000291. <https://doi.org/10.1002/adsu.202000291>.
- [5] Z. Li, C. Wang, T. Lei, H. Ma, J. Su, S. Ling, W. Wang, Arched Bamboo Charcoal as Interfacial Solar Steam Generation Integrative Device with Enhanced Water Purification Capacity, *Adv Sustain Syst.* 3 (2019) 1800144. <https://doi.org/10.1002/adsu.201800144>.
- [6] Z. Liu, Y. Pan, K. Shi, W. Wang, C. Peng, W. Li, D. Sha, Z. Wang, X. Ji, Preparation of hydrophilic luffa sponges and their water absorption performance, *Carbohydrate Polymers.* (2016). <https://doi.org/10.1016/j.carbpol.2016.04.004>.

## Highlights

# **MXene/MnO<sub>2</sub> nanocomposite coated superior salt-rejecting biodegradable luffa sponge for efficient solar steam generation**

Ahmed Mortuza Saleque<sup>1a,b</sup>, Sainan Ma<sup>2,\*</sup>, Amrit Kumar Thakur<sup>3\*</sup>, R. Saidur<sup>4a,b,\*\*</sup>, Tan Kim Han<sup>4a</sup>, Mohammad Ismail Hossain<sup>5</sup>, Wayesh Qarony<sup>6</sup>, Y. Ma<sup>3</sup>, Ravishankar Sathyamurthy<sup>7</sup>, Yuen Hong Tsang<sup>1a,b,\*</sup>

1a.) Department of Applied Physics, Photonic Research Institute, and Materials Research Center, The Hong Kong Polytechnic University, Hung Hom, Kowloon, Hong Kong

1b.) Shenzhen Research Institute, The Hong Kong Polytechnic University, 518057 Shenzhen, Guangdong, People's Republic of China

2.) Ningbo Research Institute, Zhejiang University, Ningbo 315100, China

3.) Department of Mechanical Engineering, University of California, Merced, CA, 95343, USA

4a.) Research Center for Nano-Materials and Energy Technology (RCNMET), School of Engineering and Technology, Sunway University, Bandar Sunway, Petaling Jaya 47500, Selangor Darul Ehan, Malaysia

4b.) School of Engineering, Lancaster University, Lancaster LA1 4YW, UK

5.) Department of Electrical and Computer Engineering, University of California, Davis, CA 95616, USA

6.) Department of Electrical Engineering and Computer Sciences, University of California, Berkeley, CA 94720, USA

7.) Mechanical Engineering Department, King Fahd University of Petroleum and Minerals, Dhahran, Saudi Arabia

\*) Corresponding authors.

\*\*.) Correspondence to: R. Saidur, Department of Engineering, Lancaster University, Lancaster LA1 4YW, UK.

E-mail addresses: sainanma@hotmail.com (S. Ma), saidur@sunway.edu.my (R. Saidur), amritt1@gmail.com (A. K.Thakur), yuen.tsang@polyu.edu.hk (Y. H. Tsang).



**Highlights:**

- Demonstration of MXene-MnO<sub>2</sub> nanomaterials for photothermal application.
- Demonstration of superior salt-rejecting property of luffa sponge for desalination.
- Easing restacking problem of MXene nanosheets by using MnO<sub>2</sub> interlayer barrier.
- Solar evaporation rate and efficiency of 1.36 kg m<sup>-2</sup> h<sup>-1</sup> & 85.28% under 1 sun.

Highlights

# **MXene/MnO<sub>2</sub> nanocomposite coated superior salt-rejecting biodegradable luffa sponge for efficient solar steam generation**

Ahmed Mortuza Saleque<sup>1a,b</sup>, Sainan Ma<sup>2,\*</sup>, Amrit Kumar Thakur<sup>3\*</sup>, R. Saidur<sup>4a,b,\*\*</sup>, Tan Kim Han<sup>4a</sup>, Mohammad Ismail Hossain<sup>5</sup>, Wayesh Qarony<sup>6</sup>, Y. Ma<sup>3</sup>, Ravishankar Sathyamurthy<sup>7</sup>, Yuen Hong Tsang<sup>1a,b,\*</sup>

1a.) Department of Applied Physics, Photonic Research Institute, and Materials Research Center, The Hong Kong Polytechnic University, Hung Hom, Kowloon, Hong Kong

1b.) Shenzhen Research Institute, The Hong Kong Polytechnic University, 518057 Shenzhen, Guangdong, People's Republic of China

2.) Ningbo Research Institute, Zhejiang University, Ningbo 315100, China

3.) Department of Mechanical Engineering, University of California, Merced, CA, 95343, USA

4a.) Research Center for Nano-Materials and Energy Technology (RCNMET), School of Engineering and Technology, Sunway University, Bandar Sunway, Petaling Jaya 47500, Selangor Darul Ehan, Malaysia

4b.) School of Engineering, Lancaster University, Lancaster LA1 4YW, UK

5.) Department of Electrical and Computer Engineering, University of California, Davis, CA 95616, USA

6.) Department of Electrical Engineering and Computer Sciences, University of California, Berkeley, CA 94720, USA

7.) Mechanical Engineering Department, King Fahd University of Petroleum and Minerals, Dhahran, Saudi Arabia

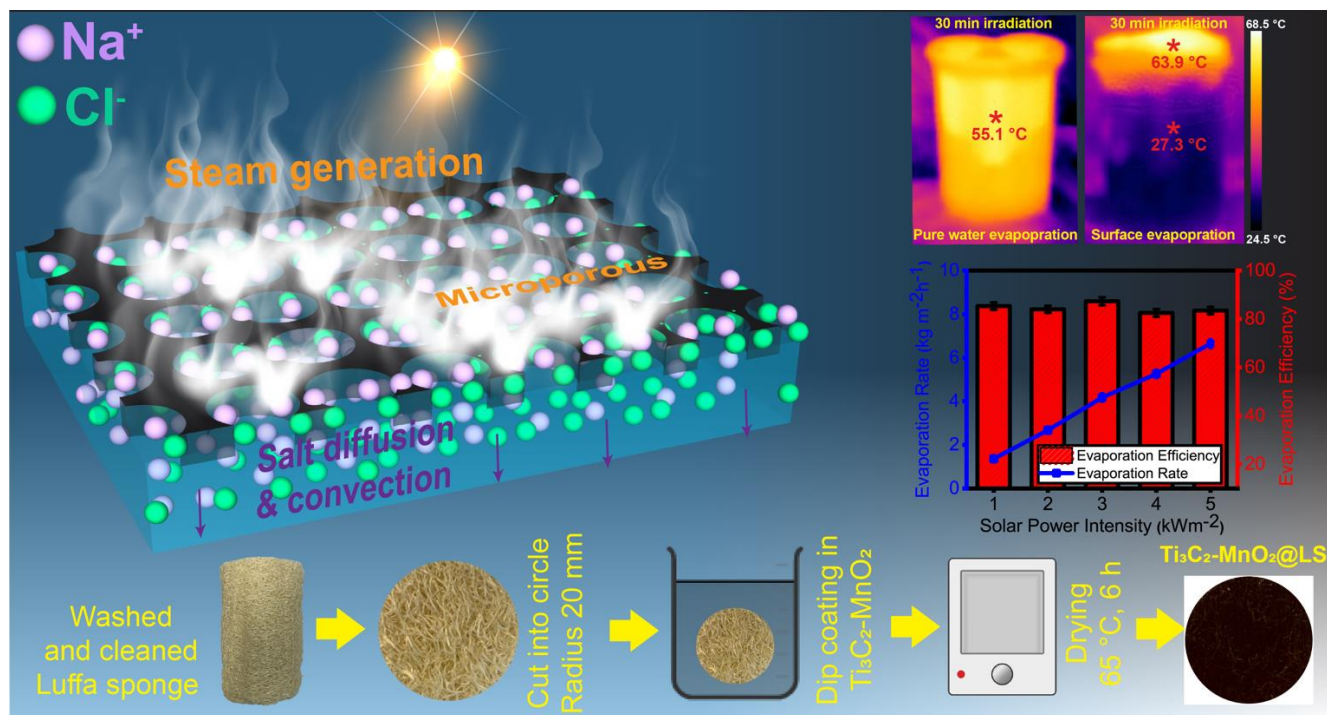
\*) Corresponding authors.

\*\*.) Correspondence to: R. Saidur, Department of Engineering, Lancaster University, Lancaster LA1 4YW, UK.

E-mail addresses: sainanma@hotmail.com (S. Ma), saidur@sunway.edu.my (R. Saidur), amritt1@gmail.com (A. K.Thakur), yuen.tsang@polyu.edu.hk (Y. H. Tsang).

**Highlights:**

- Demonstration of MXene-MnO<sub>2</sub> nanomaterials for photothermal application.
- Demonstration of superior salt-rejecting property of luffa sponge for desalination.
- Easing restacking problem of MXene nanosheets by using MnO<sub>2</sub> interlayer barrier.
- Solar evaporation rate and efficiency of 1.36 kg m<sup>-2</sup> h<sup>-1</sup> & 85.28% under 1 sun.



### Declaration of interests

The authors declare that they have no known competing financial interests or personal relationships that could have appeared to influence the work reported in this paper.

The authors declare the following financial interests/personal relationships which may be considered as potential competing interests:

Yuen Hong Tsang reports financial support was provided by Research Grants Council of Hong Kong, China. Yuen Hong Tsang reports financial support was provided by The Hong Kong Polytechnic University. Yuen Hong Tsang reports financial support was provided by Hong Kong Polytechnic University Shenzhen Research Institute, Shenzhen, China. Sainan Ma reports financial support was provided by Zhejiang Provincial Natural Science Foundation of China. Sainan Ma reports was provided by Ningbo Natural Science Foundation.

# **MXene/MnO<sub>2</sub> nanocomposite coated superior salt-rejecting biodegradable luffa sponge for efficient solar steam generation**

Ahmed Mortuza Saleque<sup>1a,b</sup>, Sainan Ma<sup>2,\*</sup>, Amrit Kumar Thakur<sup>3\*</sup>, R. Saidur<sup>4a,b,\*\*</sup>, Tan Kim Han<sup>4a</sup>, Mohammad Ismail Hossain<sup>5</sup>, Wayesh Qarony<sup>6</sup>, Y. Ma<sup>3</sup>, Ravishankar Sathyamurthy<sup>7</sup>, Yuen Hong Tsang<sup>1a,b,\*</sup>

1a.) Department of Applied Physics, Photonic Research Institute, and Materials Research Center, The Hong Kong Polytechnic University, Hung Hom, Kowloon, Hong Kong

1b.) Shenzhen Research Institute, The Hong Kong Polytechnic University, 518057 Shenzhen, Guangdong, People's Republic of China

2.) Ningbo Research Institute, Zhejiang University, Ningbo 315100, China

3.) Department of Mechanical Engineering, University of California, Merced, CA, 95343, USA

4a.) Research Center for Nano-Materials and Energy Technology (RCNMET), School of Engineering and Technology, Sunway University, Bandar Sunway, Petaling Jaya 47500, Selangor Darul Ehan, Malaysia

4b.) School of Engineering, Lancaster University, Lancaster LA1 4YW, UK

5.) Department of Electrical and Computer Engineering, University of California, Davis, CA 95616, USA

6.) Department of Electrical Engineering and Computer Sciences, University of California, Berkeley, CA 94720, USA

7.) Mechanical Engineering Department, King Fahd University of Petroleum and Minerals, Dhahran, Saudi Arabia

\*) Corresponding authors.

\*\*.) Correspondence to: R. Saidur, Department of Engineering, Lancaster University, Lancaster LA1 4YW, UK.

E-mail addresses: [sainanma@hotmail.com](mailto:sainanma@hotmail.com) (S. Ma), [saidur@sunway.edu.my](mailto:saidur@sunway.edu.my) (R. Saidur), [amritt1@gmail.com](mailto:amritt1@gmail.com) (A. K.Thakur), [yuen.tsang@polyu.edu.hk](mailto:yuen.tsang@polyu.edu.hk) (Y. H. Tsang).

## Author Statement

**Ahmed Mortuza Saleque**; Conceptualization, Methodology, Software, Investigation, Writing-Reviewing and Editing **Sainan Ma**; Data curation, Writing-Original draft preparation, Visualization **Amrit Kumar Thakur**; Formal Analysis, Software, Visualization **R. Saidur**; Data curation, Writing original draft , Supervision **Tan Kim Han**; Validation, Resources **Mohammad Ismail Hossain**; Validation, Writing-Reviewing and Editing **Wayesh Qarony**; Validation, Writing-Reviewing and Editing **Y. Ma**; Validation, Review and Editing **Ravishankar Sathyamurthy**; Validation, Writing-Reviewing and Editing **Yuen Hong Tsang**; Resources, Project Administration, Validation, Supervision, Funding acquisition.



Click here to access/download

**Video**

Supporting\_movie.mp4







[Click here to access/download](#)

**Supplementary Material**

Marked\_Supporting\_information\_DES-22-01838.docx

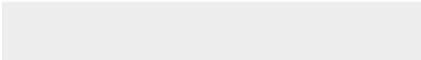





Click here to access/download

**Supplementary Material**

Non\_Marked\_Supporting\_information\_DES-22-  
01838.docx



# **MXene/MnO<sub>2</sub> nanocomposite coated superior salt-rejecting biodegradable luffa sponge for efficient solar steam generation**

Ahmed Mortuza Saleque<sup>1a,b</sup>, Sainan Ma<sup>2,\*</sup>, Amrit Kumar Thakur<sup>3\*</sup>, R. Saidur<sup>4a,b,\*\*</sup>, Tan Kim Han<sup>4a</sup>, Mohammad Ismail Hossain<sup>5</sup>, Wayesh Qarony<sup>6</sup>, Y. Ma<sup>3</sup>, Ravishankar Sathyamurthy<sup>7</sup>, Yuen Hong Tsang<sup>1a,b,\*</sup>

1a.) Department of Applied Physics, Photonic Research Institute, and Materials Research Center, The Hong Kong Polytechnic University, Hung Hom, Kowloon, Hong Kong

1b.) Shenzhen Research Institute, The Hong Kong Polytechnic University, 518057 Shenzhen, Guangdong, People's Republic of China

2.) Ningbo Research Institute, Zhejiang University, Ningbo 315100, China

3.) Department of Mechanical Engineering, University of California, Merced, CA, 95343, USA

4a.) Research Center for Nano-Materials and Energy Technology (RCNMET), School of Engineering and Technology, Sunway University, Bandar Sunway, Petaling Jaya 47500, Selangor Darul Ehan, Malaysia

4b.) School of Engineering, Lancaster University, Lancaster LA1 4YW, UK

5.) Department of Electrical and Computer Engineering, University of California, Davis, CA 95616, USA

6.) Department of Electrical Engineering and Computer Sciences, University of California, Berkeley, CA 94720, USA

7.) Mechanical Engineering Department, King Fahd University of Petroleum and Minerals, Dhahran, Saudi Arabia

\*) Corresponding authors.

\*\*.) Correspondence to: R. Saidur, Department of Engineering, Lancaster University, Lancaster LA1 4YW, UK.

E-mail addresses: [sainanma@hotmail.com](mailto:sainanma@hotmail.com) (S. Ma), [saidur@sunway.edu.my](mailto:saidur@sunway.edu.my) (R. Saidur), [amritt1@gmail.com](mailto:amritt1@gmail.com) (A. K.Thakur), [yuen.tsang@polyu.edu.hk](mailto:yuen.tsang@polyu.edu.hk) (Y. H. Tsang).

## ABSTRACT

Solar steam generation is widely regarded as one of the potential green approaches for freshwater regeneration by utilizing solar energy. Herein, the MXene/MnO<sub>2</sub> nanocomposite-coated biodegradable luffa sponge (Ti<sub>3</sub>C<sub>2</sub>-MnO<sub>2</sub>@LS) is proposed as an efficient solar evaporator for solar steam generation. The thin layer of Ti<sub>3</sub>C<sub>2</sub>-MnO<sub>2</sub> coated on the surface of the luffa sponge (LS) serves as the solar absorber and enhances the hydrophilicity of the LS, while the thermally insulating LS layer with microporous structure endows sufficient water transportation and localizes heat for interfacial water evaporation. Combining MXene with MnO<sub>2</sub> can increase the surface area as well as the stability. The Ti<sub>3</sub>C<sub>2</sub>-MnO<sub>2</sub>@LS delivers a solar evaporation rate as high as 1.36 kg m<sup>-2</sup> h<sup>-1</sup>, with a solar steam conversion efficiency of 85.28% under one sun irradiation. Furthermore, this Ti<sub>3</sub>C<sub>2</sub>-MnO<sub>2</sub>@LS exhibits superior salt-rejecting properties even under highly concentrated saltwater desalination and excellent wastewater purification performance. This work demonstrates the prospects of combining novel 2D materials with biomass-based materials for practical solar steam generation.

**Keywords:** Solar energy, desalination, 2D materials, MXene, biomaterials

## 1. INTRODUCTION

With the rapid progress of modern industry and highly increased population, water shortage has become a severe issue.[1] Intensive research have been devoted to exploring efficient, renewable, and economic water treatment strategies for fresh and clean water regeneration. Traditional desalination and wastewater treatment technologies, such as reverse osmosis, electrodialysis, thermal desalination and multi-effect distillation, still face complex equipment, high cost, high energy consumption and secondary pollution problems. Solar energy, as the most promising, and sustainable energy source, has attracted high attention to be utilized for water treatment [2,3]. However, the traditional solar steam generation system has a poor efficiency, which involves high heat loss [4,5]. Over the past decades, solar-driven interfacial steam generation has become an important research branch for seawater desalination and wastewater treatment because of its sustainability, environmental friendliness, and low cost [6–9].

For an efficient solar steam generation system, the light absorption ability, photothermal conversion efficiency, water transportability, and durability of the solar evaporator determine the solar water evaporation efficiency [10]. Various photothermal materials have been developed, including carbon materials [11,12], metal nanoparticles [13,14], semiconductor materials [15,16], and organic photothermal materials [17,18]. Among them, biomass-based materials, generally possessing natural porous structure, low thermal conductivity, and low cost, have drawn tremendous interest. For instance, a series of wood-based materials have been reported as solar evaporators for efficient solar steam generation [19–22]. Besides, carbonized bamboo, which possesses excellent water

transport channels, good mechanical strength, and effective heat localization effect, has also been explored [23–29]. Liao et al. prepared carbonized lotus seedpods with a hierarchical porous structure and good light absorption, achieving a photothermal evaporation rate and efficiency of  $1.30 \text{ kg m}^{-2} \text{ h}^{-1}$  and 86.5%, respectively [30]. Beyond these, many vegetable or fruit-based materials were investigated, such as mushroom [31], sunflower heads [32], potato [33], coconut husk [34], corncob [35], daikon [36], carrot [37], and eggplant [38]. Recently, loofah, which is a vigorous, productive, and widely distributed reticulated fibrous plant, has been investigated as good solar evaporator [39,40]. The outstanding mechanical strength and microporous structure present promising potential for continuous solar driven water transpiration.

However, for most biomass-based materials, the pristine solar absorption property is poor. Surface treatment like coating with photothermal materials can be a feasible way to enhance solar absorption. MXene, as a new family of multifunctional 2D material, has been widely applied in a variety of fields, including supercapacitor [41], microwave absorption [42], catalysis [43], and dye separation [44], etc. Wang et al. [45] reported that the  $\text{Ti}_3\text{C}_2$  MXene shows an internal light-to-heat conversion efficiency of 100% measured by a designed droplet-based light absorption and heating system, indicating the great potential of MXene as photothermal materials for solar steam generation. Because of the semi-metal character of  $\text{Ti}_3\text{C}_2$  nanosheets, the photothermal conversion mechanism of MXene is considered to be localized surface plasmon resonance effect. However, due to the commonly presented smooth surface of the  $\text{Ti}_3\text{C}_2$  nanosheets, the light absorption is weak with strong light reflection [46]. Nevertheless, the 2D  $\text{Ti}_3\text{C}_2$  nanosheets often restack spontaneously, which could hinder the water transport and

vapor escaping process. Thus, it is necessary to further modify the  $\text{Ti}_3\text{C}_2$  for efficient solar steam generation. Introducing the interlayer barrier can effectively avoid spontaneous stacking as well as increase surface area. Materials like CNTs [47], metal oxides [48], and polymers [49] have been investigated to prevent the restack of MXene nanosheets. Among them, manganese dioxide ( $\text{MnO}_2$ ) has drawn more attention due to its low cost and environmental friendliness. Wang et al. [50] demonstrated the  $\text{MnO}_2/\text{MXene}$  composite as film electrodes for electronics, in which the combination of  $\text{MnO}_2$  and MXene effectively increased the surface area and reduced the spontaneous stacking of the MXene nanosheets. Moreover,  $\text{MnO}_2$  is also a promising photothermal material for solar steam generation [51–53].

While significant advancements have been made for photothermal materials, considerable hurdles remain, particularly in regard to the problem of severe salt accumulation, which is seen as one of the largest impediments preventing their actual solar desalination applications. Water molecules undergo a phase transition from liquid to gas during solar evaporation, migrating through the porous channels of the photothermal material where salt may readily precipitate and clog the channels. The deposition of salt on the surface of photothermal materials may reduce their performance as a heat generator when exposed to light. The researchers exhibited two types of salt rejection mechanisms to solve these difficulties. A double-layered Janus structure on the photothermal material's surface hinders salt crystallization and emigration [54–56]. The simplest method is to construct aligned channels with large diameters to allow crystallized salts to dissolve quickly and be transferred back into the bulk water [57,58].

Herein, we utilized the low-cost biodegradable luffa sponge (LS), which has a 3D

microporous structure, as the solar evaporator via surface coated with  $\text{Ti}_3\text{C}_2\text{-MnO}_2$  nanocomposite. The hydrophilicity and solar absorption properties of LS have been highly enhanced by surface coating of  $\text{Ti}_3\text{C}_2\text{-MnO}_2$  nanocomposite. The water evaporation and seawater desalination performance enabled by the  $\text{Ti}_3\text{C}_2\text{-MnO}_2@\text{LS}$  are investigated and discussed. The obtained solar evaporator presents a high evaporation efficiency and long-term stability for solar water evaporation under one sun irradiation. In addition, the  $\text{Ti}_3\text{C}_2\text{-MnO}_2@\text{LS}$  shows excellent salt-rejecting performance owing to large diameters porous structure of LS which helps to dissolve crystallized salts and transferred back into the bulk water as known as salt ion diffusion backflow mechanism. Therefore, it can be used for highly concentrated saline desalination. The wastewater treatment performance has also been evaluated, in which dye contaminants can be completely removed. All of these allow the synthesized  $\text{Ti}_3\text{C}_2\text{-MnO}_2@\text{LS}$  for practical solar water treatment.

## **2. EXPERIMENTAL SECTION**

### **2.1 Synthesis of MXene ( $\text{Ti}_3\text{C}_2$ )**

MAX phase material ( $\text{Ti}_3\text{AlC}_2$ ),  $\text{NH}_4\text{HF}_2$  (95% reagent grade), and NaOH (97% purity, pellets) were purchased from Y-Carbon limited and Sigma Aldrich, USA for MXene ( $\text{Ti}_3\text{C}_2\text{T}_x$ ) synthesis. The purchased chemicals were used without being purified further. 20 ml of a 2 M solution of  $\text{NH}_4\text{HF}_2$  were prepared, followed by 1 hour of magnetic stirring at 300 rpm and 30 °C. Slowly 1 g of  $\text{Ti}_3\text{AlC}_2$  was added to a 2 M  $\text{NH}_4\text{HF}_2$  solution, which was magnetically stirred for 48 hours at 300 rpm and 30 ° C. Throughout the stirring procedure, Al was etched from the MAX phase material ( $\text{Ti}_3\text{AlC}_2$ ). Continuous pH monitoring and the addition of diluted NaOH solution allowed for the solution's pH to be



maintained at 6. After the etching procedure was complete, the solution was filtered and repeatedly washed with DI water. 4 repetitions of ultrahigh centrifugation were performed at 3500 rpm (10 mins for each cycle). The resultant multilayered  $Ti_2C_2T_x$  solution was sonicated for 1 hour with an ultrasonic probe to produce delaminated MXene (d-  $Ti_2C_2T_x$ ). Finally, the delaminated flakes of synthesized MXene were dried in a vacuum oven overnight.

## 2.2 Material Characterizations

The microstructures of the  $Ti_3C_2-MnO_2@LS$  were investigated using a scanning electron microscope (SEM, TESCAN, VEGA3, 20 kV). Energy dispersive X-ray (EDS) images were acquired using X-ray spectroscopy (INCA X-Act, Oxford) in conjunction with SEM equipment. A UV-Vis-NIR spectrometer was used to measure the absorption spectra (PerkinElmer Lambda 1050). X-ray diffraction (XRD) patterns of the materials were obtained using a Cu-K $\alpha$  radiation X-ray diffractometer (Smart Lab, Rigaku, 40 kV, 100 mA). X-ray photoelectron spectroscopy (XPS) measurements were performed using Al-K $\alpha$  radiation on a Thermo Fisher Nexsa G2 XPS instrument. The Raman spectroscopy was conducted using WITEC Confocal Raman system with 532 nm laser. The hydrophilicity of the surface was decided through the water contact angle measurement (WCA, KINO SL 200 KB). Transients hot-wire approach with computer-controlled equipment was used to measure thermal conductivity (Thermtest Instruments, THW L2). Using a linear heat source implanted in the material being tested, the hot-wire method is a transient dynamic approach that measures the temperature increase in a predetermined distance. The rate of temperature rises or fall over a certain time period is a direct measure of thermal conductivity [59].

### 2.3 Preparation of $\text{Ti}_3\text{C}_2\text{-MnO}_2\text{@LS}$ photothermal absorber

The cylindrical form of luffa sponge extracted from the ripe fruit of *Luffa cylindrica* was washed and cleaned before being tailored into a circular shape with a 20 mm radius and a 12 mm thickness. The prepared sample was ultrasonically cleaned with deionized (DI) water and dried in a 50 °C oven.  $\text{Ti}_3\text{C}_2$  MXene synthesized in a laboratory and purchased  $\text{MnO}_2$  powder were both dissolved in Isopropyl alcohol (IPA). 6 different concentrations of  $\text{Ti}_3\text{C}_2$  and  $\text{MnO}_2$  were prepared, and their corresponding average absorbance were measured. As the major objective of this solution was to improve the absorption of luffa sponge in the AM 1.5 solar spectrum, each of the produced solutions was tested in a separate cuvette for its absorption spectrum. The supporting information note S3 contains the detail description of the preparation and table S1 (supporting information) shows the various concentration of  $\text{Ti}_3\text{C}_2$  and  $\text{MnO}_2$  and their average absorbance as measured by UV-Vis-NIR spectroscopy. Based on the average absorbance,  $\text{Ti}_3\text{C}_2\text{-MnO}_2$  (2 – 5) sample provided highest average absorbance (table S1, supporting information). Therefore, it was chosen as the optimum concentration for fabricating the  $\text{Ti}_3\text{C}_2\text{-MnO}_2\text{@LS}$ .  $\text{Ti}_3\text{C}_2$  and  $\text{MnO}_2$  with a concentration of 2 mg ml<sup>-1</sup> and 5 mg ml<sup>-1</sup>, respectively are dissolved in IPA. The prepared solutions were ultrasonically treated for 4 hours. After that, 60 ml of  $\text{Ti}_3\text{C}_2$  and 40 ml of  $\text{MnO}_2$  solutions were mixed in a beaker, and the mixture was magnetically stirred at 600 rpm for 2 hours. Afterward, the prepared luffa sponge (LS) sample was dip coated several times into the  $\text{Ti}_3\text{C}_2\text{-MnO}_2$  solution. The sample was then dried in a 65 °C oven for 6 hours. The preparation method is illustrated in **Fig. 1a**. To perform sun evaporation experiments, the as-prepared  $\text{Ti}_3\text{C}_2\text{-MnO}_2\text{@LS}$  was placed on top of a beaker containing water, as shown in **Fig. 1b**.

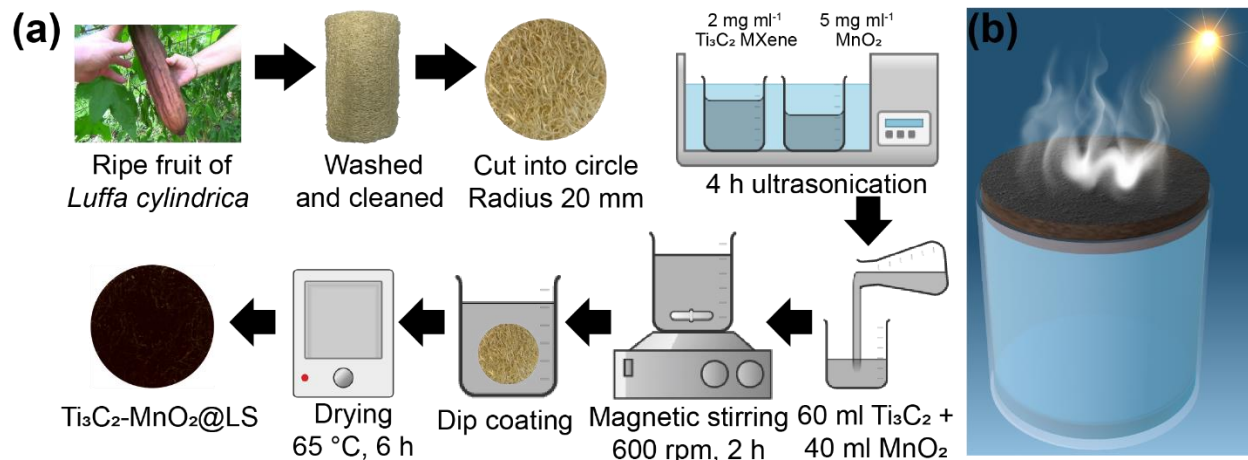


**Fig. 1** (a) Schematic representation of  $\text{Ti}_3\text{C}_2\text{-MnO}_2\text{@LS}$  preparation process; (b) Illustration of solar steam generation by  $\text{Ti}_3\text{C}_2\text{-MnO}_2\text{@LS}$ .

## 2.4 Solar-driven desalination experiment

The solar desalination experiments were conducted in a laboratory environment where the solar irradiance was provided by a xenon lamp (300 W, PLS-SXE300, Beijing Perfect Light Technology Co., Ltd). The intensity of the incident solar irradiance was measured by a power meter (THORLABS, S314C). The setup was placed on an electronic microbalance (Ohaus Corporation, C213, deviation  $\sim 0.1$  mg) to measure the mass loss. The temperature of the solar evaporator surface and underneath bulk water was recorded using an infrared camera (FLIR-E64501, Tallinn, Estonia, error range of  $\pm 2$  °C). The  $\text{Ti}_3\text{C}_2\text{-MnO}_2\text{@LS}$  structure was wrapped by an Expanded Polyethylene (EPE) foam in order to make it float and reduce the heat loss. Then, it was placed in a beaker containing seawater to conduct the solar evaporation experiments. A separate experiment was conducted without EPE foam to understand the improvement in solar evaporation rate and efficiency and the corresponding results are provided in **Fig. S2, supporting information**. At first, the thickness of the LS was varied from 6 mm to 18 mm and the

corresponding evaporation efficiency were measured under 1 sun illumination. The maximum evaporation efficiency of 85.28% has been achieved at 14 mm thickness of LS. Therefore, rest of the experiments were conducted using 14 mm thickness. The solar irradiance was varied from 1 to 5 kW/m<sup>2</sup> and the corresponding mass losses were recorded. To measure the mass loss due to the solar irradiance, the Ti<sub>3</sub>C<sub>2</sub>-MnO<sub>2</sub>@LS was put on top of a beaker holding 150 ml of seawater. The beaker was then placed within a custom-made glass structure, as shown in **Fig. S1, supporting information**. The evaporated steam is collected through an output channel on the structure's upper side. The outflow channel is linked to a pipe, with the other end connected to a container to collect the condensed water droplet. The majority of the evaporated steam flows via the output route at the top of the pipe to the water droplet collecting container. The steam gradually releases heat and condenses into water droplets as it travels along this path. However, some steam condenses inside the custom-made structure and condenses into a water droplet, which is deposited at the bottom. As a consequence, at the end of the experiment, the water deposited at the bottom of the custom-made structure was also collected. The evaporation rate and efficiency were calculated from the measured evaporated mass loss under various solar irradiance.

### **3. RESULTS AND DISCUSSION**

#### **3.1 Material Structure and Morphology**

Due to the low solar absorption of natural LS, Ti<sub>3</sub>C<sub>2</sub>-MnO<sub>2</sub> nanocomposite with excellent light absorption was utilized to coat the surface of natural LS. The surface morphology of the Ti<sub>3</sub>C<sub>2</sub>-MnO<sub>2</sub>@LS was characterized by SEM, as shown in **Fig. 2a-d**. The natural LS

possesses a fiber-shaped porous structure, which is feasible for water transport from the underneath bulk water. After coating with  $\text{Ti}_3\text{C}_2\text{-MnO}_2$ , the fiber surface of the LS is entirely covered by a large number of nanoparticles. Compared with the pristine surface (inset of **Fig. 2d**), it becomes rougher, which can be beneficial to reduce light reflection. The LS has a fibrous porous structure that is advantageous to soak the  $\text{Ti}_3\text{C}_2\text{-MnO}_2$  nanocomposite during the dip coating process.

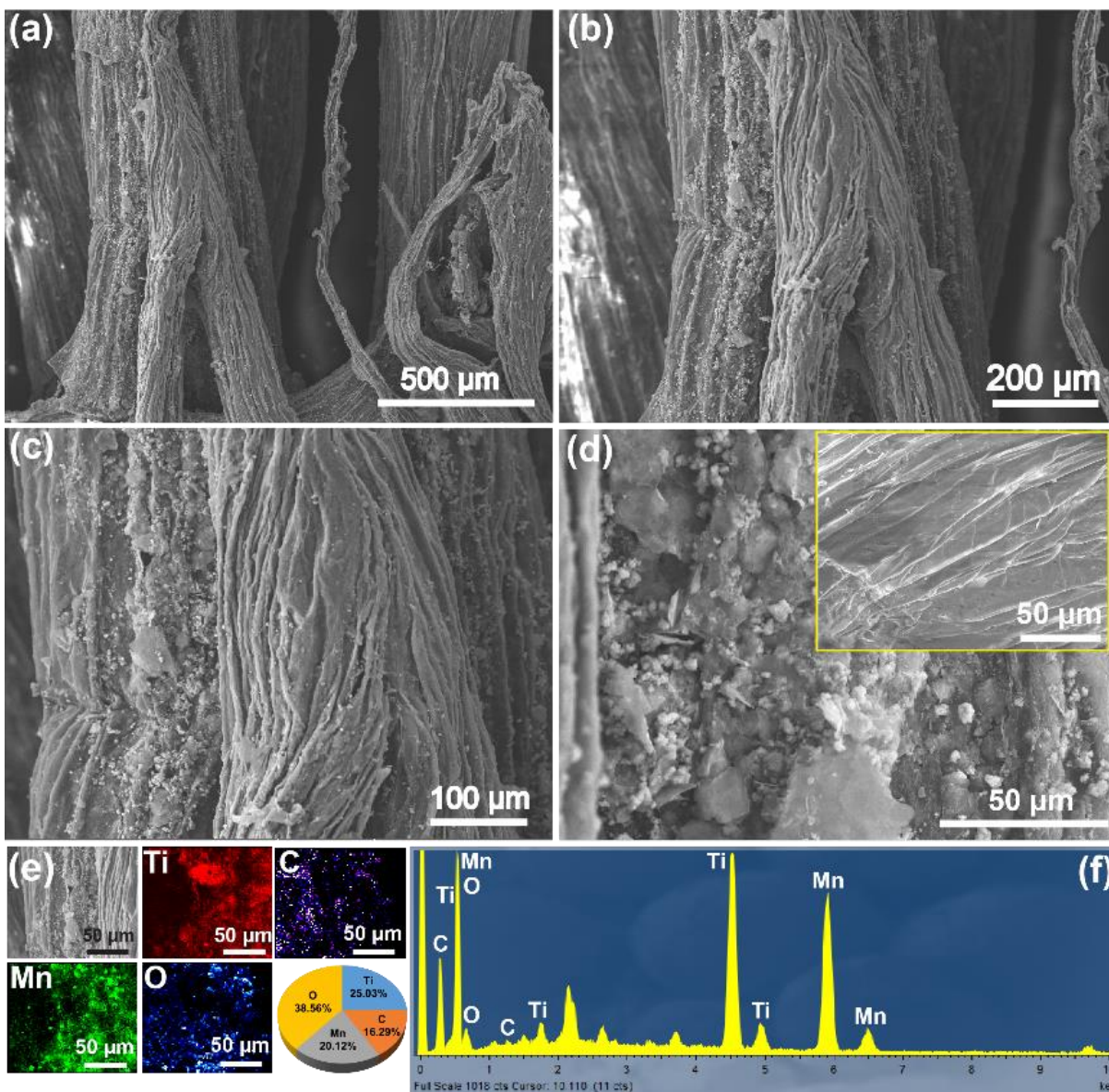


**Fig. 2** (a-d) SEM images of  $\text{Ti}_3\text{C}_2\text{-MnO}_2$ @LS in different magnitude. Inset of (d) is pristine LS; (e) EDS elemental mapping; (f) EDS spectrum with the elemental composition

analysis.

**Fig. 2e** shows the corresponding elemental distribution information by EDX elemental mapping. It is clear that the Ti, Mn, C, and O elements are homogeneously and continuously distributed throughout the LS surface, with the ratio of 25.03%, 20.12%, 16.29%, and 38.56%, respectively. The coexistence of  $\text{Ti}_3\text{C}_2$  and  $\text{MnO}_2$  is also indicated by the EDS spectrum in **Fig. 2f**.

The structural features of  $\text{Ti}_3\text{C}_2\text{-MnO}_2$  nanocomposite have been investigated by the Raman measurement as shown in **Fig. 3a**. As for the Raman spectrum of  $\text{MnO}_2$ , the two Raman bands at 486.52 and 652.81  $\text{cm}^{-1}$  are observed, corresponding to the symmetrical vibrations of  $\text{MnO}_2$ .<sup>[53,60]</sup> Generally, the two Raman bands at around 159.52 and 409.21  $\text{cm}^{-1}$  correspond to the vibrations from Ti-C bonds for  $\text{Ti}_3\text{C}_2$ , and the two bands at around 1386 and 1576.92  $\text{cm}^{-1}$  are attributed to the D band and G band of graphitic carbon.<sup>[61,62]</sup> The ratio of intensity between  $I_D$  and  $I_G$  of the  $\text{Ti}_3\text{C}_2$  is 1.048, suggesting a high graphitization degree. The Raman spectrum of  $\text{Ti}_3\text{C}_2\text{-MnO}_2$  shows both the typical characteristic bands of  $\text{MnO}_2$  and  $\text{Ti}_3\text{C}_2$ , indicating the hybrid structure of  $\text{Ti}_3\text{C}_2\text{-MnO}_2$  nanocomposite.

In order to further confirm the crystalline structure of  $\text{Ti}_3\text{C}_2\text{-MnO}_2\text{@LS}$ , XRD spectra of  $\text{MnO}_2$ ,  $\text{Ti}_3\text{C}_2$ , and  $\text{Ti}_3\text{C}_2\text{-MnO}_2$  nanocomposite were recorded, as presented in **Fig. 2b**. The diffraction peaks of the  $\text{MnO}_2$  at the angles of 29.29, 37.45, 43.07, 56.59, 72.91 are assigned to the (100), (110), (111), (211) and (301) planes, respectively. While the peaks at angles of 4.388, 14.52, 24.81, 34.89, 60.76 are assigned to the (002), (006), (008), (103) and (110) planes of  $\text{Ti}_3\text{C}_2$ , respectively. Coexisting phases of  $\text{MnO}_2$  and  $\text{Ti}_3\text{C}_2$  can be observed in  $\text{Ti}_3\text{C}_2\text{-MnO}_2$  nanocomposite.

The elemental compositions of Ti, Mn, C and O species in the  $\text{Ti}_3\text{C}_2\text{-MnO}_2$  hybrid are investigated by X-ray photoelectron spectroscopy (XPS). As shown in **Fig. 3c**, the peaks at a binding energy of 665.04, 658.67 and 453.81 eV in the  $\text{Ti}_3\text{C}_2\text{-MnO}_2$  hybrid are assigned to Mn  $2p_{1/2}$ , Mn  $2p_{3/2}$  and Ti  $2p$ , respectively. The XPS spectra indicate that the  $\text{Ti}_3\text{C}_2\text{-MnO}_2@\text{LS}$  is composed of Ti, Mn, C and O, indicating the introduction of  $\text{Ti}_3\text{C}_2\text{-MnO}_2$  hybrid into the LS. The water contact angles of the LS before and after surface coating with  $\text{Ti}_3\text{C}_2\text{-MnO}_2$  nanocomposite were measured and shown in **Fig. 3d**. The results that the contact angle decreases from  $78.56^\circ$  to  $45.21^\circ$  after coating (standard deviation  $\pm 0.05^\circ$ ), indicates that the coating can improve the hydrophilicity, which can contribute to a fast and efficient water supply from the bottom bulk water to the evaporating surface. The higher affinity for water of the  $\text{Ti}_3\text{C}_2\text{-MnO}_2$  coating in comparison to the pristine luffa sponge causes the water droplets to disperse and the water contact angle to be maximized. **Fig. 3e** shows the absorption properties of the  $\text{Ti}_3\text{C}_2\text{-MnO}_2@\text{LS}$  and uncoated LS. The solar absorption of the LS has been greatly enhanced after being coated with  $\text{Ti}_3\text{C}_2\text{-MnO}_2$ , which should be attributed to the excellent light absorption property of  $\text{Ti}_3\text{C}_2\text{-MnO}_2$  and the rougher surface with reduced reflection. The absorption covers the entire UV-Vis-NIR region and matches well with the AM 1.5 solar spectrum, which is beneficial to efficient photothermal conversion. All the above results suggest the successful synthesis of  $\text{Ti}_3\text{C}_2\text{-MnO}_2@\text{LS}$  and the great potential for application in solar steam generation.

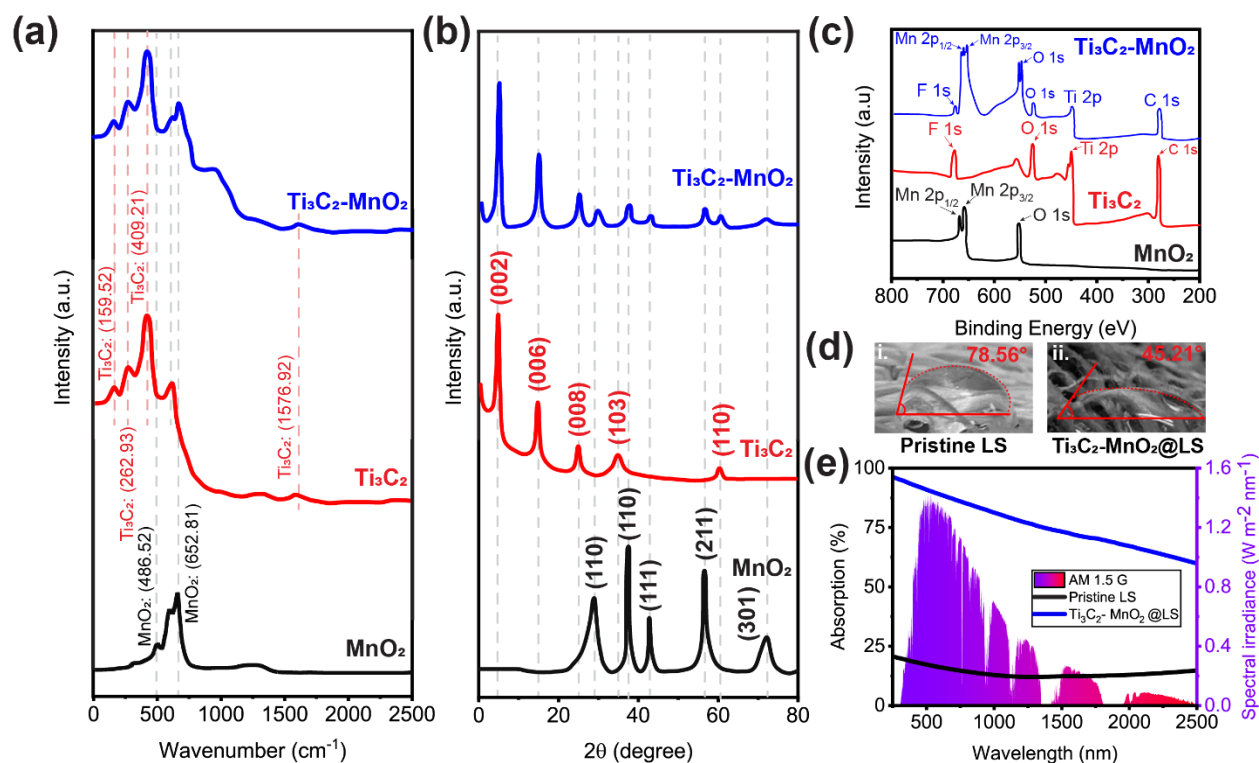


**Fig. 3** (a) Raman spectra of  $\text{Ti}_3\text{C}_2\text{-MnO}_2$ ,  $\text{Ti}_3\text{C}_2$ , and  $\text{MnO}_2$ ; (b) XRD patterns of  $\text{Ti}_3\text{C}_2\text{-MnO}_2$ ,  $\text{Ti}_3\text{C}_2$ , and  $\text{MnO}_2$ ; (c) XPS spectra of  $\text{Ti}_3\text{C}_2\text{-MnO}_2$ ,  $\text{Ti}_3\text{C}_2$ , and  $\text{MnO}_2$ ; (d) Water contact angle of pristine LS and  $\text{Ti}_3\text{C}_2\text{-MnO}_2\text{@LS}$ ; (e) UV-Vis-NIR absorption spectra of pristine LS and  $\text{Ti}_3\text{C}_2\text{-MnO}_2\text{@LS}$ .

### 3.2 Evaluation of the solar evaporation by $\text{Ti}_3\text{C}_2\text{-MnO}_2\text{@LS}$

The water evaporation performance of the synthesized  $\text{Ti}_3\text{C}_2\text{-MnO}_2\text{@LS}$  was investigated. **Fig. 4a** displays the time-dependent mass changes of water only, pristine LS and  $\text{Ti}_3\text{C}_2\text{-MnO}_2\text{@LS}$  under simulated solar irradiation of  $1 \text{ kW m}^{-2}$ . The corresponding spontaneous evaporations under dark have been subtracted. It can be observed that the water evaporation rate has been greatly enhanced in the presence of  $\text{Ti}_3\text{C}_2\text{-MnO}_2\text{@LS}$  compared to that of pristine LS. The evaporation rate of the system with  $\text{Ti}_3\text{C}_2\text{-MnO}_2\text{@LS}$  reaches to  $1.36 \text{ kg m}^{-2} \text{ h}^{-1}$ , which is more than 3.5 times higher than that of pristine LS ( $0.39 \text{ kg m}^{-2} \text{ h}^{-1}$ ) and 6.8 times higher than that of water only ( $0.20 \text{ kg m}^{-2} \text{ h}^{-1}$ ). The evaporation efficiency and rate attained are comparatively higher than several



biodegradable solar evaporators shown in the literature (table S2, supporting information). **Fig. 4b** shows the water mass change of Ti<sub>3</sub>C<sub>2</sub>-MnO<sub>2</sub>@LS under various light densities ranging from 1 kW m<sup>-2</sup> to 5 kW m<sup>-2</sup>. The evaporation rate increases almost linearly with the light density. The evaporation rate reaches up to 6.65 kg m<sup>-2</sup> h<sup>-1</sup> when the irradiation intensity scaled to 5 kW m<sup>-2</sup>.

The solar evaporation efficiency ( $\eta_{th}$ ) of the samples can be calculated by the following equation (1).

$$\eta_{th} = \frac{\dot{m}h_{LV}}{q_{solar}} \quad (1)$$

Where  $\dot{m}$  is the steady-state water evaporation rate (kg m<sup>-2</sup> h<sup>-1</sup>) excluding the evaporation rate under the dark field,  $h_{LV}$  is the total phase change enthalpy of water (2260 J/g) including the sensible heat and latent heat,  $q_{solar}$  is the power density of solar irradiation (W/m<sup>2</sup>).

The evaporation rate,  $m_e$  can be calculated by following equation:

$$m_{ev} = \frac{m_h}{A} \quad (2)$$

Where,  $m_h$  is mass loss of water per hour (kg/h) due to evaporation and  $A$  is the area (m<sup>2</sup>) of evaporation surface. As shown in **Fig. 4c**, the solar evaporation efficiency of Ti<sub>3</sub>C<sub>2</sub>-MnO<sub>2</sub>@LS can reach 85.28% under 1 sun irradiation and 83.48% under 5 sun irradiation. The slight decrease in the efficiency may be due to the increased heat loss along with higher light intensity. Another set of experiments has been carried out in order to better understand the influence of EPE sponge on solar evaporation efficiency. The evaporation efficiency has increased from 80.12% to 85.28% and 78.37% to 83.97% after surrounding the Ti<sub>3</sub>C<sub>2</sub>-MnO<sub>2</sub>@LS solar evaporator with EPE sponge under 1 sun and 2 sun

illumination, respectively. The corresponding results are provided in **Fig. S2, supporting information**. This improvement in evaporation efficiency is attributed to the EPE sponge's heat insulation property, which limits the amount of photothermal induced heat that is radiated into the environment, hence aiding in heat localization. The cycling stability of the  $\text{Ti}_3\text{C}_2\text{-MnO}_2@\text{LS}$  for solar evaporation was measured by repeating the same evaporation experiment for 25 cycles under 1 sun irradiation. The results are presented in **Fig. 4d**, in which the water evaporation rates are quite stable with ignorable fluctuation. It demonstrates that the as-prepared  $\text{Ti}_3\text{C}_2\text{-MnO}_2@\text{LS}$  has a very stable solar evaporation ability.

Besides, the solar water evaporation performances of  $\text{Ti}_3\text{C}_2\text{-MnO}_2@\text{LS}$  with different thicknesses of LS under 1 sun were investigated to find out the most efficient thickness. As shown in **Fig. 4e**, the evaporation efficiency increases from 50% to 85.28% as the thickness increases from 6 mm to 12 mm and reaches the highest at a thickness of 14 mm. After that, the efficiency drops as the thickness continues to increase. Similarly, the evaporation rate at 6 mm of luffa sponge thickness is just  $0.79 \text{ kg m}^{-2} \text{ h}^{-1}$ . At 14 mm thickness, the evaporation rate reaches its maximum value of  $1.36 \text{ kg m}^{-2} \text{ h}^{-1}$ . The rate of evaporation then reduces with increasing thickness, reaching  $1.15 \text{ kg m}^{-2} \text{ h}^{-1}$  at 18 mm thickness. When the thickness of LS is small, more heat loss occurs to the underlying bulk water. Whereas when the thickness increases to be too thick, water may not be sufficiently transported to the evaporation surface due to the long transfer path, leading to the lower evaporation efficiency. **Fig. 4f** shows that the thermal conductivity of the LS is extremely low, which is  $0.18 \text{ W m}^{-1} \text{ K}^{-1}$  in dry state and  $0.35 \text{ W m}^{-1} \text{ K}^{-1}$  in wet state with

a standard deviation of  $\pm 0.007 \text{ W m}^{-1} \text{ K}^{-1}$ , indicating the good heat confinement effect of LS.

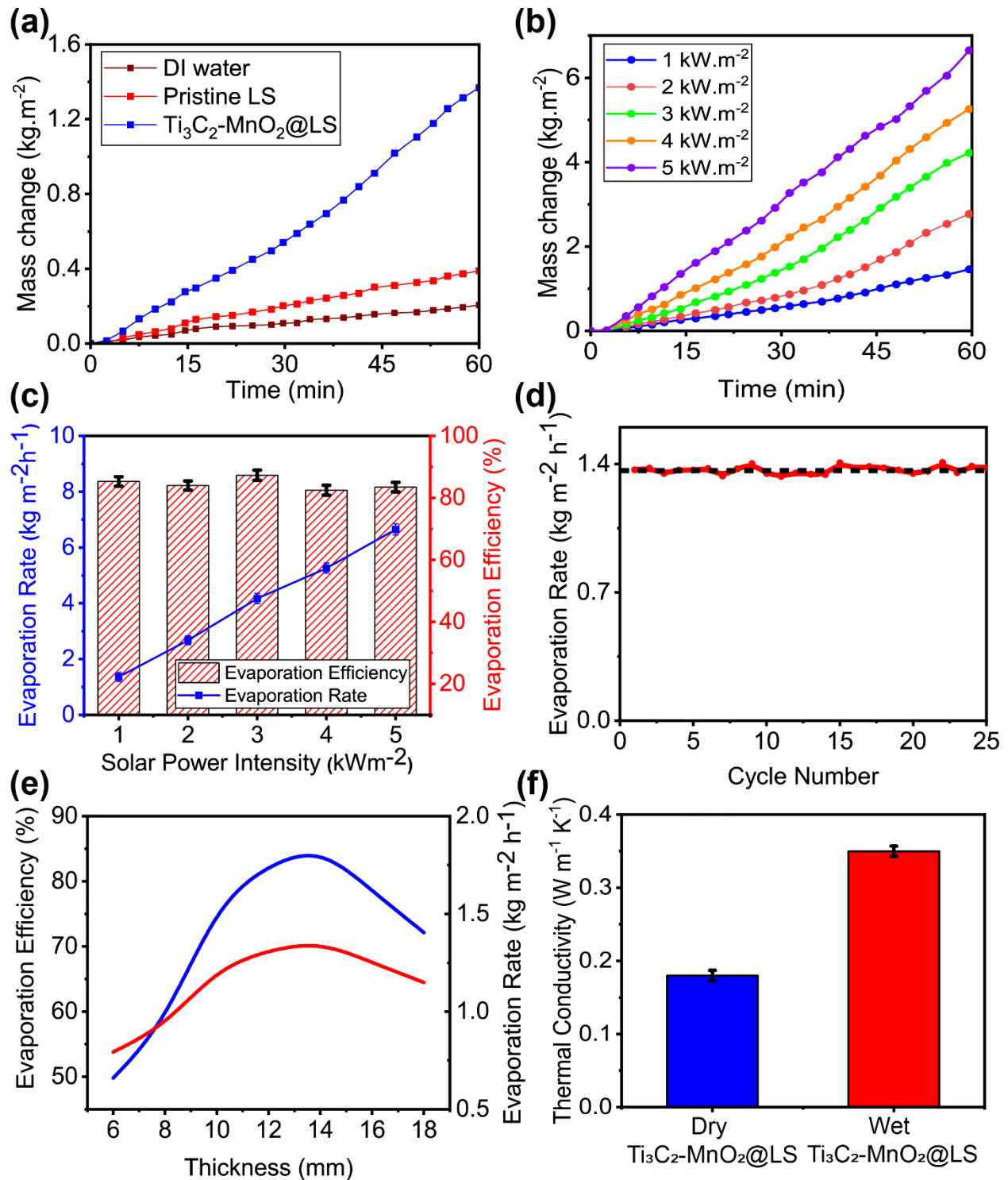


**Fig. 4** The solar water evaporation mass change over time of the system with water only,

pristine LS, and  $\text{Ti}_3\text{C}_2\text{-MnO}_2@\text{LS}$  under one sun irradiation; (b) Solar evaporation performance of  $\text{Ti}_3\text{C}_2\text{-MnO}_2@\text{LS}$  under various light intensity irradiation; (c) Corresponding evaporation rate (line) and evaporation efficiency (bars) under various solar irradiance with error bars; (d) The cyclic performance of the  $\text{Ti}_3\text{C}_2\text{-MnO}_2@\text{LS}$  for water evaporation for 1h over 25 cycles. (e) Evaporation efficiency and rate at different thickness; (f) Thermal conductivity of  $\text{Ti}_3\text{C}_2\text{-MnO}_2@\text{LS}$  at dry and wet state.

The heat confinement performance was further investigated by measuring the cross-sectional temperature distribution of the beaker with and without  $\text{Ti}_3\text{C}_2\text{-MnO}_2@\text{LS}$  floating on the air-water interface under 1 sun irradiation via the IR camera. As shown in **Fig. 5a**, after 30 mins illumination, the beaker with water only presents a homogeneously increased temperature distribution. In contrast, from the cross-sectional IR image of the system with  $\text{Ti}_3\text{C}_2\text{-MnO}_2@\text{LS}$ , an obvious temperature gradient can be observed between the top layer and underlying bulk water. A temperature of as high as 63.9 °C can be achieved at the top surface, whereas the temperature of underlying bulk water was only slightly higher than room temperature (~ 27.3 °C).

### 3.3 Desalination and salt rejecting performance evaluation

To evaluate the desalination performance of the prepared  $\text{Ti}_3\text{C}_2\text{-MnO}_2@\text{LS}$ , seawater collected from Whampoa Harbor, Hong Kong and high concentration NaCl solutions including 10, 20, and 30 wt% were prepared for solar evaporation under simulated 1 sun irradiation. As shown in **Fig. 5b**, the evaporation rate drops with the increasing saline concentration owing to the fact that the vapor pressure of water decreases with the increased salinity.[63] Nonetheless, the evaporation rate of seawater keeps above 1.3 kg  $\text{m}^{-2} \text{h}^{-1}$  and even for 30 wt% NaCl solution, the evaporation rate is still larger than 1.1 kg  $\text{m}^{-2} \text{h}^{-1}$ , indicating the excellent desalination performance of  $\text{Ti}_3\text{C}_2\text{-MnO}_2@\text{LS}$ . Furthermore, the salt-resistant performance of the  $\text{Ti}_3\text{C}_2\text{-MnO}_2@\text{LS}$  has also been evaluated.

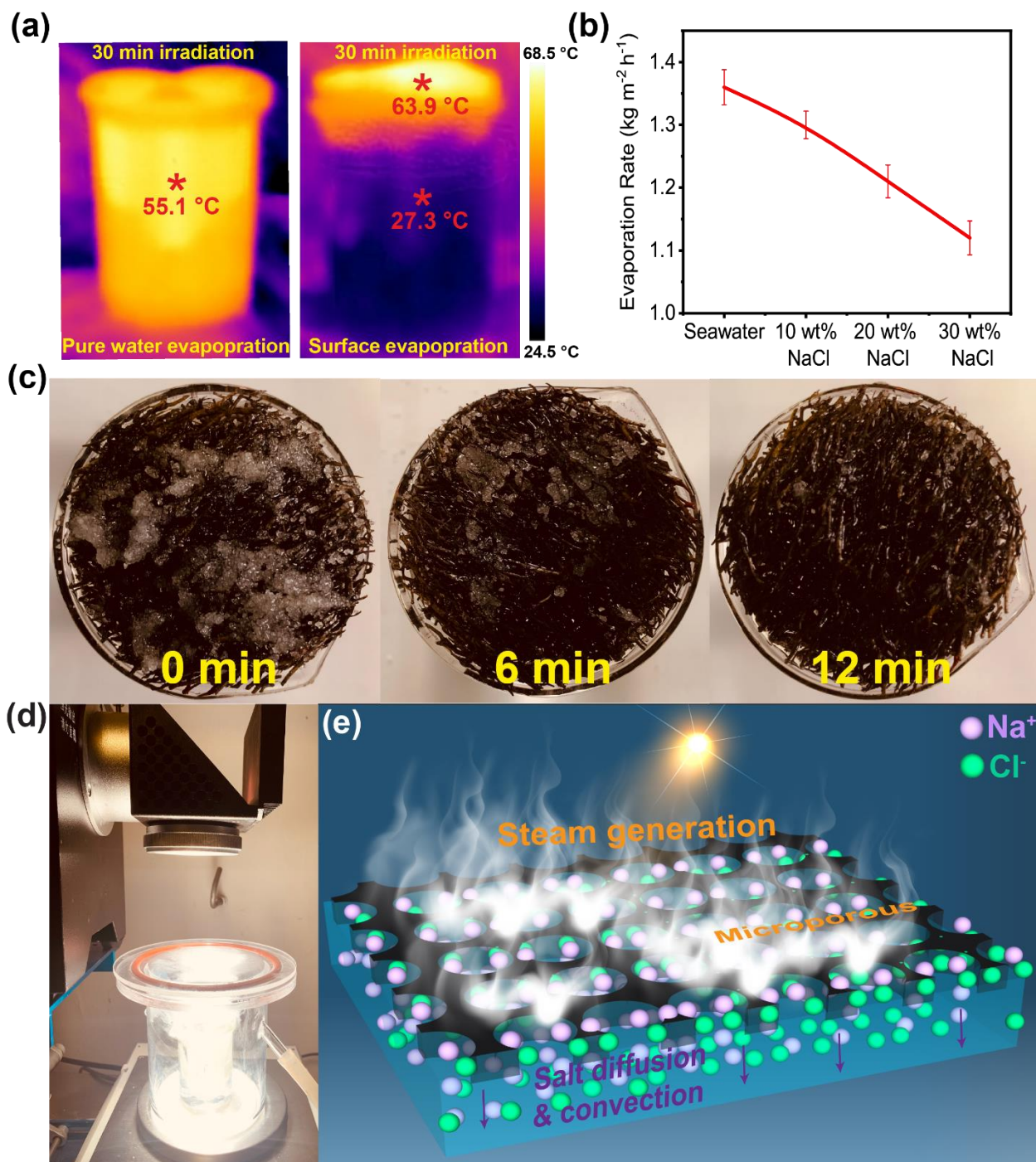


**Fig. 5** (a) IR images of the side view temperature distribution of the system with water only and  $\text{Ti}_3\text{C}_2\text{-MnO}_2@\text{LS}$  after 30 min irradiation; (b) Solar evaporation rate of  $\text{Ti}_3\text{C}_2\text{-MnO}_2@\text{LS}$  under different salinity (seawater, 10, 20, 30 wt%); (c) Progression of salt-resistance under 1 sun irradiation; (d) Image of the homemade setup for seawater desalination; (e) Schematic illustration of the possible salt rejection mechanism of the  $\text{Ti}_3\text{C}_2\text{-MnO}_2@\text{LS}$ .

As illustrated in Fig. 5c, 5 g NaCl salt crystals were directly placed on the top surface of  $\text{Ti}_3\text{C}_2\text{-MnO}_2@\text{LS}$ , irradiating the surface with 1 sun solar illumination. The solid NaCl is gradually dissolved within 12 min, confirming the remarkable salt ion diffusion backflow property of  $\text{Ti}_3\text{C}_2\text{-MnO}_2@\text{LS}$ . **Supporting movie** demonstrates the salt rejection and ion back flow of the proposed the  $\text{Ti}_3\text{C}_2\text{-MnO}_2@\text{LS}$ . The salt rejection property of the evaporator of the interfacial solar desalination is of great importance. Salt accumulation will block the water transportation channels as well as hinder solar absorption, resulting in a lower evaporation efficiency. The mechanism of salt ion diffusion backflow may be described as follows. First, luffa sponge's porous structure provides linked channels for rapid water transport and vapor escape. The hydrophilic characteristic of the luffa sponge keeps it moist, allowing for adequate water flow through capillary action and rapid steam production.

The salt particles formed on the surface of the  $\text{Ti}_3\text{C}_2\text{-MnO}_2@\text{LS}$  solar evaporator dissolve rapidly and create a high salt region at the interface between the solar evaporator and bulk water. The difference in salt concentration between the high salt region and the bulk water induces diffusion and convection, therefore reducing salt concentration in the solar evaporator and preventing salt deposition. **Fig. 5e** illustrates that due to the natural microporous structure of LS, efficient salt ion diffusion backflow mechanism can be achieved. Thus, the  $\text{Ti}_3\text{C}_2\text{-MnO}_2@\text{LS}$  can effectively prevent salt deposition during the desalination process. To demonstrate the potential applicability for seawater and wastewater purification, the solar desalination experiment was conducted on a homemade setup with natural seawater and simulated wastewater, as shown in **Fig. 5d**. The vapor will condense in the chamber and be collected for further analysis.

To evaluate the quality of purified water (i.e., desalinated water), the potential of hydrogen (pH), salinity, total dissolved solids (TDS), and conductivity of actual seawater, desalinated water, and DI water were measured. As shown in **Fig. 6a**, the pH of three water samples is kept neutral, while the salinity of desalinated water is very close to zero. **Fig. 6b** shows that the TDS and conductivity of desalinated water are both reduced by more than 2 orders of magnitude compared to the actual seawater, indicating a greatly improvement in water quality. The ion ( $\text{Na}^+$ ,  $\text{K}^+$ ,  $\text{Ca}^{2+}$ ,  $\text{Mg}^{2+}$ ) concentrations of actual seawater before and after desalination were measured by inductive-coupled plasma mass spectrometry. As presented in **Fig. 6c**, the ion concentration of desalinated water treated by  $\text{Ti}_3\text{C}_2\text{-MnO}_2@\text{LS}$  is nearly 3-4 orders of magnitude significantly reduced compared to the actual seawater, which is far below the salinity levels for drinkable water defined by the World Health Organization (WHO). Moreover, wastewater treatment experiment was further conducted to evaluate the wastewater treatment performance of  $\text{Ti}_3\text{C}_2\text{-MnO}_2@\text{LS}$ . Methylene blue (MB) solution was chosen to simulate wastewater. As shown in **Fig. 6d**, the absorbance of purified water is similar to that of DI water without the characteristic peaks of MB shown, indicating that the MB should be completely removed from the purified water. All the above results indicate that the  $\text{Ti}_3\text{C}_2\text{-MnO}_2@\text{LS}$  has great prospects to be applied in practical solar water treatment to address the issues of freshwater shortage.

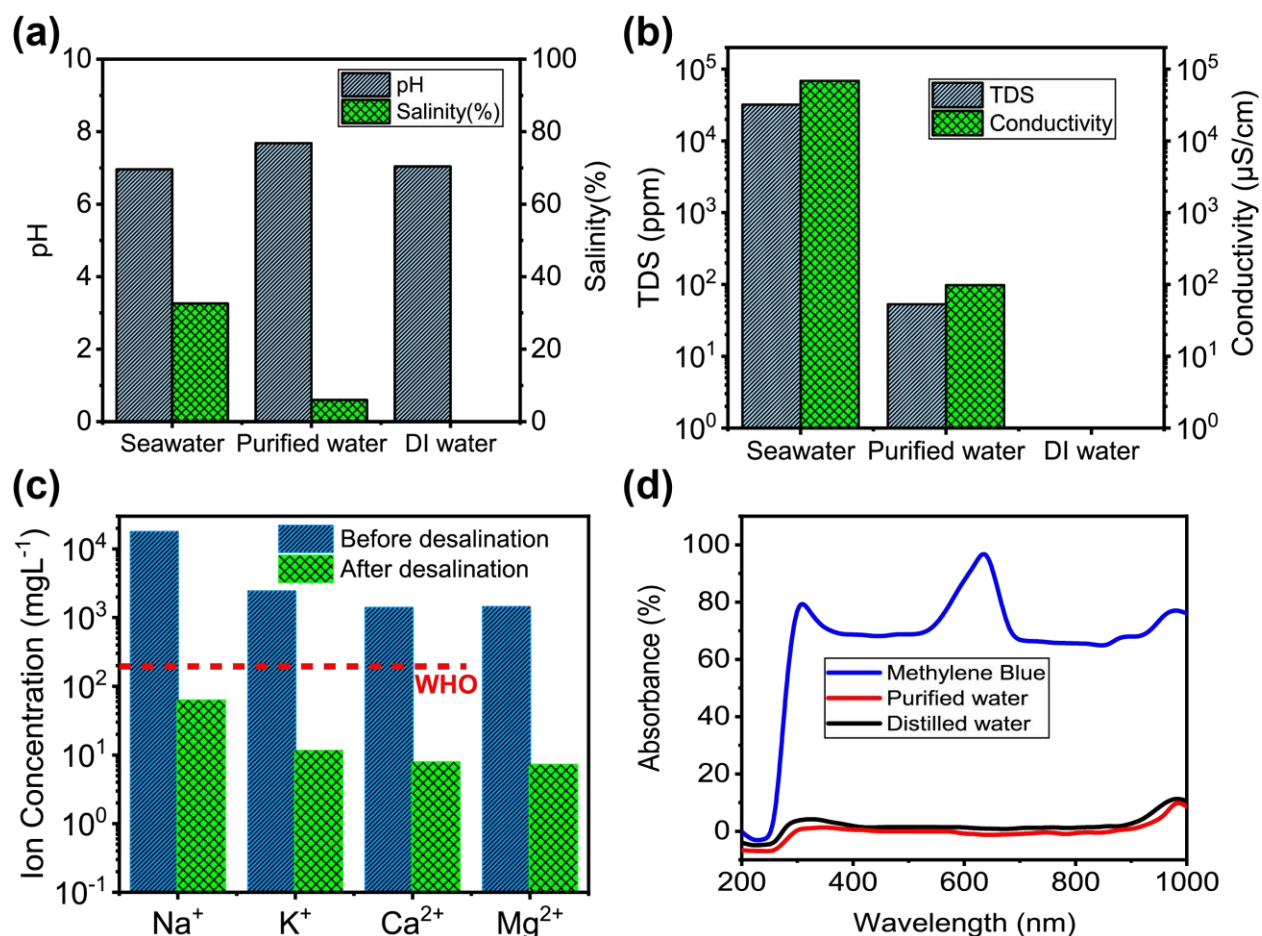


**Fig. 6** (a) pH and salinity of seawater, desalted water, and DI water; (b) TDS and conductivity of seawater, desalted water, and DI water; (c) Concentration of four main salt ions of actual seawater before and after desalination. (d) The UV-Vis spectra of methylene blue before and after solar thermal purification with  $\text{Ti}_3\text{C}_2\text{-MnO}_2@\text{LS}$  under one sun irradiation.

#### 4. Conclusion

In summary, highly effective  $\text{Ti}_3\text{C}_2\text{-MnO}_2$  nanocomposite coated LS has been developed for interfacial solar steam generation. The  $\text{Ti}_3\text{C}_2\text{-MnO}_2@\text{LS}$  was synthesized by a facial dip-drying method to improve the solar absorption and hydrophilicity of pristine biodegradable LS. The as-prepared evaporator achieves a superb water evaporation rate of  $1.36 \text{ kg m}^{-2} \text{ h}^{-1}$  and photothermal conversion efficiency of 85.28% under one sun irradiation. Excellent desalination performance has also been achieved, in which an



evaporation rate of above  $1.1 \text{ kg m}^{-2} \text{ h}^{-1}$  can be realized even under 30 wt% saline evaporation. The outstanding performance could be attributed to the excellent photothermal conversion efficiency of  $\text{Ti}_3\text{C}_2$  composited with  $\text{MnO}_2$  and the natural microporous structure and low thermal conductivity of LS. The porous structure of the luffa sponge provides salt ion diffusion backflow mechanism to reject the salt deposition on the surface of the evaporator. Moreover, the  $\text{Ti}_3\text{C}_2\text{-MnO}_2\text{@LS}$  is also feasible for efficient wastewater purification. The long-term durability, outstanding evaporation rate, low cost, and excellent salt rejection make it possible for widespread practical solar water evaporation to meet the freshwater demand.

## **Acknowledgments**

This work is financially supported by the Innovation and Technology Fund, Hong Kong, China (GHP/040/19SZ), the Hong Kong Polytechnic University (Project number: 1-ZE14), Photonic Research Institute, The Hong Kong Polytechnic University (Project number: 1-CD6V), the Hong Kong Polytechnic University Shenzhen Research Institute, Shenzhen, China (Grant Code: the science and technology innovation commission of Shenzhen (JCYJ20210324141206017)), Zhejiang Provincial Natural Science Foundation of China (Grant No. LQ21E020009), Ningbo Natural Science Foundation (Grant No. 2021J172), NSF (Award # 1856112) and California DWR (No. RS-2014-08).

## **Conflicts of interest**

There is no conflict to declare.

## Reference

- [1] H. Cheng, Y. Hu, J. Zhao, Meeting China's Water Shortage Crisis: Current Practices and Challenges, *Environ Sci Technol.* 43 (2009) 240–244. <https://doi.org/10.1021/es801934a>.
- [2] J. Gong, C. Li, M.R. Wasielewski, Advances in solar energy conversion, *Chem Soc Rev.* 48 (2019) 1862–1864. <https://doi.org/10.1039/C9CS90020A>.
- [3] K. Yu, P. Shao, P. Meng, T. Chen, J. Lei, X. Yu, R. He, F. Yang, W. Zhu, T. Duan, Superhydrophilic and highly elastic monolithic sponge for efficient solar-driven radioactive wastewater treatment under one sun, *J Hazard Mater.* 392 (2020) 122350. <https://doi.org/10.1016/j.jhazmat.2020.122350>.
- [4] A. Lenert, E.N. Wang, Optimization of nanofluid volumetric receivers for solar thermal energy conversion, *Solar Energy.* 86 (2012) 253–265. <https://doi.org/10.1016/j.solener.2011.09.029>.
- [5] G. Ahmadi, D. Toghraie, A. Azimian, O.A. Akbari, Evaluation of synchronous execution of full repowering and solar assisting in a 200 MW steam power plant, a case study, *Appl Therm Eng.* 112 (2017) 111–123. <https://doi.org/10.1016/j.applthermaleng.2016.10.083>.
- [6] A.M. Saleque, S. Ahmed, Md.N.A.S. Ivan, M.I. Hossain, W. Qarony, P.K. Cheng, J. Qiao, Z.L. Guo, L. Zeng, Y.H. Tsang, High-temperature solar steam generation by MWCNT-HfTe<sub>2</sub> van der Waals heterostructure for low-cost sterilization, *Nano Energy.* 94 (2022) 106916. <https://doi.org/10.1016/j.nanoen.2022.106916>.
- [7] A.M. Saleque, N. Nowshin, Md.N.A.S. Ivan, S. Ahmed, Y.H. Tsang, Natural Porous Materials for Interfacial Solar Steam Generation toward Clean Water Production, *Solar RRL.* (2022) 2100986. <https://doi.org/10.1002/solr.202100986>.
- [8] Z. Wang, T. Horseman, A.P. Straub, N.Y. Yip, D. Li, M. Elimelech, S. Lin, Pathways and challenges for efficient solar-thermal desalination, *Sci Adv.* 5 (2019). <https://doi.org/10.1126/sciadv.aax0763>.
- [9] A.K. Menon, I. Haechler, S. Kaur, S. Lubner, R.S. Prasher, Enhanced solar evaporation using a photo-thermal umbrella for wastewater management, *Nat Sustain.* 3 (2020) 144–151. <https://doi.org/10.1038/s41893-019-0445-5>.
- [10] P. Tao, G. Ni, C. Song, W. Shang, J. Wu, J. Zhu, G. Chen, T. Deng, Solar-driven

- interfacial evaporation, *Nat Energy*. 3 (2018) 1031–1041. <https://doi.org/10.1038/s41560-018-0260-7>.
- [11] P. Cao, L. Zhao, Z. Yang, P. Yuan, Y. Zhang, Q. Li, Carbon Nanotube Network-Based Solar-Thermal Water Evaporator and Thermoelectric Module for Electricity Generation, *ACS Appl Nano Mater.* 4 (2021) 8906–8912. <https://doi.org/10.1021/acsanm.1c01551>.
- [12] T. Yang, H. Lin, K.-T. Lin, B. Jia, Carbon-based absorbers for solar evaporation: Steam generation and beyond, *Sustainable Materials and Technologies*. 25 (2020) e00182. <https://doi.org/10.1016/j.susmat.2020.e00182>.
- [13] Z. Wang, Y. Liu, P. Tao, Q. Shen, N. Yi, F. Zhang, Q. Liu, C. Song, D. Zhang, W. Shang, T. Deng, Bio-Inspired Evaporation Through Plasmonic Film of Nanoparticles at the Air-Water Interface, *Small*. 10 (2014) 3234–3239. <https://doi.org/10.1002/smll.201401071>.
- [14] H. Wang, R. Zhang, D. Yuan, S. Xu, L. Wang, Gas Foaming Guided Fabrication of 3D Porous Plasmonic Nanoplatfrom with Broadband Absorption, Tunable Shape, Excellent Stability, and High Photothermal Efficiency for Solar Water Purification, *Adv Funct Mater.* 30 (2020) 2003995. <https://doi.org/10.1002/adfm.202003995>.
- [15] T. Wang, S. Gao, G. Wang, H. Wang, J. Bai, S. Ma, B. Wang, Three-dimensional hierarchical oxygen vacancy-rich WO<sub>3</sub>-decorated Ni foam evaporator for high-efficiency solar-driven interfacial steam generation, *J Colloid Interface Sci.* 602 (2021) 767–777. <https://doi.org/10.1016/j.jcis.2021.06.065>.
- [16] W. Huang, P. Su, Y. Cao, C. Li, D. Chen, X. Tian, Y. Su, B. Qiao, J. Tu, X. Wang, Three-dimensional hierarchical Cu<sub>x</sub>S-based evaporator for high-efficiency multifunctional solar distillation, *Nano Energy*. 69 (2020) 104465. <https://doi.org/10.1016/j.nanoen.2020.104465>.
- [17] Z. Li, X. Ma, D. Chen, X. Wan, X. Wang, Z. Fang, X. Peng, Polyaniline-Coated MOFs Nanorod Arrays for Efficient Evaporation-Driven Electricity Generation and Solar Steam Desalination, *Advanced Science*. 8 (2021) 2004552. <https://doi.org/10.1002/advs.202004552>.
- [18] X. Wang, Q. Liu, S. Wu, B. Xu, H. Xu, Multilayer Polypyrrole Nanosheets with Self-Organized Surface Structures for Flexible and Efficient Solar–Thermal Energy

- Conversion, *Advanced Materials*. 31 (2019) 1807716. <https://doi.org/10.1002/adma.201807716>.
- [19] G. Xue, K. Liu, Q. Chen, P. Yang, J. Li, T. Ding, J. Duan, B. Qi, J. Zhou, Robust and Low-Cost Flame-Treated Wood for High-Performance Solar Steam Generation, *ACS Appl Mater Interfaces*. 9 (2017) 15052–15057. <https://doi.org/10.1021/acsami.7b01992>.
- [20] C. Jia, Y. Li, Z. Yang, G. Chen, Y. Yao, F. Jiang, Y. Kuang, G. Pastel, H. Xie, B. Yang, S. Das, L. Hu, Rich Mesostructures Derived from Natural Woods for Solar Steam Generation, *Joule*. 1 (2017) 588–599. <https://doi.org/10.1016/j.joule.2017.09.011>.
- [21] M.M. Ghafurian, H. Niazmand, E. Ebrahimnia-Bajestan, R.A. Taylor, Wood surface treatment techniques for enhanced solar steam generation, *Renew Energy*. 146 (2020) 2308–2315. <https://doi.org/10.1016/j.renene.2019.08.036>.
- [22] L. Huang, L. Ling, J. Su, Y. Song, Z. Wang, B.Z. Tang, P. Westerhoff, R. Ye, Laser-Engineered Graphene on Wood Enables Efficient Antibacterial, Anti-Salt-Fouling, and Lipophilic-Matter-Rejection Solar Evaporation, *ACS Appl Mater Interfaces*. 12 (2020) 51864–51872. <https://doi.org/10.1021/acsami.0c16596>.
- [23] J. Liu, J. Yao, Y. Yuan, Q. Liu, W. Zhang, X. Zhang, J. Gu, Surface-Carbonized Bamboos with Multilevel Functional Biostructures Deliver High Photothermal Water Evaporation Performance, *Adv Sustain Syst*. 4 (2020) 1–8. <https://doi.org/10.1002/adsu.202000126>.
- [24] C. Sheng, N. Yang, Y. Yan, X. Shen, C. Jin, Z. Wang, Q. Sun, Bamboo decorated with plasmonic nanoparticles for efficient solar steam generation, *Appl Therm Eng*. 167 (2020) 114712. <https://doi.org/10.1016/j.applthermaleng.2019.114712>.
- [25] Y. Bian, Q. Du, K. Tang, Y. Shen, L. Hao, D. Zhou, X. Wang, Z. Xu, H. Zhang, L. Zhao, S. Zhu, J. Ye, H. Lu, Y. Yang, R. Zhang, Y. Zheng, S. Gu, Carbonized Bamboos as Excellent 3D Solar Vapor-Generation Devices, *Adv Mater Technol*. 4 (2019) 1800593. <https://doi.org/10.1002/admt.201800593>.
- [26] Z. Li, C. Wang, T. Lei, H. Ma, J. Su, S. Ling, W. Wang, Arched Bamboo Charcoal as Interfacial Solar Steam Generation Integrative Device with Enhanced Water Purification Capacity, *Adv Sustain Syst*. 3 (2019) 1800144.

- <https://doi.org/10.1002/adsu.201800144>.
- [27] B. Gong, H. Yang, S. Wu, Y. Tian, X. Guo, C. Xu, W. Kuang, J. Yan, K. Cen, Z. Bo, K. (Ken) Ostrikov, Multifunctional solar bamboo straw: Multiscale 3D membrane for self-sustained solar-thermal water desalination and purification and thermoelectric waste heat recovery and storage, *Carbon* N Y. 171 (2021) 359–367. <https://doi.org/10.1016/j.carbon.2020.09.033>.
- [28] Md.N.A.S. Ivan, A.M. Saleque, S. Ahmed, Z.L. Guo, D. Zu, L. Xu, T.I. Alam, S.U. Hani, Y.H. Tsang, Jute stick derived self-regenerating sustainable solar evaporators with different salt mitigation mechanisms for highly efficient solar desalination, *J Mater Chem A Mater.* (2023). <https://doi.org/10.1039/D2TA08237C>.
- [29] A.M. Saleque, Md.N.A.S. Ivan, S. Ahmed, Y.H. Tsang, Light-trapping texture bio-hydrogel with anti-biofouling and antibacterial properties for efficient solar desalination, *Chemical Engineering Journal.* 458 (2023) 141430. <https://doi.org/10.1016/j.cej.2023.141430>.
- [30] Y. Liao, J. Chen, D. Zhang, X. Wang, B. Yuan, P. Deng, F. Li, H. Zhang, Lotus leaf as solar water evaporation devices, *Mater Lett.* 240 (2019) 92–95. <https://doi.org/10.1016/j.matlet.2018.12.133>.
- [31] N. Xu, X. Hu, W. Xu, X. Li, L. Zhou, S. Zhu, J. Zhu, Mushrooms as Efficient Solar Steam-Generation Devices, *Advanced Materials.* 29 (2017) 1–5. <https://doi.org/10.1002/adma.201606762>.
- [32] P. Sun, W. Zhang, I. Zada, Y. Zhang, J. Gu, Q. Liu, H. Su, D. Pantelić, B. Jelenković, D. Zhang, 3D-Structured Carbonized Sunflower Heads for Improved Energy Efficiency in Solar Steam Generation, *ACS Appl Mater Interfaces.* 12 (2020) 2171–2179. <https://doi.org/10.1021/acsami.9b11738>.
- [33] C. Wang, J. Wang, Z. Li, K. Xu, T. Lei, W. Wang, Superhydrophilic porous carbon foam as a self-desalting monolithic solar steam generation device with high energy efficiency, *J Mater Chem A Mater.* 8 (2020) 9528–9535. <https://doi.org/10.1039/D0TA01439G>.
- [34] T.T. Pham, T.H. Nguyen, T.A.H. Nguyen, D.D. Pham, D.C. Nguyen, D.B. Do, H.V. Nguyen, M.H. Ha, Z.H. Nguyen, Durable, scalable and affordable iron (III) based coconut husk photothermal material for highly efficient solar steam generation,

- Desalination. 518 (2021) 115280. <https://doi.org/10.1016/j.desal.2021.115280>.
- [35] Y. Sun, Z. Zhao, G. Zhao, L. Wang, D. Jia, Y. Yang, X. Liu, X. Wang, J. Qiu, High performance carbonized corncob-based 3D solar vapor steam generator enhanced by environmental energy, *Carbon N Y.* 179 (2021) 337–347. <https://doi.org/10.1016/j.carbon.2021.04.037>.
- [36] M. Zhu, J. Yu, C. Ma, C. Zhang, D. Wu, H. Zhu, Carbonized daikon for high efficient solar steam generation, *Solar Energy Materials and Solar Cells.* 191 (2019) 83–90. <https://doi.org/10.1016/j.solmat.2018.11.015>.
- [37] Y. Long, S. Huang, H. Yi, J. Chen, J. Wu, Q. Liao, H. Liang, H. Cui, S. Ruan, Y.-J. Zeng, Carrot-inspired solar thermal evaporator, *J Mater Chem A Mater.* 7 (2019) 26911–26916. <https://doi.org/10.1039/C9TA08754K>.
- [38] Y. Kong, Y. Gao, B. Gao, Y. Qi, W. Yin, S. Wang, F. Yin, Z. Dai, Q. Yue, Tubular polypyrrole enhanced elastomeric biomass foam as a portable interfacial evaporator for efficient self-desalination, *Chemical Engineering Journal.* 445 (2022) 136701. <https://doi.org/10.1016/j.cej.2022.136701>.
- [39] C. Liu, K. Hong, X. Sun, A. Natan, P. Luan, Y. Yang, H. Zhu, An “antifouling” porous loofah sponge with internal microchannels as solar absorbers and water pumps for thermal desalination, *J Mater Chem A Mater.* 8 (2020) 12323–12333. <https://doi.org/10.1039/d0ta03872e>.
- [40] A.M. Saleque, S. Ma, S. Ahmed, M.I. Hossain, W. Qarony, Y.H. Tsang, Solar Driven Interfacial Steam Generation Derived from Biodegradable Luffa Sponge, *Adv Sustain Syst.* 5 (2021) 2000291. <https://doi.org/10.1002/adsu.202000291>.
- [41] J. Zheng, X. Pan, X. Huang, D. Xiong, Y. Shang, X. Li, N. Wang, W.-M. Lau, H.Y. Yang, Integrated NiCo<sub>2</sub>-LDHs@MXene/rGO aerogel: Componential and structural engineering towards enhanced performance stability of hybrid supercapacitor, *Chemical Engineering Journal.* 396 (2020) 125197. <https://doi.org/10.1016/j.cej.2020.125197>.
- [42] Y. Li, F. Meng, Y. Mei, H. Wang, Y. Guo, Y. Wang, F. Peng, F. Huang, Z. Zhou, Electrospun generation of Ti<sub>3</sub>C<sub>2</sub>T<sub>x</sub> MXene@graphene oxide hybrid aerogel microspheres for tunable high-performance microwave absorption, *Chemical Engineering Journal.* 391 (2020) 123512.

- <https://doi.org/10.1016/j.cej.2019.123512>.
- [43] G. Liu, Q. Xiong, Y. Xu, Q. Fang, K.C.-F. Leung, M. Sang, S. Xuan, L. Hao, Sandwich-structured MXene@Au/polydopamine nanosheets with excellent photothermal-enhancing catalytic activity, *Colloids Surf A Physicochem Eng Asp.* 633 (2022) 127860. <https://doi.org/10.1016/j.colsurfa.2021.127860>.
- [44] Q. Lin, Y. Liu, G. Zeng, X. Li, B. Wang, X. Cheng, A. Sengupta, X. Yang, Z. Feng, Bionics inspired modified two-dimensional MXene composite membrane for high-throughput dye separation, *J Environ Chem Eng.* 9 (2021) 105711. <https://doi.org/10.1016/j.jece.2021.105711>.
- [45] R. Li, L. Zhang, L. Shi, P. Wang, MXene Ti<sub>3</sub>C<sub>2</sub>: An Effective 2D Light-to-Heat Conversion Material, *ACS Nano.* 11 (2017) 3752–3759. <https://doi.org/10.1021/acsnano.6b08415>.
- [46] X. Zhao, X.-J. Zha, L.-S. Tang, J.-H. Pu, K. Ke, R.-Y. Bao, Z. Liu, M.-B. Yang, W. Yang, Self-assembled core-shell polydopamine@MXene with synergistic solar absorption capability for highly efficient solar-to-vapor generation, *Nano Res.* 13 (2020) 255–264. <https://doi.org/10.1007/s12274-019-2608-0>.
- [47] Y. Dall’Agnese, P. Rozier, P.-L. Taberna, Y. Gogotsi, P. Simon, Capacitance of two-dimensional titanium carbide (MXene) and MXene/carbon nanotube composites in organic electrolytes, *J Power Sources.* 306 (2016) 510–515. <https://doi.org/10.1016/j.jpowsour.2015.12.036>.
- [48] J. Zhu, Y. Tang, C. Yang, F. Wang, M. Cao, Composites of TiO<sub>2</sub> Nanoparticles Deposited on Ti<sub>3</sub>C<sub>2</sub> MXene Nanosheets with Enhanced Electrochemical Performance, *J Electrochem Soc.* 163 (2016) A785–A791. <https://doi.org/10.1149/2.0981605jes>.
- [49] M. Pi, X. Wang, Z. Wang, R. Ran, Sustainable MXene/PDA hydrogel with core-shell structure tailored for highly efficient solar evaporation and long-term desalination, *Polymer (Guildf).* 230 (2021) 124075. <https://doi.org/10.1016/j.polymer.2021.124075>.
- [50] D. Wen, G. Ying, L. Liu, C. Sun, Y. Li, Y. Zhao, Z. Ji, Y. Wu, J. Zhang, J. Zhang, X. Wang, Flexible and High-Performance MXene/MnO<sub>2</sub> Film Electrodes Fabricated by Inkjet Printing: Toward a New Generation Supercapacitive Application, *Adv*

- Mater Interfaces. 8 (2021) 2101453. <https://doi.org/10.1002/admi.202101453>.
- [51] Z. Zhang, P. Mu, J. Han, J. He, Z. Zhu, H. Sun, W. Liang, A. Li, Superwetting and mechanically robust MnO<sub>2</sub> nanowire–reduced graphene oxide monolithic aerogels for efficient solar vapor generation, *J Mater Chem A Mater.* 7 (2019) 18092–18099. <https://doi.org/10.1039/C9TA04509K>.
- [52] D. Li, D. Han, C. Guo, C. Huang, Facile Preparation of MnO<sub>2</sub>-Deposited Wood for High-Efficiency Solar Steam Generation, *ACS Appl Energy Mater.* 4 (2021) 1752–1762. <https://doi.org/10.1021/acsaem.0c02902>.
- [53] M.S. Irshad, X. Wang, M.S. Abbasi, N. Arshad, Z. Chen, Z. Guo, L. Yu, J. Qian, J. You, T. Mei, Semiconductive, Flexible MnO<sub>2</sub> NWs/Chitosan Hydrogels for Efficient Solar Steam Generation, *ACS Sustain Chem Eng.* 9 (2021) 3887–3900. <https://doi.org/10.1021/acssuschemeng.0c08981>.
- [54] G. Ni, S.H. Zandavi, S.M. Javid, S. V. Boriskina, T.A. Cooper, G. Chen, A salt-rejecting floating solar still for low-cost desalination, *Energy Environ Sci.* 11 (2018) 1510–1519. <https://doi.org/10.1039/C8EE00220G>.
- [55] Y. Liu, J. Chen, D. Guo, M. Cao, L. Jiang, Floatable, Self-Cleaning, and Carbon-Black-Based Superhydrophobic Gauze for the Solar Evaporation Enhancement at the Air–Water Interface, *ACS Appl Mater Interfaces.* 7 (2015) 13645–13652. <https://doi.org/10.1021/acsami.5b03435>.
- [56] X. Wang, Y. He, X. Liu, Synchronous steam generation and photodegradation for clean water generation based on localized solar energy harvesting, *Energy Convers Manag.* 173 (2018) 158–166. <https://doi.org/10.1016/j.enconman.2018.07.065>.
- [57] Y. Kuang, C. Chen, S. He, E.M. Hitz, Y. Wang, W. Gan, R. Mi, L. Hu, A High-Performance Self-Regenerating Solar Evaporator for Continuous Water Desalination, *Advanced Materials.* 31 (2019) 1900498. <https://doi.org/10.1002/adma.201900498>.
- [58] F. Wang, D. Wei, Y. Li, T. Chen, P. Mu, H. Sun, Z. Zhu, W. Liang, A. Li, Chitosan/reduced graphene oxide-modified spacer fabric as a salt-resistant solar absorber for efficient solar steam generation, *J Mater Chem A Mater.* 7 (2019) 18311–18317. <https://doi.org/10.1039/C9TA05859A>.



- [59] H. Xie, H. Gu, M. Fujii, X. Zhang, Short hot wire technique for measuring thermal conductivity and thermal diffusivity of various materials, *Meas Sci Technol.* 17 (2006) 208–214. <https://doi.org/10.1088/0957-0233/17/1/032>.
- [60] Y. Wu, Y. Liu, W. Wang, J. Wang, C. Zhang, Z. Wu, P. Yan, K. Li, Microwave absorption enhancement and loss mechanism of lamellar MnO<sub>2</sub> nanosheets decorated reduced graphene oxide hybrid, *Journal of Materials Science: Materials in Electronics.* 30 (2019) 842–854. <https://doi.org/10.1007/s10854-018-0354-9>.
- [61] M. Boota, B. Anasori, C. Voigt, M.-Q. Zhao, M.W. Barsoum, Y. Gogotsi, Pseudocapacitive Electrodes Produced by Oxidant-Free Polymerization of Pyrrole between the Layers of 2D Titanium Carbide (MXene), *Advanced Materials.* 28 (2016) 1517–1522. <https://doi.org/10.1002/adma.201504705>.
- [62] R. Zhao, H. Di, X. Hui, D. Zhao, R. Wang, C. Wang, L. Yin, Self-assembled Ti<sub>3</sub>C<sub>2</sub> MXene and N-rich porous carbon hybrids as superior anodes for high-performance potassium-ion batteries, *Energy Environ Sci.* 13 (2020) 246–257. <https://doi.org/10.1039/C9EE03250A>.
- [63] L. Li, N. He, B. Jiang, K. Yu, Q. Zhang, H. Zhang, D. Tang, Y. Song, Highly Salt-Resistant 3D Hydrogel Evaporator for Continuous Solar Desalination via Localized Crystallization, *Adv Funct Mater.* 2104380 (2021) 2104380. <https://doi.org/10.1002/adfm.202104380>.